Elastic Beams in Three Dimensions

Lars Andersen and Søren R.K. Nielsen

ISSN 1901-7286
DCE Lecture Notes No. 23

Department of Civil Engineering

Aalborg University
Department of Civil Engineering
Structural Mechanics

DCE Lecture Notes No. 23

Elastic Beams in Three Dimensions

by

Lars Andersen and Søren R.K. Nielsen

August 2008

Scientific Publications at the Department of Civil Engineering

Technical Reports are published for timely dissemination of research results and scientific work carried out at the Department of Civil Engineering (DCE) at Aalborg University. This medium allows publication of more detailed explanations and results than typically allowed in scientific journals.

Technical Memoranda are produced to enable the preliminary dissemination of scientific work by the personnel of the DCE where such release is deemed to be appropriate. Documents of this kind may be incomplete or temporary versions of papers—or part of continuing work. This should be kept in mind when references are given to publications of this kind.

Contract Reports are produced to report scientific work carried out under contract. Publications of this kind contain confidential matter and are reserved for the sponsors and the DCE. Therefore, Contract Reports are generally not available for public circulation.

Lecture Notes contain material produced by the lecturers at the DCE for educational purposes. This may be scientific notes, lecture books, example problems or manuals for laboratory work, or computer programs developed at the DCE.

Theses are monograms or collections of papers published to report the scientific work carried out at the DCE to obtain a degree as either PhD or Doctor of Technology. The thesis is publicly available after the defence of the degree.

Latest News is published to enable rapid communication of information about scientific work carried out at the DCE. This includes the status of research projects, developments in the laboratories, information about collaborative work and recent research results.

Published 2008 by
Aalborg University
Department of Civil Engineering
Sohngaardsholmsvej 57,
DK-9000 Aalborg, Denmark

Printed in Denmark at Aalborg University

ISSN 1901-7286 DCE Lecture Notes No. 23

Preface

This textbook has been written for the course Statics IV on spatial elastic beam structures given at the 5th semester of the undergraduate programme in Civil Engineering at Aalborg University. The book provides a theoretical basis for the understanding of the structural behaviour of beams in three-dimensional structures. In the course, the text is supplemented with laboratory work and hands-on exercises in commercial structural finite-element programs as well as MATLAB. The course presumes basic knowledge of ordinary differential equations and structural mechanics. A prior knowledge about plane frame structures is an advantage though not mandatory. The authors would like to thank Mrs. Solveig Hesselvang for typing the manuscript.

Aalborg, August 2008 Lars Andersen and Søren R.K. Nielsen

Contents

CHAPTER 1
Beams in three dimensions

This chapter gives an introduction is given to elastic beams in three dimensions. Firstly, the equations of equilibrium are presented and then the classical beam theories based on Bernoulli-Euler and Timoshenko beam kinematics are derived. The focus of the chapter is the flexural deformations of three-dimensional beams and their coupling with axial deformations. Only a short introduction is given to torsional deformations, or twist, of beams in three dimensions. A full description of torsion and shear stresses is given in the next chapters. At the end of this chapter, a stiffness matrix is formulated for a three-dimensional Timosheko beam element. This element can be used for finite-element analysis of elastic spatial frame structures.

1.1 Introduction

In what follows, the theory of three-dimensional beams is outlined.

1.2 Equations of equilibrium for spatial beams

An initially straight beam is considered. When the beam is free of external loads, the beam occupies a so-called referential state. In the referential state the beam is cylindrical with the length l, *i.e.* the cross-sections are everywhere identical. The displacement and rotation of the beam is described in a referential (x, y, z)-coordinate system with base unit vectors $\{\mathbf{i}, \mathbf{j}, \mathbf{k}\}$, the origin O placed on the left end-section, and the x-axis parallel with the cylinder and orientated into the beam, see Fig. 1–1. For the time being, the position of O and the orientation of the y- and z-axes may be chosen freely.

The beam is loaded by a distributed load per unit length of the referential scale defined by the vector field $\mathbf{q} = \mathbf{q}(x)$ and a distributed moment load vector per unit length $\mathbf{m} = \mathbf{m}(x)$. A differential beam element of the length dx is then loaded by the external force vector $\mathbf{q}dx$ and external moment vector $\mathbf{m}dx$ as shown in Fig. 1–1. The length of the differential beam element may change during deformations due to axial strains. However, this does not affect the indicated load vectors which have been defined per unit length of the referential state. Measured in the (x, y, z)-coordinate system, $\mathbf{q}$ and $\mathbf{m}$ have the components

$$\mathbf{q} = \begin{bmatrix} q_x \\ q_y \\ q_z \end{bmatrix}, \qquad \mathbf{m} = \begin{bmatrix} m_x \\ m_y \\ m_z \end{bmatrix}. \tag{1–1}$$

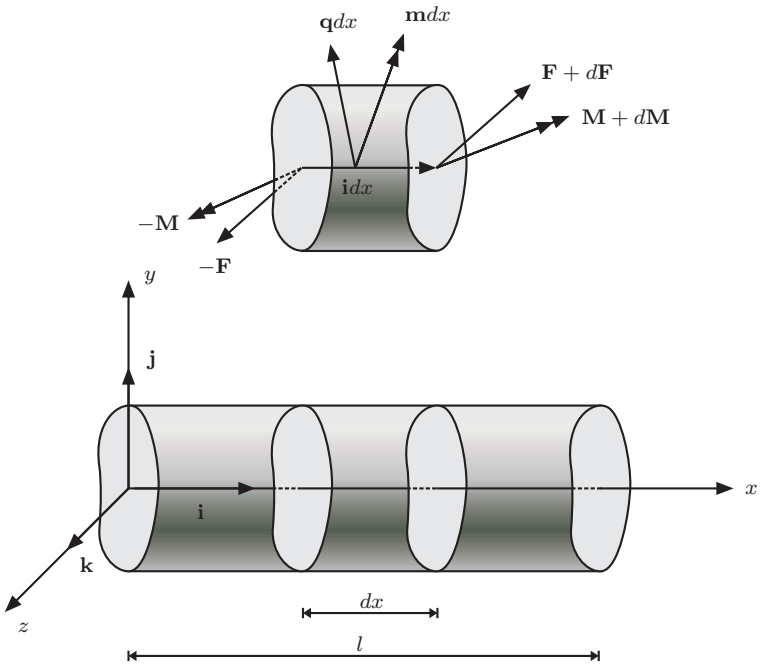

Figure 1–1 Beam in referential state.

As a consequence of the external loads, the beam is deformed into the so-called current state where the external loads are balanced by an internal section force vector $\mathbf{F} = \mathbf{F}(x)$ and an internal section moment vector $\mathbf{M} = \mathbf{M}(x)$. These vectors act on the cross-section with the base unit vector $\mathbf{i}$ of the x-axis as outward directed normal vector. With reference to Fig. 1–2, the components of $\mathbf{F}$ and $\mathbf{M}$ in the (x, y, z)-coordinate system are:

$$\mathbf{F} = \begin{bmatrix} N \\ Q_y \\ Q_z \end{bmatrix}, \qquad \mathbf{M} = \begin{bmatrix} M_x \\ M_y \\ M_z \end{bmatrix} \tag{1–2}$$

Here, $N = N(x)$ is the *axial force*, whereas the components $Q_y = Q_y(x)$ and $Q_z = Q_z(x)$ signify the *shear force* components in the y- and z-directions. The axial component $M_x = M_x(x)$ of the section moment vector is denoted the *torsional moment*. The components $M_y = M_y(x)$ and $M_z = M_z(x)$ in the y- and z-directions represent the *bending moments*. The torsional moment is not included in two-dimensional beam theory. However, in the design of three-dimensional frame structures, a good understanding of the torsional behaviour of beams is crucial.

Assuming that the displacements remain small, the equation of static equilibrium can be established in the referential state. With reference to Fig. 1–1, the left end-section of the element is loaded with the section force vector $-\mathbf{F}$ and the section moment vector $-\mathbf{M}$. At the right end-section, these vectors are changed differentially into $\mathbf{F} + d\mathbf{F}$ and $\mathbf{M} + d\mathbf{M}$, respectively. Force equilibrium and moment equilibrium formulated at the point of attack of the section force vector $-\mathbf{F}$ at the left end-section then provides the following equations of force and moment

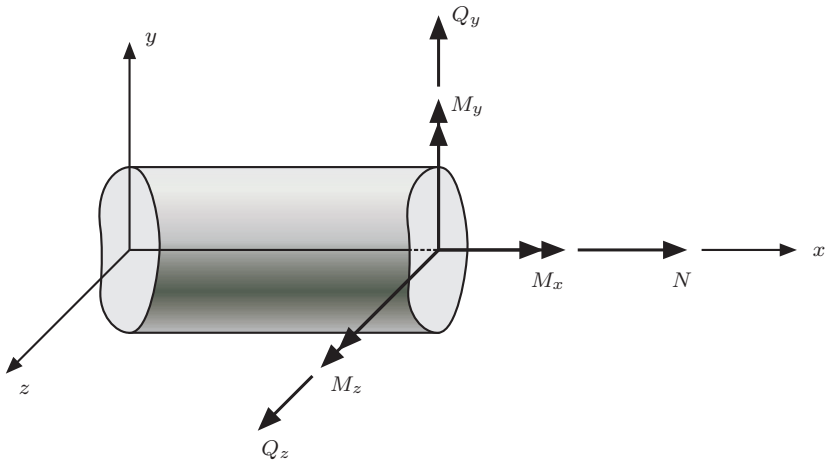

Figure 1–2 Components of the section force vector and the section moment vector.

equilibrium of the differential beam element:

$$-\mathbf{F} + \mathbf{F} + d\mathbf{F} + \mathbf{q}dx = \mathbf{0} \Rightarrow$$

$$\frac{dF}{dx} + \mathbf{q} = \mathbf{0} \tag{1–3a}$$

$$-\mathbf{M} + \mathbf{M} + dM + \mathbf{i}dx \times (\mathbf{F} + d\mathbf{F}) + \mathbf{m}dx = \mathbf{0} \Rightarrow$$

$$\frac{d\mathbf{M}}{dx} + \mathbf{i} \times \mathbf{F} + \mathbf{m} = \mathbf{0} \tag{1–3b}$$

From Eqs. (1–1) and (1–2) follows that Eqs. (1–3a) and (1–3b) are equivalent to the following component relations:

$$\frac{dN}{dx} + q_x = 0, \qquad \frac{dQ_y}{dx} + q_y = 0, \qquad \frac{dQ_z}{dx} + q_z = 0, \tag{1–4a}$$

$$\frac{dM_x}{dx} + m_x = 0, \qquad \frac{dM_y}{dx} - Q_z + m_y = 0, \qquad \frac{dM_z}{dx} + Q_y + m_z = 0. \tag{1–4b}$$

At the derivation of Eq. (1–4b), it has been utilised that

$$\mathbf{i} \times \mathbf{F} = \mathbf{i} \times (N\mathbf{i} + Q_y\mathbf{j} + Q_z\mathbf{k}) = N\mathbf{i} \times \mathbf{i} + Q_y\mathbf{i} \times j Q_z\mathbf{i} \times \mathbf{k} = 0\mathbf{i} - Q_z\mathbf{j} + Q_y\mathbf{k}. \tag{1–5}$$

Hence, $\mathbf{i} \times \mathbf{F}$ has the components $\{0, -Q_z, Q_y\}$. It is noted that a non-zero normal-force component is achieved when the moment equilibrium equations are formulated in the deformed state. This may lead to coupled lateral-flexural instability as discussed in a later chapter.

1.2.1 Section forces and stresses in a beam

On the cross-section with the outward directed unit vector co-directional to the x-axis, the normal stress σ_{xx} and the shear stresses σ_{xy} and σ_{xz} act as shown in Fig. 1–3. These stresses must be

statically equivalent to the components of the force vector $\mathbf{F}$ and the section moment vector $\mathbf{M}$ as indicated by the following relations:

$$N = \int_A \sigma_{xx} dA, \qquad Q_y = \int_A \sigma_{xy} dA, \qquad Q_z = \int_A \sigma_{xz} dA, \tag{1–6a}$$

$$M_x = \int_A (\sigma_{xz} y - \sigma_{xy} z) dA, \qquad M_y = \int_A z \sigma_{xx} dA, \qquad M_z = -\int_A y \sigma_{xx} dA. \tag{1–6b}$$

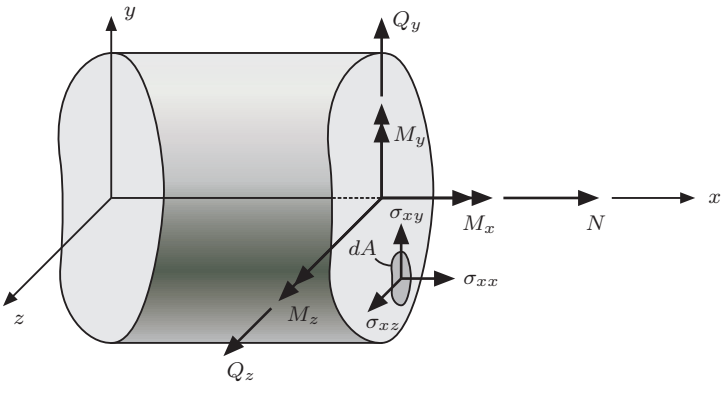

Figure 1–3 Stresses and stress resultant on a cross-section of the beam.

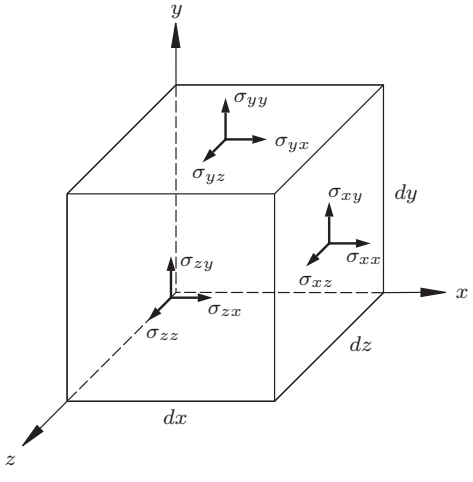

Figure 1–4 Components of the stress tensor.

On sections orthogonal to the y- and z-axes, the stresses $\{\sigma_{yy}, \sigma_{yx}, \sigma_{yz}\}$ and $\{\sigma_{zz}, \sigma_{zx}, \sigma_{zy}\}$ act as shown in Fig. 1–4. The first index indicates the coordinate axis co-directional to the outward normal vector of the section, whereas the second index specifies the direction of action of the stress component. The stresses shown in Fig.1–4 form the components of the stress tensor

$\boldsymbol{\sigma}$ in the (x, y, z)-coordinate system given as

$$\boldsymbol{\sigma} = \begin{bmatrix} \sigma_{xx} & \sigma_{yx} & \sigma_{zx} \\ \sigma_{xy} & \sigma_{yy} & \sigma_{zy} \\ \sigma_{xz} & \sigma_{yz} & \sigma_{zz} \end{bmatrix}. \tag{1–7}$$

Moment equilibrium of the cube shown in Fig. 1–4 requires that

$$\sigma_{xy} = \sigma_{yx}, \qquad \sigma_{xz} = \sigma_{zx}, \qquad \sigma_{yz} = \sigma_{zy}. \tag{1–8}$$

Hence, $\boldsymbol{\sigma}$ is a symmetric tensor.

1.2.2 Kinematics and deformations of a beam

The basic assumption in the classical beam theory is that a cross-section orthogonal to the x-axis at the coordinate x remains plane and keeps its shape during deformation. In other words, the cross-section translates and rotates as a rigid body. Especially, this means that Poisson contractions in the transverse direction due to axial strains are ignored. Hence, the deformed position of the cross-section is uniquely described by a position vector $\mathbf{w} = \mathbf{w}(x)$ and a rotation vector $\boldsymbol{\theta} = \boldsymbol{\theta}(x)$ with the following components in the (x, y, z)-coordinate system:

$$\mathbf{w} = \begin{bmatrix} w_x \\ w_y \\ w_z \end{bmatrix}, \qquad \boldsymbol{\theta} = \begin{bmatrix} \theta_x \\ \theta_y \\ \theta_z \end{bmatrix}. \tag{1–9}$$

Further, only linear beam theory will be considered. This means that the displacement components w_x, w_y and w_z in Eq. (1–9) all small compared to the beam length l. Further the rotation components θ_x, θ_y and θ_z are all small. Especially, this means that

$$\sin\theta \simeq \tan\theta \simeq \theta, \tag{1–10}$$

where θ represents any of the indicated rotation components measured in radians. The various displacement and rotation components have been illustrated in Fig. 1–5. The rotation component around the x-axis is known as the twist of the beam.

Now, a material point on the cross-section with the coordinates (x, y, z) in the referential state achieves a displacement vector $\mathbf{u} = \mathbf{u}(x, y, z)$ with the components $\{u_x, u_y, u_z\}$ in the (x, y, z)-coordinate system given as (see Fig. 1–5):

$$u_x(x, y, z) = w_x(x) + z\theta_y(x) - y\theta_z(x), \tag{1–11a}$$

$$u_y(x, y, z) = w_y(x) - z\theta_x(x), \tag{1–11b}$$

$$u_z(x, y, z) = w_z(x) + y\theta_x(x). \tag{1–11c}$$

It follows that the displacement of any material point is determined if only the 6 components of $\mathbf{w}(x)$ and $\boldsymbol{\theta}(x)$ are known at the beam coordinate x. Hence, the indicated kinematic constraint reduces the determination of the continuous displacement field $\mathbf{u} = \mathbf{u}(x, y, z)$ to the determination of the 6 deformation components $w_x = w_x(x)$, $w_y = w_y(x)$, $w_z = w_z(x)$, $\theta_x = \theta_x(x)$, $\theta_y = \theta_y(x)$ and $\theta_z = \theta_z(x)$ of a single spatial coordinate along the beam axis.

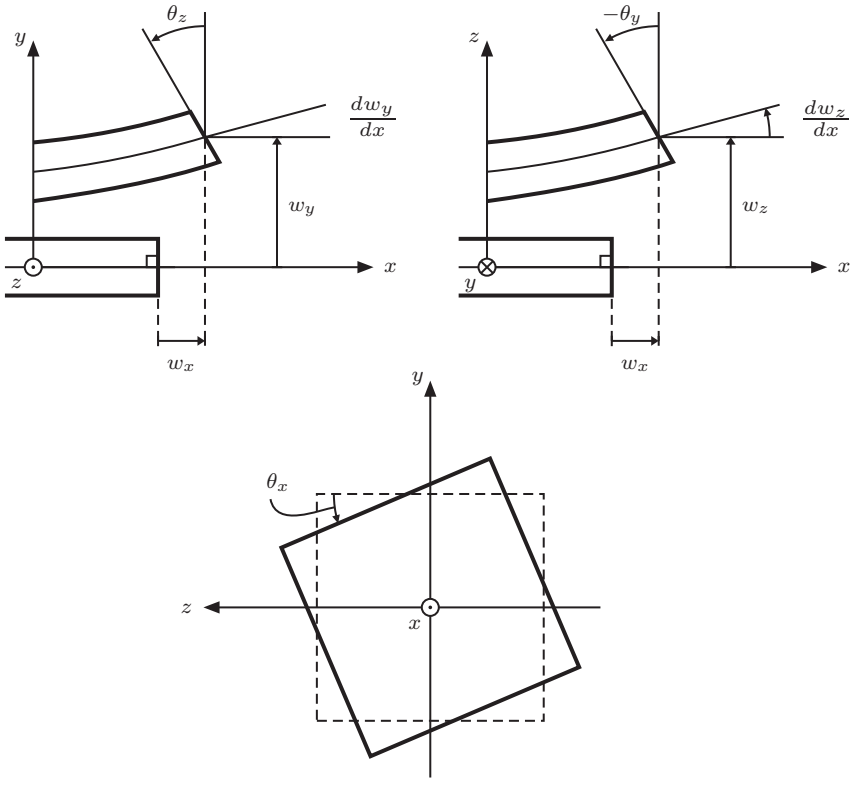

Figure 1–5 Deformation components in beam theory.

The strains conjugated to σ_{xx}, σ_{xy} and σ_{xz} are the axial strain ε_{xx} and the angular strains $\gamma_{xy} = 2\varepsilon_{xy}$ and $\gamma_{xz} = 2\varepsilon_{xz}$. They are related to displacement components as follows:

$$\varepsilon_{xx} = \frac{\partial u_x}{\partial x} = \frac{dw_x}{dx} + z\frac{d\theta_y}{dx} - y\frac{d\theta_z}{dx}, \tag{1–12a}$$

$$\gamma_{xy} = \frac{\partial u_x}{\partial y} + \frac{\partial u_y}{\partial x} = \frac{dw_y}{dx} - z\frac{d\theta_x}{dx} - \theta_z(x), \tag{1–12b}$$

$$\gamma_{xz} = \frac{\partial u_x}{\partial z} + \frac{\partial u_z}{\partial x} = \frac{dw_y}{dx} + y\frac{d\theta_x}{dx} + \theta_y(x). \tag{1–12c}$$

From Eq. (1–12) follows that $\gamma_{xy} = \gamma_{xy}(x, z)$ is independent of y as a consequence of the presumed plane deformation of the cross-section. Then, the shear stress $\sigma_{xy} = \sigma_{xy}(x, z)$ must also be constant over the cross-section. Especially, $\sigma_{xy} \neq 0$ at the upper and lower edge of the cross-section as illustrated in Fig. 1–6a. However, if the cylindrical surface is free of surface shear tractions, then $\sigma_{yx} = 0$ at the edge. Hence, $\sigma_{xy} \neq \sigma_{yx}$ in contradiction to Eq. (1–8). In reality $\sigma_{xy} = 0$ at the edges, corresponding to $\gamma_{xy} = 0$. This means that the deformed cross-section forms a right angle to the cylindrical surface as shown in Fig. 1–6b.

The displacement fields Eq. (1–11) are only correct for beams with cross-sections which are circular symmetric around the x-axis. In all other cross-sections, the torsional moment M_x will

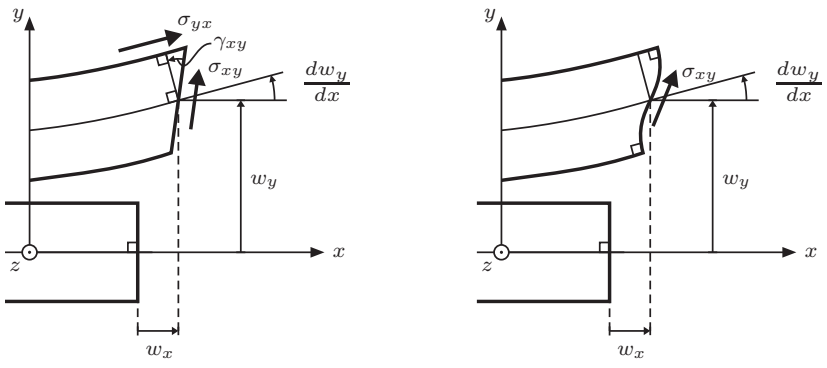

Figure 1–6 Shear stresses on deformed beam section: (a) Deformation of cross-section in beam theory and (b) real deformation of cross-section.

induce an additional non-planar displacement in the x-axis, which generally can be written in the form $u_x(x, y, z) = \omega(y, z)d\theta_x/dx$. This is illustrated in Fig. 1–7. Hence, the final expression for the axial displacement reads

$$u_x(x, y, z) = w_x(x) + z\theta_y(x) - y\theta_z(x) + \omega(y, z)\frac{d\theta_x}{dx}. \tag{1–13}$$

The expressions for u_y and u_z in Eq. (1–11) remain unchanged, and $\omega(y, z)$ is called the *warping function*. Whereas y and z in Eq. (1–13) may be considered as shape functions for the deformations caused by the rotations $\theta_z(x)$ and $\theta_y(x)$, the warping function is a shape function defining the axial deformation of the cross-section from the rotation component. The definition and determination of the warping function is considered in a subsequent section.

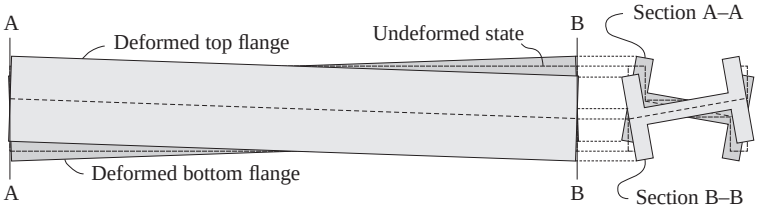

Figure 1–7 Warping deformations in an I-beam induced by homogeneous torsion. The cross sections A–A and B–B are shown with the top flange on the left and the bottom flange on the right.

As a consequence of the inclusion of the warping, the strain components in Eq. (1–12) are modified as follows:

$$\varepsilon_{xx} = \frac{\partial u_x}{\partial x} = \frac{dw_x}{dx} + z\frac{d\theta_y}{dx} - y\frac{d\theta_z}{dx} + \omega\frac{d^2\theta_x}{dx^2}, \tag{1–14a}$$

$$\gamma_{xy} = \frac{\partial u_x}{\partial y} + \frac{\partial u_y}{\partial x} = \frac{dw_y}{dx} - \theta_z + \left(\frac{\partial \omega}{\partial y} - z\right)\frac{d\theta_x}{dx}, \tag{1–14b}$$

$$\gamma_{xz} = \frac{\partial u_x}{\partial z} + \frac{\partial u_z}{\partial x} = \frac{dx_z}{dx} + \theta_y + \left(\frac{\partial \omega}{\partial z} + y\right)\frac{d\theta_x}{dx}. \tag{1–14c}$$

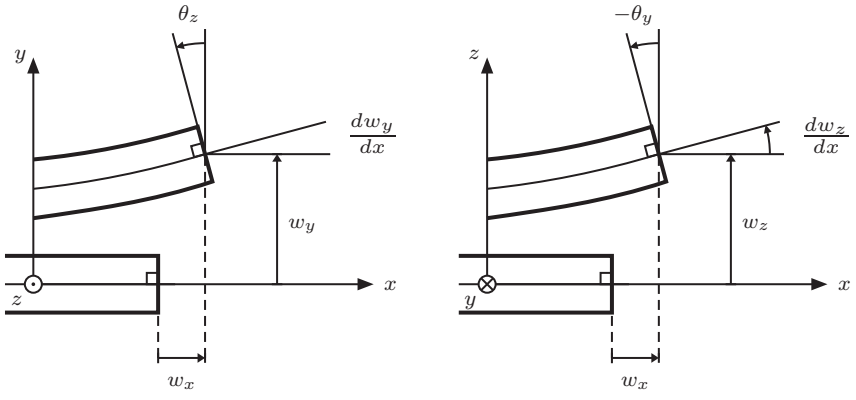

Figure 1–8 Kinematics of Bernoulli-Euler beam theory.

Bernoulli-Euler beam kinematics presumes that the rotated cross-section is always orthogonal to the deformed beam axis. This involves the following additional kinematical constraints on the deformation of the cross-section (see Fig. 1–8):

$$\theta_y = -\frac{dw_z}{dx}, \qquad \theta_z = \frac{dw_y}{dx}. \tag{1–15}$$

Assuming temporarily that $\theta_x \equiv 0$ in bending deformations, *i.e.* disregarding the twist of the beam, Eqs. (1–14) and (1–15) then provide:

$$\gamma_{xy} = \gamma_{xz} = 0. \tag{1–16}$$

Equation (1–16) implies that the shear stresses are $\sigma_{xy} = \sigma_{xz} = 0$, and in turn that the shear forces become $Q_y = Q_z = 0$, cf. Eq. (1–6). However, non-zero shear forces are indeed present in bending of Bernoulli-Euler beams. The apparent paradox is dissolved by noting that the shear forces in Bernoulli-Euler beam theory cannot be derived from the kinematic condition, but has to be determined from the static equations.

The development of the classical beam theory is associated with names like Galilei (1564–1642), Mariotte (1620–1684), Leibner (1646–1716), Jacob Bernoulli (1654–1705), Euler (1707–1783), Coulomb (1736–1806) and Navier (1785–1836), leading to the mentioned Bernoulli-Euler beam based on the indicated kinematic constraint. The inclusion of transverse shear deformation was proposed in 1859 by Bresse (1822–1883) and extended to dynamics in 1921 by Timoshenko (1878–1972). Due to this contribution, the resulting beam theory based on the strain relations Eq. (1–12), is referred to as Timoshenko beam theory (Timoshenko 1921).

The first correct analysis of torsion in beams was given by St. Venant (1855). The underlying assumption was that $d\theta_x/dx$ in Eq. (1–13) was constant, so the warping in all cross-sections become identical. Then, the axial strain ε_{xx} from torsion vanishes and the distribution of the shear strains γ_{xy} and γ_{xz} are identical in all sections. Because of this, St. Venant torsion is also referred to as *homogeneous torsion*.

Whenever the twist or the warping is prevented at one or more cross-sections, $d\theta_x/dx$ is no longer constant as a function of x. Hence, axial strains occur and, as a consequence of this, axial stresses arise and the shear strains and shear stresses are varying along the beam. These phenomena were systematically analysed by Vlasov (1961) for thin-walled beams, for which reason the resulting theory is referred to as *Vlasov torsion* or *non-homogeneous torsion*. Notice that the shear stresses from Vlasov torsion have not been included in the present formulation. These will be considered in a subsequent chapter.

Seen from an engineering point of view, the primary advantage of Vlasov torsion theory is that it explains a basic feature of beams, namely that *prevention of warping leads to a much stiffer structural elements* than achieved in the case of homogeneous warping, *i.e.* a given torsional moment will induce a smaller twist. Warping of the cross-section may, for example, be counteracted by the inclusion of a thick plate orthogonal to the beam axis and welded to the flanges and the web. The prevention of torsion in this manner is particularly useful in the case of slender beams with open thin-walled cross-sections that are prone to coupled flexural–torsional buckling. Obviously, Vlasov torsion theory must be applied for the analysis of such problems as discussed later in the book.

Next, the deformation of the cross-section may be decomposed into bending and shear components. The bending components are caused by the bending moments M_y and M_z and deform as a Bernoulli-Euler beam. Hence, the bending components are causing the rotations θ_y and θ_z of the cross-section. The shear components are caused by the shear forces Q_y and Q_z. These cause the angular shear strains γ_{xy} and γ_{xz} without rotating the cross-section. Further, the displacement of the beam axis in shear takes place without curvature. Hence, the curvature of the beam axis is strictly related to the bending components, see Fig. 1–9.

With reference to Fig. 1–10, the radii of curvatures r_y and r_z are related to the rotation increments $d\theta_z$ and $-d\theta_y$ of the end-sections in the bending deformations of a differential beam element of the length dx as follows

$$\left.\begin{array}{r} r_y d\theta_z = dx \\ \\ -r_z d\theta_y = dx \end{array}\right\} \quad \Rightarrow \quad \left\{\begin{array}{l} \kappa_y = -1/r_z = d\theta_y/dx \\ \\ \kappa_z = \quad 1/r_y = d\theta_z/dx \end{array}\right. \tag{1–17}$$

Here, κ_y and κ_z denote the components of the curvature vector $\boldsymbol{\kappa}$ of the x-axis. Especially, for a Bernoulli-Euler beam the curvature components become, cf. Eq. (1–15),

$$\kappa_y = -\frac{d^2 w_z}{dx^2}, \qquad \kappa_z = \frac{d^2 w_y}{dx^2}. \tag{1–18}$$

From Eqs. (1–14) and (1–17) follows that the axial strain may be written as

$$\varepsilon_{xx}(x,y,z) = \varepsilon(x) + z\kappa_y(x) - y\kappa_z(x) + \omega(y,z)\frac{d^2\theta_x}{dx^2}, \tag{1–19}$$

where $\varepsilon(x)$ denotes the axial strain of the beam along the x-axis given as

$$\varepsilon(x) = \frac{dw_x}{dx}. \tag{1–20}$$

Here, $\varepsilon(x)$, $\kappa_y(x)$ and $\kappa_y(x)$ define the axial strain and curvatures of the beam axis, *i.e.* the (x)-axis.

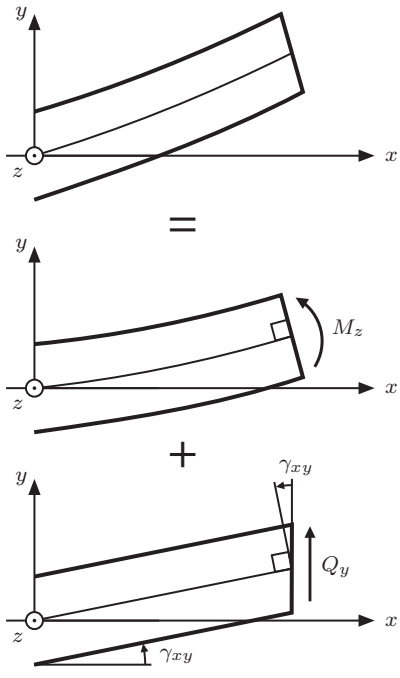

Figure 1–9 Decomposition of cross-section deformation into bending and shear components.

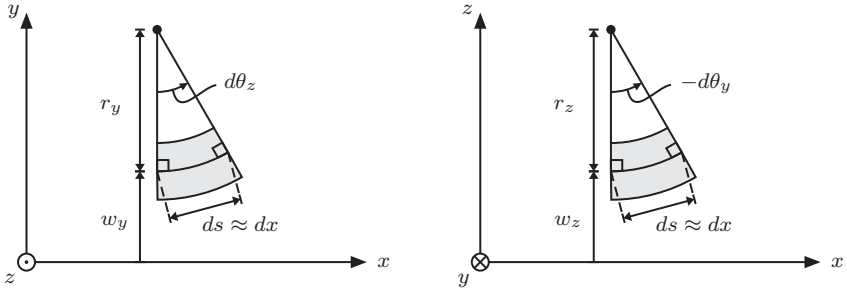

Figure 1–10 Definition of curvature.

1.2.3 Constitutive relations for an elastic beam

In what follows we shall refer to $N(x)$, $Q_y(x)$, $Q_z(x)$, $M_x(x)$, $M_y(x)$ and $M_z(x)$ as *generalised stresses*. These are stored in the column matrix

$$\boldsymbol{\sigma}(x) = \begin{bmatrix} N(x) \\ Q_y(x) \\ Q_z(x) \\ M_x(x) \\ M_y(x) \\ M_z(x) \end{bmatrix}. \tag{1–21}$$

The internal virtual work of these quantities per unit length of the beam is given as

$$\delta\omega = N\delta\varepsilon + Q_y\delta\gamma_{xy} + Q_z\delta\gamma_{xz} + M_x\delta\theta_x + M_y\delta\kappa_y + M_z\delta\kappa_z = \boldsymbol{\sigma}^T\delta\boldsymbol{\varepsilon}, \tag{1–22}$$

where

$$\boldsymbol{\varepsilon}(x) = \begin{bmatrix} \varepsilon(x) \\ \gamma_{xy}(x) \\ \gamma_{xz}(x) \\ \theta_x(x) \\ \kappa_y(x) \\ \kappa_z(x) \end{bmatrix}. \tag{1–23}$$

The components of $\boldsymbol{\varepsilon}(x)$ are referred to as the *generalised strains*. The components of $\boldsymbol{\sigma}(x)$ and $\boldsymbol{\varepsilon}(x)$ are said to be virtual work conjugated because these quantities define the internal virtual work per unit length of the beam.

Let E and G denote the elasticity modulus and the shear modulus. Then, the normal stress σ_{xx} and the shear stresses σ_{xy} and σ_{xz} may be calculated from Eq. (1–14) as follows:

$$\sigma_{xx} = E\varepsilon_{xx} = E\left(\frac{dw_x}{dx} + z\frac{d\theta_y}{dx} - y\frac{d\theta_z}{dx} + \omega(y,z)\frac{d^2\theta_x}{dx^2}\right), \tag{1–24a}$$

$$\sigma_{xy} = G\gamma_{xy} = G\left(\frac{dw_y}{dx} - \theta_z + \left(\frac{\partial\omega}{\partial y} - z\right)\frac{d\theta_x}{dx}\right), \tag{1–24b}$$

$$\sigma_{xz} = G\gamma_{xz} = G\left(\frac{dw_2}{dx} + \theta_y + \left(\frac{\partial\omega}{\partial z} + y\right)\frac{d\theta_x}{dx}\right). \tag{1–24c}$$

By integration over the cross-sectional area, it then follows that

$$N = E\left(A\frac{dw_x}{dx} + S_y\frac{d\theta_y}{dx} - S_z\frac{d\theta_2}{dx} + S_\omega\frac{d^2\theta_x}{dx^2}\right), \tag{1–25a}$$

$$Q_y = G\left(A_y\left(\frac{dw_y}{dx} - \theta_z\right) + R_y\frac{d\theta_x}{dx}\right), \tag{1–25b}$$

$$Q_z = G\left(A_z\left(\frac{dw_z}{dx} + \theta_y\right) + R_z\frac{d\theta_x}{dx}\right), \tag{1–25c}$$

$$M_x = G\left(S_z\left(\frac{dw_z}{dx} + \theta_y\right) - S_y\left(\frac{dw_y}{dx} - \theta_z\right) + K\frac{d\theta_x}{dx}\right), \tag{1–25d}$$

$$M_y = E\left(S_y\frac{dw_x}{dx} + I_{yy}\frac{d\theta_y}{dx} - I_{yz}\frac{d\theta_z}{dx} + I_{\omega z}\frac{d\theta_x}{dx}\right), \tag{1–25e}$$

$$M_z = E\left(-S_z\frac{dw_x}{dx} - I_{yz}\frac{d\theta_y}{dx} + I_{zz}\frac{d\theta_z}{dx} - I_{\omega y}\frac{d\theta_x}{dx}\right), \tag{1–25f}$$

where A_y, A_z, R_y, R_z, S_y, S_z, S_ω, K, I_{yy}, I_{zz}, $I_{yz} = I_{zy}$, $I_{\omega y}$ and $I_{\omega z}$ are cross-sectional (or geometrical) constants identified as:

$$A = \int_A dA, \qquad A_y = \alpha_y A, \qquad A_z = \alpha_z A, \tag{1–26a}$$

$$R_y = \int_A \left(\frac{\partial \omega}{\partial y} - z \right) dA, \qquad R_z = \int_A \left(\frac{\partial \omega}{\partial z} + y \right) dA, \tag{1–26b}$$

$$S_y = \int_A z dA, \qquad S_z = \int_A y dA, \qquad S_\omega = \int_A \omega dA, \tag{1–26c}$$

$$I_{yy} = \int_A z^2 dA, \qquad I_{zz} = \int_A y^2 dA, \tag{1–26d}$$

$$I_{yz} = \int_A yz dA, \qquad I_{\omega y} = \int_A \omega y dA, \qquad I_{\omega z} = \int_A \omega z dA, \tag{1–26e}$$

$$K = \int_A \left(y^2 + z^2 + y \frac{\partial \omega}{\partial z} - z \frac{\partial \omega}{\partial y} \right) dA. \tag{1–26f}$$

Here, A is the cross-sectional area, whereas A_y and A_z signify the so-called shear areas. Beam theory presumes a constant variation of the shear stresses in bending, whereas the actual variation is at least quadratic. The constant variation results in an overestimation of the stiffness against shear deformations, which is compensated by the indicated shear reduction factors α_y and α_z. If the actual distribution of the shear stresses is parabolic, these factors become $\alpha_y = \alpha_z = 5/6$. For an I-profile, the shear area is approximately equal to the web area.

For $GA_y \to \infty$ we have $\gamma_{xy} = Q_y/(GA_y) = 0$. Bernoulli-Euler beam theory is characterised by $\gamma_{xy} = 0$. Hence, Timoshenko theory must converge towards Bernoulli-Euler theory for the shear areas passing towards infinity. The magnitude of the shear deformations in proportion to the bending deformations depends on the quantity $(h/l)^2$, where h is the height and l is the length of the beam. This relation is illustrated in Example 1-3.

R_y and R_z are section constants which depend on the warping mode shape $\omega(y, z)$ as well as the bending modes via y and z. Further, the section constants S_y and S_z are denoted the static moments around the y- and z-axes. S_ω specifies a corresponding static moment of the warping shape function.

I_{yy} and I_{zz} signify the *bending moments of inertia* around the y- and z-axes, respectively. I_{yz} is denoted the *centrifugal moment of inertia*, whereas $I_{\omega y}$ and $I_{\omega z}$ are the corresponding *centrifugal moments of the warping* shape function and the bending mode shapes.

K is the so-called *torsion constant*. This defines merely the torsional stiffness in St. Venant torsion. As mentioned above, the additional contribution to M_x from Vlasov torsion will be considered in a subsequent section.

1.3 Differential equations of equilibrium for beams

In what follows, the governing differential equations for Timoshenko and Bernoulli-Euler beams are derived. At this stage, the twist θ_x and the torsional moment M_x are ignored. With no further assumptions and simplifications, Eq. (1–25) reduces to

$$\begin{bmatrix} N \\ M_y \\ M_z \\ Q_y \\ Q_z \end{bmatrix} = \begin{bmatrix} EA & -ES_y & -ES_z & 0 & 0 \\ ES_y & EI_{yy} & -EI_{yz} & 0 & 0 \\ -ES_z & -EI_{yz} & EI_{zz} & 0 & 0 \\ 0 & 0 & 0 & GA_y & 0 \\ 0 & 0 & 0 & 0 & GA_z \end{bmatrix} \begin{bmatrix} dw_x/dx \\ d\theta_y/dx \\ d\theta_z/dx \\ dw_y/dx - \theta_z \\ dw_z/dx + \theta_y \end{bmatrix}. \tag{1–27}$$

The coefficient matrix of Eq. (1–27) is symmetric. When formulated in a similar matrix format, the corresponding matrix in Eq. (1–25) is not symmetric. This is a consequence of the ignorance of the Vlasov torsion in M_x.

1.3.1 Governing equations for a Timoshenko beam

Next, Eq. (1–27) is inserted into the equilibrium equations (1–4a) and (1–4b), which results in the following system of coupled ordinary differential equations for the determination of w_x, w_y, w_z, θ_y and θ_z:

$$\begin{bmatrix} dN/dx \\ dM_y/dx \\ dM_z/dx \\ dQ_y/dx \\ dQ_z/dx \end{bmatrix} = \begin{bmatrix} 0 \\ Q_z \\ -Q_y \\ 0 \\ 0 \end{bmatrix} - \begin{bmatrix} q_x \\ m_y \\ m_z \\ q_y \\ q_z \end{bmatrix} \Rightarrow$$

$$\frac{d}{dx}\left(\begin{bmatrix} EA & ES_y & -ES_z & 0 & 0 \\ ES_y & EI_{yy} & -EI_{yz} & 0 & 0 \\ -ES_z & -EI_{yz} & EI_{zz} & 0 & 0 \\ 0 & 0 & 0 & GA_y & 0 \\ 0 & 0 & 0 & 0 & GA_z \end{bmatrix} \begin{bmatrix} dw_x/dx \\ d\theta_y/dx \\ d\theta_z/dx \\ dw_y/dx - \theta_z \\ dw_z/dx + \theta_y \end{bmatrix} \right)$$
$$= \begin{bmatrix} 0 & 0 & 0 & 0 & 0 \\ 0 & 0 & 0 & 0 & GA_z \\ 0 & 0 & 0 & -GA_y & 0 \\ 0 & 0 & 0 & 0 & 0 \\ 0 & 0 & 0 & 0 & 0 \end{bmatrix} \begin{bmatrix} dw_x/dx \\ d\theta_y/dx \\ d\theta_z/dx \\ d\theta_z/dx - \theta_z \\ dw_z/dx + \theta_y \end{bmatrix} - \begin{bmatrix} q_x \\ m_y \\ m_z \\ q_y \\ q_z \end{bmatrix}. \qquad (1\text{–}28)$$

Equation (1–28) specifies the differential equations for Timoshenko beam theory. These should be solved with proper boundary condition at the end-sections of the beam. Let x_0 denote the abscissa of any of the two end-sections, *i.e.* $x_0 = 0$ or $x_0 = l$, where l is the length of the beam. At $x = x_0$ either kinematical or mechanical boundary conditions may be prescribed.

Kinematical boundary conditions mean that values of w_x, w_y, w_z, θ_y and θ_z are prescribed,

$$\left.\begin{array}{rcl} w_x(x_0) & = & w_{x,0} \\ w_y(x_0) & = & w_{y,0} \\ w_z(x_0) & = & w_{z,0} \\ \theta_y(x_0) & = & \theta_{y,0} \\ \theta_z(x_0) & = & \theta_{z,0} \end{array}\right\}, \qquad x_0 = 0, l, \qquad (1\text{–}29)$$

whereas mechanical boundary conditions imply the prescription of N, Q_y, Q_z, M_y and M_z,

$$\left.\begin{array}{rcl} N(x_0) & = & N_0 \\ Q_y(x_0) & = & Q_{y,0} \\ Q_z(x_0) & = & Q_{z,0} \\ M_y(x_0) & = & M_{y,0} \\ M_z(x_0) & = & M_{z,0} \end{array}\right\}, \qquad x_0 = 0, l. \qquad (1\text{–}30)$$

In Eq. (1–30), the left-hand sides are expressed in kinematical quantities by means of Eq. (1–27). Of the 10 possible boundary conditions at $x = x_0$ specified by Eqs. (1–35) and (1–30), only 5 can be specified. The 5 boundary conditions at $x_0 = 0$ and $x_0 = l$ can be selected independently from Eq. (1–35) and Eq. (1–30).

With given boundary conditions Eq. (1–28) can be solved uniquely for the 5 kinematic quantities w_x, w_y, w_z, θ_y, θ_z, which make up the degrees of freedom of the cross-section. Although an analytical solution may be cumbersome, a numerical integration is always within reach.

1.3.2 Governing equations for a Bernoulli-Euler beam

Next, similar differential equations are specified for a Bernoulli-Euler beam. At first the shear forces Q_y and Q_z in the equations of equilibrium for M_y and M_z in Eq. (1–4b) are eliminated by means of the 2nd and 3rd equations in Eq. (1–4a):

$$\left.\begin{array}{l} d^2M_y/dx^2 - dQ_z/dx + dm_y/dx = 0 \\ \\ d^2M_z/dx^2 + dQ_y/dx + dm_z/dx = 0 \end{array}\right\} \Rightarrow \left\{\begin{array}{l} d^2M_y/dx^2 + q_z + dm_y/dx = 0 \\ \\ d^2M_z/dx^2 - q_y + dm_z/dx = 0. \end{array}\right. \tag{1–31}$$

Using the Bernoulli-Euler kinematical constraint Eq. (1–15), the constitutive equations for the resulting section forces may be written as

$$\begin{bmatrix} N \\ M_y \\ M_z \end{bmatrix} = \begin{bmatrix} EA & ES_y & -ES_z \\ ES_y & EI_{yy} & -EI_{yz} \\ -ES_{zz} & -EI_{yz} & EI_{zz} \end{bmatrix} \begin{bmatrix} dw_x/dx \\ -d^2w_z/dx^2 \\ d^2w_y/dx^2 \end{bmatrix}. \tag{1–32}$$

Then, the equations of equilibrium Eq. (1–4a) and Eq. (1–31) may be recasted as the following system of coupled ordinary differential equations

$$\frac{d}{dx}\left(EA\frac{dw_x}{dx} - ES_y\frac{d^2w_z}{dx^2} - ES_z\frac{d^2w_y}{dx^2}\right) + q_x = 0, \tag{1–33a}$$

$$\frac{d^2}{dx^2}\left(ES_y\frac{dw_x}{dx} - EI_{yy}\frac{d^2w_z}{dx^2} - EI_{yz}\frac{d^2w_y}{dx^2}\right) + q_z + \frac{dm_y}{dx} = 0, \tag{1–33b}$$

$$\frac{d^2}{dx^2}\left(-ES_z\frac{dw_x}{dx} + EI_{yz}\frac{d^2w_z}{dx^2} + EI_{zz}\frac{d^2w_y}{dx^2}\right) + q_y + \frac{dm_z}{dx} = 0. \tag{1–33c}$$

The governing equations (1–33) should be solved with 5 of the same boundary conditions as indicated by Eqs. (1–35) and (1–30). The difference is that $\theta_y(x_0)$, $\theta_z(x_0)$, $Q_y(x_0)$ and $Q_z(x_0)$ are represented as, cf. Eqs. (1–4b) and (1–15),

$$-\frac{dw_z(x_0)}{dx} = \theta_{y,0}, \qquad \frac{dw_z(x_0)}{dx} = \theta_{z,0}, \tag{1–34a}$$

$$-\frac{dM_z(x_0)}{dx} - m_z(x_0) = Q_{y,0}, \qquad \frac{dM_y(x_0)}{dx} + m_y(x_0) = Q_{z,0}. \tag{1–34b}$$

With this in mind, the kinematic boundary conditions for Bernoulli-Euler beams are given in the form

$$\left.\begin{array}{rcl} w_x(x_0) & = & w_{x,0} \\ w_y(x_0) & = & w_{y,0} \\ w_z(x_0) & = & w_{z,0} \\ dw_z(x_0)/dx & = & \theta_{y,0} \\ dw_y(x_0)/dx & = & \theta_{z,0} \end{array}\right\}, \qquad x_0 = 0, l, \tag{1–35}$$

whereas the mechanical boundary conditions defined in Eq. (1–30) are still valid.

1.4 Uncoupling of axial and bending deformations

Up to now the position of the origin O and the orientation of the y- and z-axes in the cross-section have been chosen arbitrarily. As a consequence of this, the deformations from the axial force and the deformation from the bending moments M_y and M_z will generally be coupled. This means that the axial force N referred to the origin O will not merely induce a uniform displacement w_x of the cross-section, but also non-zero displacements w_y and w_z of O as well as rotations θ_y and θ_z. Similarly, the bending moment M_y will not merely cause a displacement w_y and a rotation θ_y of the cross-section, but also a non-zero displacement w_y and a rotation θ_z in the orthogonal direction in addition to an axial displacement w_y of the origin. The indicated mechanical couplings are the reason for the couplings in the differential equations (1–28) and (1–33). The couplings may have a significant impact on the structural behaviour and stability of an engineering structure and the position of the origin for a given beam element as well as the orientation of the coordinate axes must be implemented correctly in a computational model.

In this section, two coordinate transformations will be indicated, in which the axial force referred to the new origin B, called the *bending centre*, only induces a uniform axial displacement over the cross-section. Similarly, the bending moments M_y and M_z around the new rotated y- and z-axes, referred to as the *principal axes*, will only induce the non-zero deformation components (w_z, θ_y) and (w_y, θ_z), respectively. Especially, the moments will induce the displacement $w_x = 0$ of the bending centre, B.

1.4.1 Determination of the bending centre

The position of the bending centre B is given by the position vector $\mathbf{r}_B$ with the components $\{0, y_B, z_B\}$ in the (x, y, z)-coordinate system. In order to determine the components y_B and z_B, a translation of the (x, y, z)-coordinate system to a new (x', y', z')-coordinate system with origin in the yet unknown bending centre is performed (see Fig. 1–11). The relations between the new and the old coordinates read

$$x = x', \qquad y = y' + y_B, \qquad z = z' + z_B, \tag{1–36}$$

In the new coordinate system, the displacement of B (the new origin) in the x'-direction (the new beam axis) becomes (see Fig. 1–11):

$$w'_x = w_x + z_B\theta_y - y_B\theta_z. \tag{1–37}$$

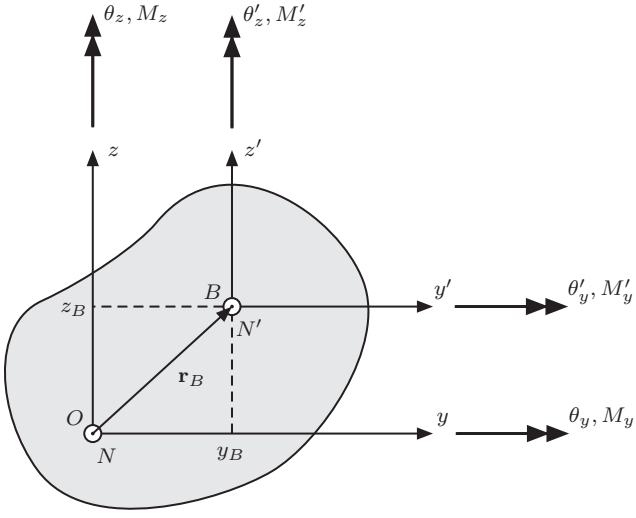

Figure 1–11 Translation of coordinate system.

The axial strain of fibres placed on the new beam axis becomes

$$\varepsilon'(x') = \frac{dw'}{dx'} = \frac{dw'}{dx} = \varepsilon + z_B\kappa_y - y_B\kappa_z, \tag{1–38}$$

where Eq. (1–17), Eq. (1–20) and Eq. (1–37) have been used. The components of the rotation vector $\boldsymbol{\theta}$ of the cross-section are identical, *i.e.*

$$\theta'_x = \theta_x, \qquad \theta'_y = \theta_y, \qquad \theta'_z = \theta_z. \tag{1–39}$$

In turn, this means that the components of the curvature vector $\boldsymbol{\kappa}$ in the two coordinate systems are identical as well

$$\kappa'_y = \frac{d\theta'_y}{dx'} = \frac{d\theta_y}{dx} = \kappa_y, \qquad \kappa'_z = \frac{d\theta'_z}{dx'} = \frac{d\theta_z}{dx} = \kappa_z. \tag{1–40}$$

Further, the components of the section force vector $\mathbf{F}$ in the two coordinate systems become identical, *i.e.*

$$N' = N, \qquad Q'_y = Q_y \qquad Q'_z = Q_z. \tag{1–41}$$

As a consequence of referring the axial force $N = N'$ to the new origin B, the components of the section vector in the (x', y', z')-coordinate system are related to the components in the (x, y, z)-coordinate as follows:

$$M'_x = M_x, \quad M'_y = M_y - z_B N, \quad M'_z = M_z + y_B N. \tag{1–42}$$

Equations (1–38) and (1–40) provide the following relation for ε in terms of ε', κ'_y and κ_z:

$$\varepsilon = \varepsilon' - z_B\kappa_y + y_B\kappa_z = \varepsilon' - z_B\kappa'_y + y_B\kappa'_z. \tag{1–43}$$

Then the relation between $\{N, M_y, M_z\}$ and $\{N', M'_y, M'_z\}$ and $\{\varepsilon, \kappa_y, \kappa_z\}$ and $\{\varepsilon', \kappa'_y, \kappa_z\}$ may be specified in the following matrix formulation:

$$\boldsymbol{\sigma}' = \mathbf{A}^T \boldsymbol{\sigma}, \tag{1–44a}$$

$$\boldsymbol{\varepsilon} = \mathbf{A} \boldsymbol{\varepsilon}', \tag{1–44b}$$

where

$$\boldsymbol{\sigma} = \begin{bmatrix} N \\ M_y \\ M_z \end{bmatrix}, \qquad \boldsymbol{\varepsilon} = \begin{bmatrix} \varepsilon \\ \kappa_y \\ \kappa_z \end{bmatrix}, \tag{1–45a}$$

$$\boldsymbol{\sigma}' = \begin{bmatrix} N' \\ M'_y \\ M'_z \end{bmatrix}, \qquad \boldsymbol{\varepsilon}' = \begin{bmatrix} \varepsilon' \\ \kappa'_y \\ \kappa'_y \end{bmatrix}, \tag{1–45b}$$

$$\mathbf{A} = \begin{bmatrix} 1 & -z_B & y_B \\ 0 & 1 & 0 \\ 0 & 0 & 1 \end{bmatrix}. \tag{1–45c}$$

The components $\{N, M_y, M_z\}$ and $\{\varepsilon, \kappa_y, \kappa_z\}$ of $\boldsymbol{\sigma}$ and $\boldsymbol{\varepsilon}$ may be interpreted as work conjugated generalised stresses and strains.

With reference to Eq. (1–32), the constitutive relation between $\boldsymbol{\sigma}$ and $\boldsymbol{\varepsilon}$ is given as

$$\boldsymbol{\sigma} = \mathbf{C} \boldsymbol{\varepsilon}, \tag{1–46}$$

where $\mathbf{C}$ denotes the constitutive matrix,

$$\mathbf{C} = E \begin{bmatrix} A & S_y & -S_z \\ S_y & I_{yy} & -I_{yz} \\ -S_z & -I_{yz} & I_{zz} \end{bmatrix}. \tag{1–47}$$

Likewise, the constitutive relation in the (x', y', z')-coordinate system reads

$$\boldsymbol{\sigma}' = \mathbf{C}' \boldsymbol{\varepsilon}' \tag{1–48}$$

where the constitutive matrix has the form

$$\mathbf{C}' = E \begin{bmatrix} A & S_{y'} & -S_{z'} \\ S_{y'} & I_{y'y'} & -I_{y'z'} \\ -S_{z'} & -I_{y'z'} & I_{z'z'} \end{bmatrix}. \tag{1–49}$$

Obviously, as given by Eqs. (1–47) and (1–49), the cross-sectional area A is invariant to a rotation of the cross-section about the x-axis and a translation in the y- and z-directions.

From Eqs. (1–44a), (1–44b) and (1–46) follows that

$$\boldsymbol{\sigma}' = \mathbf{A}^T \mathbf{C} \boldsymbol{\varepsilon} = \mathbf{A}^T \mathbf{C} \mathbf{A} \boldsymbol{\varepsilon}' \qquad \Rightarrow$$

$$\mathbf{C}' = \mathbf{A}^T \mathbf{C} \mathbf{A} = E \begin{bmatrix} 1 & 0 & 0 \\ -z_B & 1 & 0 \\ y_B & 0 & 1 \end{bmatrix} \begin{bmatrix} A & S_y & -S_z \\ S_y & I_{yy} & -I_{yz} \\ -S_z & -I_{yz} & I_{zz} \end{bmatrix} \begin{bmatrix} 1 & -z_B & y_B \\ 0 & 1 & 0 \\ 0 & 0 & 1 \end{bmatrix} \qquad \Rightarrow$$

$$\mathbf{C}' = E \begin{bmatrix} A & S_y - z_B A & -(S_z - y_B A) \\ S_y - z_B A & I_{yy} - 2z_B S_y + z_B^2 A & -I_{yz} + y_B S_y + z_B(S_z - y_B A) \\ -(S_z - y_B A) & -I_{yz} + y_B S_y + z_B(S_z - y_B A) & I_{zz} - 2y_B S_z + y_B^2 A \end{bmatrix}. \tag{1–50}$$

The idea is now to use the translational coordinate transformation to uncouple the axial deformations from the bending deformations. This requires that $S_{y'} = S_{z'} = 0$. Upon comparison of Eq. (1–49) and Eq. (1–50), this provides the following relations for the deformation of the coordinates of the bending centre:

$$y_B = \frac{S_z}{A}, \qquad z_B = \frac{S_y}{A}. \tag{1–51}$$

With y_B and z_B given by Eq. (1–51), the bending moments of inertia, $I_{y'y'}$ and $I_{z'z'}$, and the centrifugal moment of inertia, $I_{y'z'}$, in the new coordinate system can be expressed in terms of the corresponding quantities in the old coordinate system as follows:

$$I_{y'y'} = I_{yy} - 2z_B(Az_B) + z_B^2 A = I_{yy} - z_B^2 A, \tag{1–52a}$$

$$I_{z'z'} = I_{zz} - 2y_B(Ay_B) + y_B^2 A = I_{zz} - y_B^2 A, \tag{1–52b}$$

$$I_{y'z'} = I_{yz} - y_B(Az_B) - z_B(Ay_B) + y_B z_B A = I_{yz} - y_B z_B A. \tag{1–52c}$$

The final results in Eq. (1–52) are known as *König's theorem*.

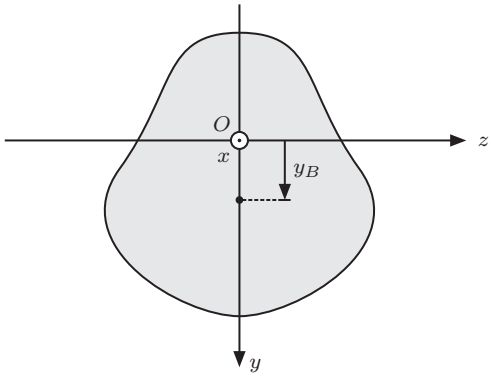

Figure 1–12 Single-symmetric cross-section.

If the cross-section is symmetric around a single line, and the y-axis is placed so that it coincides with this line of symmetry, then the static moment S_y vanishes, *i.e.*

$$S_y = \int_A z dA = 0 \tag{1–53}$$

As a result of this, the bending centre B will always be located on the line of symmetry in a single-symmetric cross-section, see Fig. 1–12. Obviously, if the cross-section is double symmetric, then the position of B is found at the intersection of the two lines of symmetry.

Example 1.1 Determination of bending and centrifugal moments of inertia of non-symmetric thin-walled cross-section

The position of the bending centre of the cross-section shown in Fig. A is determined along with the bending moments of inertia $I_{y'y'}$ and $I_{z'z'}$ and the centrifugal moment of inertia $I_{y'z'}$.

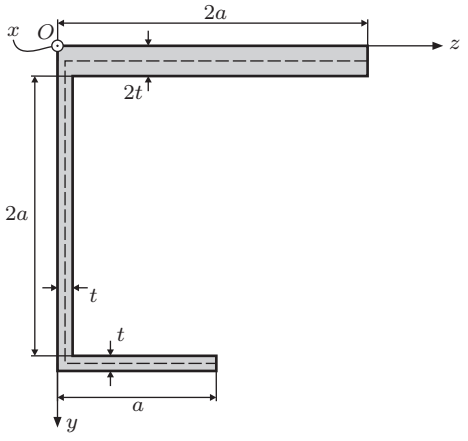

Figure A Thin-walled cross-section.

The (x, y, z)-coordinate system is placed as shown in Fig. A. Then, the following cross-sectional constants are calculated:

$$A = 2a \cdot 2t + 2a \cdot t + a \cdot t = 7at, \tag{a}$$

$$S_y = 2a \cdot 2t \cdot a + 2a \cdot t \cdot \frac{t}{2} + a \cdot t \cdot \frac{a}{2} = \frac{1}{2}(2t + 9a) + ta, \tag{b}$$

$$S_z = 2a \cdot 2t \cdot t + 2a \cdot t \cdot (2t + a) + a \cdot t \cdot \left(2t + 2a + \frac{t}{2}\right) = \frac{1}{2}(21t + 8a)ta, \tag{c}$$

$$I_{yy} = \frac{1}{3} \cdot 2t \cdot (2a)^3 + \frac{1}{3} \cdot 2a \cdot t^3 + \frac{1}{3} \cdot t \cdot a^3 = \frac{1}{3}\left(2t^2 + 17a^2\right) ta, \tag{d}$$

$$I_{zz} = \frac{1}{3} \cdot 2a \cdot 2a \cdot (2t)^3 + \frac{1}{12}(2a)^3 \cdot t + 2a \cdot t \cdot (2t + a)^2 + \frac{1}{12} \cdot a \cdot t^3 + a \cdot t \cdot \left(2t + 2a + \frac{t}{2}\right)^2$$
$$= \frac{1}{3}\left(59t^2 + 54ta + 20a^2\right) ta, \tag{e}$$

$$I_{yz} = 2a \cdot 2t \cdot t \cdot a + 2a \cdot t \cdot (2t + a) \cdot \frac{1}{2} + a \cdot t \cdot \left(2t + 2a + \frac{t}{2}\right) \cdot \frac{a}{2} = \frac{1}{4}\left(8t^2 + 25ta + 4a^2\right) ta. \tag{f}$$

Here, use has been made of König's theorem at the calculation of contributions to I_{yy}, I_{zz} and I_{yz} from the three rectangles forming the cross-section.

The coordinates of the bending centre follow from Eq. (1–51) and Eqs. (a) to (c). Thus,

$$y_B = \frac{S_z}{A} = \frac{3}{2}t + \frac{4}{7}a, \qquad z_B = \frac{S_y}{A} = \frac{1}{7}t + \frac{9}{14}a. \tag{g}$$

(continued)

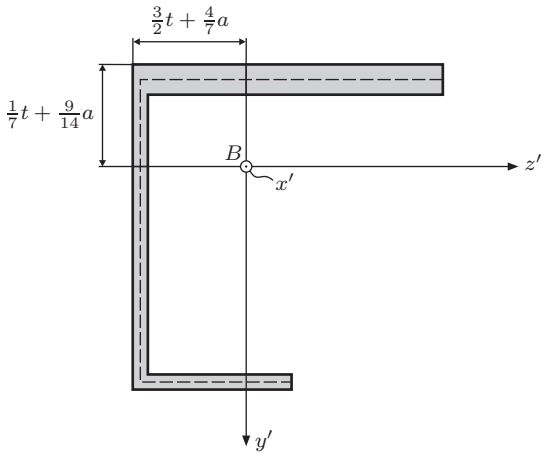

Figure B Position of bending centre in the thin-walled cross-section.

Subsequently, the moments of inertia around the axes of the (x', y', z')-coordinate system follow from Eq. (1–52), Eq. (1–53) and Eqs. (d) to (f):

$$I_{y'y'} = \frac{1}{3}(2t^2 + 17a^2)ta - \left(\frac{1}{7}t + \frac{9}{14}a\right)^2 \cdot 7ta = \frac{1}{84}(44t^2 - 108ta + 233a^2)ta, \tag{h}$$

$$I_{z'z'} = \frac{1}{3}(59t^2 + 54ta + 20a^2)ta - \left(\frac{3}{2}t + \frac{4}{7}a\right)^2 \cdot 7ta = \frac{1}{84}(329t^2 + 504ta + 368a^2)ta, \tag{i}$$

$$I_{y'z'} = \frac{1}{4}(8t^2 + 25ta + 4a^2)ta - \left(\frac{1}{7}t + \frac{9}{14}a)\right)\left(\frac{3}{2}t + \frac{4}{7}a\right) \cdot 7ta = \frac{1}{14}(7t^2 - 15ta - 22a^2)ta. \tag{j}$$

Now, for a thin-walled cross-section the thickness of the flanges and the web is much smaller than the widths of the flanges and the height of the web. In the present case this means that $t \ll a$. With this in mind, Eqs. (g) to (j) reduce to

$$y_B \simeq \frac{4}{7}a, \qquad z_B \simeq \frac{9}{14}a \tag{k}$$

and

$$I_{y'y'} \simeq \frac{233}{84}ta^3, \qquad I_{z'z'} \simeq \frac{92}{21}ta^3, \qquad I_{y'z'} \simeq -\frac{11}{7}ta^3. \tag{l}$$

It is noted that the error on $I_{z'z'}$ estimated by Eq. (l) increases rapidly with increasing values of t/a. Thus, for $t/a = 0.1$, the error is about 13%. The errors related to the estimated values of $I_{y'y'}$ and $I_{y'z'}$ are somewhat smaller, *i.e.* about 5% and 7%, respectively. □

From now on, the origin of the (x, y, z)-coordinate system is placed at the bending centre. Then, the constitutive matrix given by Eq. (1–47) takes the form

$$\mathbf{C} = E \begin{bmatrix} A & 0 & 0 \\ 0 & I_{yy} & -I_{yz} \\ 0 & -I_{yz} & I_{zz} \end{bmatrix}. \tag{1–54}$$

As a result of this, an axial force N no longer induces deformations in the y- and z-directions, and the bending moments M_y and M_z do not induce axial displacements. However, the bending moment M_y will still induce displacements in the y-direction in addition to the expected displacements in the z-direction. Similarly, the bending moment M_z induces displacements in both the y- and z-directions.

1.4.2 Determination of the principal axes

In order to uncouple the bending deformations, so that M_y will only induce deformations in the z-direction, and M_z only deformations in the y-direction, a new (x', y', z')-coordinate system is introduced with origin in B and rotated the angle φ around the x-axis as shown in Fig. 1–13.

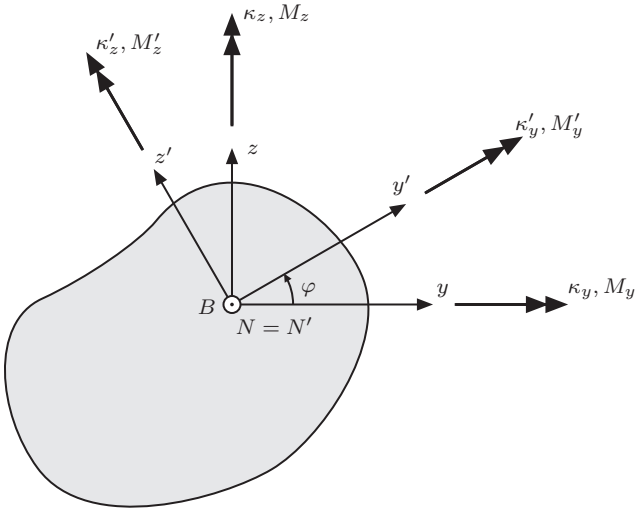

Figure 1–13 Rotation of coordinate system.

Let $\{N, M_y, M_z\}$ and $\{N', M_y', M_z'\}$ denote the components of the generalised stresses in the (x, y, z)-coordinate system and the (x', y', z')-coordinate system, respectively. The two sets of generalised stresses are related as

$$\boldsymbol{\sigma} = \mathbf{B}\boldsymbol{\sigma}', \tag{1–55a}$$

where

$$\boldsymbol{\sigma}' = \begin{bmatrix} N' \\ M_y' \\ M_z' \end{bmatrix}, \qquad \boldsymbol{\sigma} = \begin{bmatrix} N \\ M_y \\ M_z \end{bmatrix}, \qquad \mathbf{B} = \begin{bmatrix} 1 & 0 & 0 \\ 0 & \cos\varphi & -\sin\varphi \\ 0 & \sin\varphi & \cos\varphi \end{bmatrix}. \tag{1–55b}$$

Likewise, the components of the generalised strains in the two coordinate systems are denoted as $\{\varepsilon', \kappa_y', \kappa_z'\}$ and $\{\varepsilon, \kappa_y, \kappa_z\}$, respectively. These are related as

$$\boldsymbol{\varepsilon} = \mathbf{B}\boldsymbol{\varepsilon}', \tag{1–56a}$$

where

$$\boldsymbol{\varepsilon}' = \begin{bmatrix} \varepsilon' \\ \kappa_y' \\ \kappa_z' \end{bmatrix}, \qquad \boldsymbol{\varepsilon} = \begin{bmatrix} \varepsilon \\ \kappa_y \\ \kappa_z \end{bmatrix}, \qquad \mathbf{B} = \begin{bmatrix} 1 & 0 & 0 \\ 0 & \cos\varphi & -\sin\varphi \\ 0 & \sin\varphi & \cos\varphi \end{bmatrix}. \tag{1–56b}$$

The constitutive relation in the (x', y', z')-coordinate system reads

$$\boldsymbol{\sigma}' = \mathbf{C}'\boldsymbol{\varepsilon}', \qquad \mathbf{C}' = E \begin{bmatrix} A & 0 & 0 \\ 0 & I_{y'y'} & -I_{y'z'} \\ 0 & -I_{y'z'} & I_{z'z'} \end{bmatrix}. \tag{1–57}$$

The corresponding constitutive relation in the (x, y, z)-coordinate system is given by Eq. (1–46) with $\mathbf{C}$ given by Eq. (1–54). Use of Eqs. (1–55a) and (1–56a) in Eq. (1–46) provides

$$\mathbf{B}\boldsymbol{\sigma}' = \mathbf{C}\boldsymbol{\varepsilon} = \mathbf{C}\mathbf{B}\boldsymbol{\varepsilon}' \qquad \Rightarrow \qquad \boldsymbol{\sigma}' = \mathbf{B}^T\mathbf{C}\mathbf{B}\boldsymbol{\varepsilon}', \tag{1–58}$$

where it has been utilised that $\mathbf{B}^{-1} = \mathbf{B}^T$. Comparison of Eq. (1–57) and Eq. (1–58) leads the following relation between the constitutive matrices

$$\begin{aligned} \mathbf{C}' &= \mathbf{B}^T\mathbf{C}\mathbf{B} \\ &= E \begin{bmatrix} 1 & 0 & 0 \\ 0 & \cos\varphi & \sin\varphi \\ 0 & -\sin\varphi & \cos\varphi \end{bmatrix} \begin{bmatrix} A & 0 & 0 \\ 0 & I_{yy} & -I_{yz} \\ 0 & -I_{yz} & I_{zz} \end{bmatrix} \begin{bmatrix} 1 & 0 & 0 \\ 0 & \cos\varphi & -\sin\varphi \\ 0 & \sin\varphi & \cos\varphi \end{bmatrix} \\ &= E \begin{bmatrix} A & 0 & 0 \\ 0 & C_{22}' & C_{23}' \\ 0 & C_{32}' & C_{33}' \end{bmatrix}. \end{aligned} \tag{1–59a}$$

where

$$C_{22}' = \cos^2\varphi I_{yy} - 2\cos\varphi\sin\varphi I_{yz} + \sin^2\varphi I_{zz}, \tag{1–59b}$$

$$C_{23}' = C_{32}' = -\sin\varphi\cos\varphi(I_{yy} - I_{zz}) - (\cos^2\varphi - \sin^2\varphi)I_{yz}, \tag{1–59c}$$

$$C_{33}' = \cos^2\varphi I_{zz} + 2\cos\varphi\sin\varphi I_{yz} + \sin^2\varphi I_{zz}. \tag{1–59d}$$

From Eq. (1–57) and Eq. (1–59) follows that

$$I_{y'y'} = \frac{1}{2}(I_{yy} + I_{zz}) + \frac{1}{2}(I_{yy} - I_{zz})\cos(2\varphi) - I_{yz}\sin(2\varphi), \tag{1–60a}$$

$$I_{y'z'} = -\frac{1}{2}\sin(2\varphi)(I_{yy} - I_{zz}) - \cos(2\varphi)I_{yz}, \tag{1–60b}$$

$$I_{z'z'} = \frac{1}{2}(I_{yy} + I_{zz}) - \frac{1}{2}(I_{yy} - I_{zz})\cos(2\varphi) + I_{yz}\sin(2\varphi), \tag{1–60c}$$

where use has been made of the relations

$$\sin(2\varphi) = 2\sin\varphi\cos\varphi, \qquad \cos(2\varphi) = \cos^2\varphi - \sin^2\varphi,$$

$$\cos^2\varphi = \frac{1}{2}(1 + \cos 2\varphi), \qquad \sin^2\varphi = \frac{1}{2}(1 - \cos^2\varphi).$$

Uncoupling of bending deformations in the (x', y', z')-coordinate system requires that $I_{y'z'} = 0$. This provides the following relation for the determination of the rotation angle φ:

$$-\frac{1}{2}\sin(2\varphi)(I_{yy} - I_{zz}) - \cos(2\varphi)I_{yz} = 0 \;\Rightarrow\; \begin{cases} \tan(2\varphi) = \frac{2I_{yz}}{I_{zz}-I_{yy}} & \text{for} \quad I_{yy} \neq I_{zz}, \\ \cos(2\varphi) = 0 & \text{for} \quad I_{yy} = I_{zz}. \end{cases} \tag{1–61}$$

Note that $\cos(2\varphi) = 0$ implies that $\sin(2\varphi) = \pm 1$. The sign of $\sin(2\varphi)$ is chosen as follows:

$$\left.\begin{array}{lll} \sin(2\varphi) = \quad 1 \quad \Rightarrow \quad \varphi = \frac{1}{4}\pi \quad \text{for} \quad I_{yz} < 0 \\ \sin(2\varphi) = -1 \quad \Rightarrow \quad \varphi = \frac{3}{4}\pi \quad \text{for} \quad I_{yz} > 0 \end{array}\right\}. \tag{1–62}$$

Then, Eq. (1–60) provides the following solutions for $I_{y'y'}$ and $I_{z'z'}$:

$$I_{y'y'} = \frac{1}{2}(I_{yy} + I_{zz}) + \mid I_{yz} \mid, \qquad I_{z'z'} = \frac{1}{2}(I_{yy} + I_{zz}) - \mid I_{yz} \mid . \tag{1–63}$$

For $I_{yy} \neq I_{zz}$ the solution for $\tan(2\varphi)$ is fulfilled for the following two alternative solutions for $\sin(2\varphi)$ and $\cos(2\varphi)$:

$$\sin(2\varphi) = -\frac{2I_{yz}}{J}, \qquad \cos(2\varphi) = \quad \frac{I_{yy} - I_{zz}}{J}, \tag{1–64a}$$

$$\sin(2\varphi) = \quad \frac{2I_{yz}}{J}, \qquad \cos(2\varphi) = -\frac{I_{yy} - I_{zz}}{J}, \tag{1–64b}$$

where

$$J = \sqrt{(I_{yy} - I_{zz})^2 + 4I_{yz}^2}. \tag{1–65}$$

The sign definition in Eq. (1–64a) is chosen. This implies that

$$2\varphi \in [0, \pi] \quad \text{for} \quad I_{yz} < 0 \qquad \text{and} \qquad 2\varphi \in [\pi, 2\pi] \quad \text{for} \quad I_{yz} > 0. \tag{1–66}$$

Insertion of the solution for $\sin(2\varphi)$ and $\cos(2\varphi)$ into Eq. (1–60) provides the following results for $I_{y'y'}$ and $I_{z'z'}$:

$$I_{y'y'} = \frac{1}{2}(I_{yy} + I_{zz}) + \frac{1}{2}\frac{(I_{yy} - I_{zz})^2 + 4I_{yz}^2}{J}, \tag{1–67a}$$

$$I_{z'z'} = \frac{1}{2}(I_{yy} + I_{zz}) - \frac{1}{2}\frac{(I_{yy} - I_{zz})^2 + 4I_{yz}^2}{J}, \tag{1–67b}$$

or, by insertion of J, cf. Eq. (1–65),

$$I_{y'y'} = \frac{1}{2}(I_{yy} + I_{zz}) + \frac{1}{2}\sqrt{(I_{yy} - I_{zz})^2 + 4I_{yz}^2}, \tag{1–68a}$$

$$I_{z'z'} = \frac{1}{2}(I_{yy} + I_{zz}) - \frac{1}{2}\sqrt{(I_{yy} - I_{zz})^2 + 4I_{yz}^2}. \tag{1–68b}$$

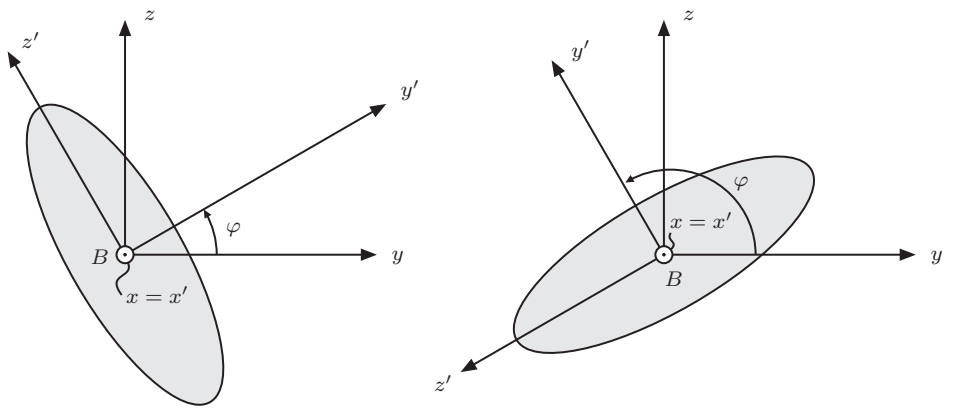

Figure 1–14 Position of principal axes: (a) $I_{yz} < 0$ and (b) $I_{yz} > 0$.

The coordinate axes y' and z' are known as the *principal axes* of the cross-section, whereas $I_{y'y'}$ and $I_{z'z'}$ are called the *principal moments of inertia*. It follows from Eqs. (1–63) and (1–67) that the choices of signs for $\sin(2\varphi)$ implies that $I_{y'y'}$ becomes the larger of the principal moments of inertia and $I_{z'z'}$ is the smaller principal moment of inertia. It is emphasised that this choice is performed merely to have a unique determination of φ. Three other choices of φ are possible obtained by additional rotations of the magnitudes $\frac{\pi}{2}$, π and $\frac{3}{2}\pi$ relative to the indicated.

If the cross-section has a symmetry line, and the y-axis is placed along this line, then $I_{yz} = 0$. Hence, a symmetry line is always a principal axis. Since the principal axes are orthogonal, the z-axis is also a principal axis—even if the cross-section is not symmetric around the axis.

Example 1.2 Determination of principal axes coordinate system

The cross-section analysed in Example 1.1 is reconsidered. The thin-wall approximation is used, so the moments of inertia are given by Eq. (l) in Example 1.1 and repeated here (without the primes):

$$I_{yy} \simeq \frac{233}{84}ta^3 \approx 2.7738 \cdot ta^3, \quad I_{zz} \simeq \frac{92}{21}ta^3 \approx 4.3810 \cdot ta^3, \quad I_{yz} \simeq -\frac{11}{7}ta^3 \approx -1.5714 \cdot ta^3. \tag{a}$$

The position of the bending centre relatively to the top-left corner of the cross-section is provided in Fig. A. From Eq. (a) and Eq. (1–65) follows that

$$J = \sqrt{\left(\frac{233}{84}ta^3 - \frac{92}{21}ta^3\right)^2 + 4\left(-\frac{11}{7}ta^3\right)^2} = ta^3 \cdot \frac{\sqrt{9769}}{28}, \tag{b}$$

which by insertion into Eq. (1–64) provides:

$$\sin(2\varphi) = -\frac{2 \cdot \left(-\frac{11}{7}ta^3\right) \cdot 28}{ta^3 \cdot \sqrt{9769}} = \frac{88}{\sqrt{9769}} \approx 0.8903, \tag{c}$$

$$\cos(2\varphi) = \frac{\left(\frac{233}{84}ta^3 - \frac{92}{21}ta^3\right) \cdot 28}{ta^3 \cdot \sqrt{9769}} = -\frac{3780}{84 \cdot \sqrt{9769}} \approx -0.4553. \tag{d}$$

(continued)

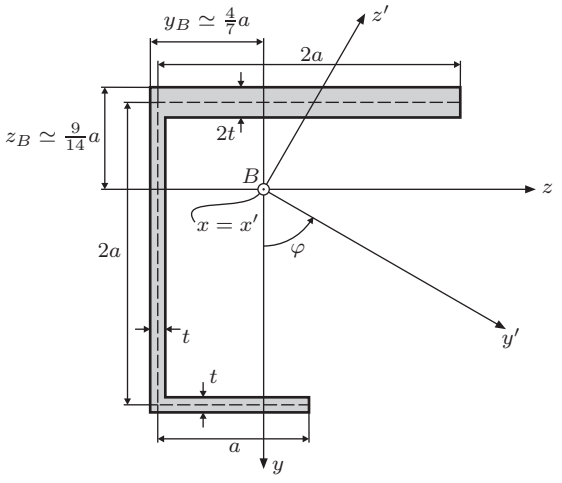

Figure A Position of principal axes coordinated system for the thin-walled cross-section.

From Eqs. (c) and (d) it is found that $\varphi = 1.0217$ radians corresponding to $\varphi = 58.5418^\circ$. Hence, $\varphi \in [0, \frac{\pi}{2}]$ in agreement with $I_{yz} = -\frac{11}{7}ta^3 < 0$.

Finally, the moments of inertia in the principal axes coordinate system follow from Eq. (1–67), *i.e.*

$$\left.\begin{matrix} I_{y'y'} \\ I_{z'z'} \end{matrix}\right\} = \left(\frac{1}{2}\left(\frac{233}{84}+\frac{92}{21}\right) \pm \frac{1}{2}\sqrt{\left(\frac{233}{84}-\frac{92}{21}\right)^2 + 4\left(\frac{11}{7}\right)^2}\right) ta^3 = \begin{cases} 5.3423\, ta^3, \\ 1.8124\, ta^3. \end{cases} \tag{e}$$

Clearly, $I_{y'y'}$ is greater than any of I_{yy} or I_{zz}, whereas $I_{y'y'}$ is smaller than the bending moments of inertia defined with respect to the original y- and z-axes. □

1.4.3 Equations of equilibrium in principal axes coordinates

From now on it will be assumed that the (x, y, z)-coordinate system forms a principal axes coordinate system with origin at the bending centre. In this case, the system of differential equations (1–28) for a Timoshenko beam uncouples into three differential subsystems. Thus, the axial deformation is governed by the equation

$$\frac{d}{dx}\left(EA\frac{dw_x}{dx}\right) + q_x = 0, \tag{1–69}$$

whereas bending deformation in the y-direction is defined by the coupled equations

$$\frac{d}{dx}\left(EI_z\frac{d\theta_z}{dx}\right) + GA_z\left(\frac{dw_y}{dx} - \theta_z\right) + m_z = 0, \tag{1–70a}$$

$$\frac{d}{dx}\left(GA_y\left(\frac{dw_y}{dx} - \theta_z\right)\right) + q_y = 0, \tag{1–70b}$$

where the double index yy on the bending moment of inertia has been replaces by a single index y in order to indicate that the principal-axes coordinates are utilised.

Similarly, the flexural deformations in the z-directions are determined by

$$\frac{d}{dx}\left(EI_y\frac{d\theta_y}{dx}\right) - GA_z\left(\frac{dw_z}{dx}+\theta_y\right) + m_y = 0, \tag{1–71a}$$

$$\frac{d}{dx}\left(GA_z\left(\frac{dw_z}{dx}+\theta_y\right)\right) + q_z = 0, \tag{1–71b}$$

where again the double index on the bending moment of inertia has been replaced by a single index. As seen from Eqs. (1–70) and (1–71), $\{w_y, \theta_z\}$ and $\{w_z, \theta_y\}$ are still determined by pairwise coupled ordinary differential equations of the second order.

For a Bernoulli-Euler beam, the system of ordinary differential equations (1–33) uncouples completely into the following differential equations for the determination of w_x, w_y and w_z:

$$\frac{d}{dx}\left(EA\frac{dw_x}{dx}\right) + q_x = 0, \tag{1–72a}$$

$$\frac{d^2}{dx^2}\left(EI_z\frac{d^2w_y}{dx^2}\right) - q_y + \frac{dm_z}{dx} = 0, \tag{1–72b}$$

$$\frac{d^2}{dx^2}\left(EI_y\frac{d^2w_z}{dx^2}\right) - q_z - \frac{dm_y}{dx} = 0. \tag{1–72c}$$

Example 1.3 Plane, fixed Timoshenko beam with constant load per unit length

Figure A shows a plane Timoshenko beam of the length l with constant bending stiffness EI_z and shear stiffness GA_y. The beam is fixed at both end-sections and is loaded with a constant load q_y and a constant moment load m_z. The displacement $w_y(x)$, the rotation $\theta_z(x)$, the shear force $Q_y(x)$ and the bending moment are to be determined.

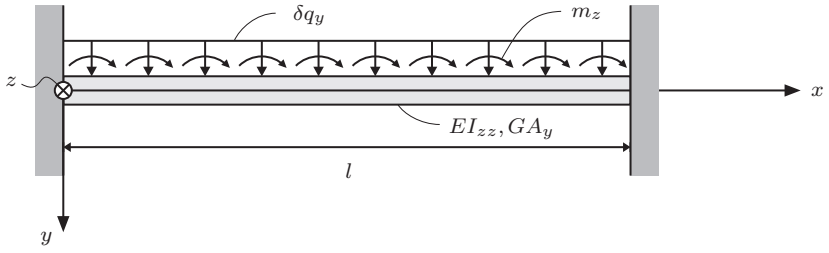

Figure A Fixed beam with constant load per unit length.

The differential equations for determination of $w_y(x)$ and $\theta_z(x)$ follow from Eq. (1–70). Thus,

$$EI_z\frac{d^2\theta_z}{dx^2} + GA_y\left(\frac{dw_y}{dx}-\theta_z\right) + m_z = 0, \qquad \frac{d}{dx}\left(GA_y\left(\frac{dw_y}{dx}-\theta_z\right)\right) + q_y = 0. \tag{a}$$

According to Eq. (1–35), the boundary conditions are:

$$w_y(0) = w_y(l) = 0, \qquad \theta_z(0) = \theta_z(l) = 0. \tag{b}$$

(continued)

Integration of the second equation in Eq. (a) provides:

$$Q_y = GA_y\left(\frac{dw_y}{dx} - \theta_z\right) = -q_y x + c_1 \tag{c}$$

Then, the following solution is obtained for $\theta_z(x)$ from the first equation in Eq. (a):

$$EI_z\frac{d^2\theta_z}{dx^2} = q_y x - (c_1 + m_z) \qquad \Rightarrow \qquad EI_z\theta_z(x) = \frac{1}{6}q_y x^3 - \frac{1}{2}(c_1 + m_z)x^2 + c_2 x + c_3. \tag{d}$$

Further, the boundary conditions $\theta_z(0) = \theta_z(l) = 0$ provide

$$c_3 = 0, \qquad c_2 = -\frac{1}{6}q_y l^2 + \frac{1}{2}(c_1 + m_z)l. \tag{e}$$

Hence, the following reduced form is obtained for $\theta_z(x)$:

$$\theta_z(x) = \frac{1}{6EI_z}\left(q_y(x^3 - xl^2) - 3(c_1 + m_z)(x^2 - xl)\right). \tag{f}$$

Next, Eq. (f) is inserted into Eq. (c) which is subsequently integrated with respect to x, leading to the following solution for $w_y(x)$:

$$GA_y\frac{dw_y}{dx} = -q_y x + c_1 + \frac{GA_y}{6EI_z}\left(q_y(x^3 - xl^2) - 3(c_1 + m_z)x^2 - xl)\right) \qquad \Rightarrow$$
$$GA_y w_y(x) = -\frac{1}{2}q_y x^2 + c_1 x + c_4 + \frac{GA_y}{6EI_z}\left(\frac{1}{4}q_y(x^4 - 2x^2l^2) - \frac{1}{2}(c_1 + m_z)(2x^3 - 3x^2 l)\right). \tag{g}$$

The boundary conditions $w_y(0) = w_y(l) = 0$ provide the integration constants

$$c_4 = 0, \qquad c_1 = \frac{1}{2}q_y l - \frac{1}{\Phi_y + 1}m_z, \tag{h}$$

where

$$\Phi_y = 12\frac{EI_z}{GA_y l^2} \tag{i}$$

Then, Eq. (a) and Eq. (f) provide the following solutions:

$$w_y(x) = \frac{q_y}{2GA_y}(l - x)x + \frac{q_y}{24EI_z}(l - x)^2x^2 - \frac{m_z}{GA_y}\frac{x}{\Phi_y + 1} - \frac{m_z}{12EI_z}\frac{\Phi_y}{\Phi_y + 1}(2x^3 - 3x^2 l) \quad \Rightarrow$$
$$w_y(x) = \frac{q_y}{24EI_z}\left((l - x)^2x^2 + \Phi_y l^2(l - x)x\right) - \frac{m_z}{12EI_z}\frac{\Phi_y}{\Phi_y + 1}(2x^3 - 3x^2 l + xl^2), \tag{j}$$

$$\theta_z(x) = \frac{q_y}{12EI_z}(2x^3 - 3x^2 l + xl^2) + \frac{m_z}{2EI_z}\frac{\Phi_y}{\Phi_y + 1}(l - x)x. \tag{k}$$

The non-dimensional parameter Φ_y is a measure of the influence of the shear deformations. For a rectangular cross-section with the height h we have $I_z = \frac{1}{12}h^2A$ and $A_y = \frac{5}{6}A$. Then Φ_y becomes

$$\Phi_y = \frac{72}{5}\cdot\frac{h^2}{l^2}\frac{E}{G}. \tag{l}$$

Hence, shear deformations are primarily of importance for short and high beams. On the other hand, for long beams with a small height of the cross-section, shear deformations are of little importance, *i.e.* only the bending deformation is significant. *(continued)*

For Bernoulli-Euler beams we have $\gamma_{xy} = 0$, corresponding to $GA_y = \infty$, cf. Eqs. (1–16) and (1–27). Then, $\Phi_y = 0$ and Eqs. (j) and (k) reduce to

$$w_y(x) = \frac{q_y}{24EI_z}(l-x)^2x^2, \tag{m}$$

$$\theta_z(x) = \frac{q_y}{12EI_z}(2x^3 - 3x^3l + xl). \tag{n}$$

It is remarkable that the distributed moment load m_z does not induce any displacements or rotations in the considered beam with Bernoulli-Euler kinematics.

The shear force $Q_y(x)$ and bending moment $M_z(x)$ follow from Eq. (c), Eq. (h) and Eq. (k), respectively, *i.e.*

$$Q_y(x) = -q_yx + c_1 = \frac{1}{2}q_y(l-2x) - \frac{1}{\Phi_y+1}m_z, \tag{o}$$

$$M_z(x) = EI_z\frac{d\theta_z}{dx} = \frac{q_y}{12}(6x^2 - 6xl + l^2) + \frac{m_z}{2}\frac{\Phi_y}{\Phi_y+1}(l-2x). \tag{p}$$

For a Bernoulli-Euler beam these results reduce to

$$Q_y(x) = \frac{1}{2}q_y(l-2x) - m_z, \tag{q}$$

$$M_z(x) = \frac{q_y}{12}(6x^2 - 6xl + l^2). \tag{r}$$

The constant moment load m_z only induces a constant shear force of magnitude $-m_z$, whereas $M_z(x)$ is not affected by this load. Especially, for $x = 0$ and $x = l$, Eq. (o) and Eq. (p) provide

$$Q_y(0) = \frac{1}{2}q_yl - m_z, \qquad M_y(0) = \frac{1}{12}q_yl + \frac{1}{2}\frac{\Phi_y}{\Phi_y+1}m_zl, \tag{s}$$

$$Q_y(l) = -\frac{1}{2}q_yl - m_z, \qquad M_y(l) = \frac{1}{12}q_yl^2 - \frac{1}{2}\frac{\Phi_y}{\Phi_y+1}m_zl. \tag{t}$$

The displacement at the midpoint $x = l/2$ follows from Eq. (k):

$$w_y(l/2) = \frac{q_yl^4}{384EI_z}(1+4\Phi_y). \tag{u}$$

The first and second terms within the parenthesis specify the contributions from bending and shear, respectively. Again the parameter Φ_y reveals itself as a measure of the relative contribution from shear deformations. □

1.5 Normal stresses in beams

For at beam without warping, the normal stress $\sigma_{xx}(x,y,z)$ in terms of the generalised strains follows from Eqs. (1–17), (1–20) and (1–24):

$$\sigma_{xx} = E(\varepsilon - \kappa_zy + \kappa_yz). \tag{1–73}$$

In the principal axes coordinate system, where $S_y = S_z = I_{yz} = 0$, the generalised strains $\{\varepsilon, \kappa_y, \kappa_z\}$ are related to the conjugated generalised stresses $\{N, M_y, M_z\}$ as determined from

Eqs. (1–45a), (1–45b), (1–46) and (1–47) for $S_y = S_z = I_{yz} = 0$, *i.e.*

$$\varepsilon = \frac{N}{EA}, \qquad \kappa_y = \frac{M_y}{EI_y}, \qquad \kappa_z = \frac{M_z}{EI_z}. \tag{1–74}$$

Insertion of Eq. (1–74) into Eqs. (1–19) and (1–24) provides the result for the axial stress in terms of the generalised stresses,

$$\sigma_{xx} = \frac{N}{A} - \frac{M_z}{I_z}y + \frac{M_y}{I_y}z. \tag{1–75}$$

Equation (1–75) is due to Navier, and is therefore referred to as *Navier's formula*. It should be noticed that Eq. (1–75) presumes that the stresses are formulated in a principal axes coordinate system, so I_y and I_z indicate the principal moments of inertia. The relation is valid for both Timoshenko and Bernoulli-Euler beams. This is so because only the relation (1–15), but not the relation (1–18) has been utilised. Hence, Eq. (1–75) is based on the assumption that plane cross-sections remain plane, but not that they remain orthogonal to the beam axis.

The so-called *zero line* specifies the line in the (y, z)-plane on which $\sigma_x = 0$. The analytical expression for the zero line becomes

$$\frac{N}{A} - \frac{M_z}{I_z}y + \frac{M_y}{I_y}z = 0. \tag{1–76}$$

It is finally noted that warping introduces displacements in the axial direction in addition to those provided by bending. However, if the torsion is homogeneous, these displacements will not introduce any normal strains and therefore no normal stresses. Hence, Navier's formula is also valid in the case of St. Venant torsion, but in the case of Vlasov torsion, or inhomogeneous torsion, additional terms must be included in Eq. (1–75).

1.6 The principle of virtual forces

In this section the *principle of virtual forces* is derived for a plane Timoshenko beam of the length l. The deformation of the beam is taking place in the (x, y)-plane. In the referential state, the left end-section is placed at the origin of the coordinate system and the x-axis is placed along the bending centres of the cross-sections, see Fig. 1–15.

The principle of virtual forces is the dual to the *principle of virtual displacements*. In the principle of virtual displacements the actual sectional forces and sectional moments are assumed to be in equilibrium with the loads and the reaction forces applied at the end sections. The virtual displacements and rotations are considered as arbitrary increments to the actual displacements and they only need to fulfil homogeneous kinematic boundary conditions, so that the combined field made up by the actual and the virtual fields always fulfils the actual non-homogeneous boundary conditions as given by Eq. (1–35). Further, the generalised virtual strains defining the internal virtual work must be derived from the virtual displacement and rotation fields.

In contrast, the principle of virtual forces presumes that the displacements and rotations of the beam are fulfilling the kinematic boundary conditions, and that the generalised internal strains are compatible to these fields. The actual loads on the beam are superimposed with the virtual incremental loads per unit length δq_x and δq_y, the virtual moment load per unit length δm_z,

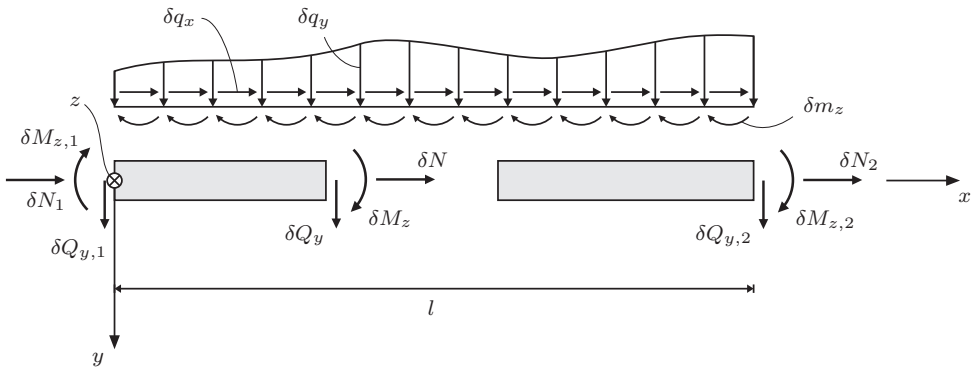

Figure 1–15 Virtual internal and external forces.

the virtual reaction forces δN_j and $\delta Q_{y,j}$ along the x- and y-directions, and the virtual reaction moments δM_z in the z-directions, where $j = 1$ and $j = 2$ indicate the left and right end-sections, respectively. Due to the load increments, the internal section forces and section moment achieve increments δN, δQ_y and δM_z, see Fig. 1–15. These variational fields are assumed to be in equilibrium with the variational load fields $\delta q_x, \delta q_y$ and δm_z, and to comply with the variations $\delta N_j, \delta Q_{y,j}$ and $\delta M_{z,j}$ of the reaction forces and reaction moments. In what follows, δN, δQ_y and δM_z will be referred to as the virtual internal forces, whereas δq_x, δq_y, δm_z, δN_j, $\delta Q_{y,j}$ and $\delta M_{z,j}$ are called the virtual external forces.

The starting point is taken in the kinematical conditions provided by Eqs. (1–12) and (1–17) and rewritten in the form

$$\frac{dw_x}{dx} - \varepsilon = 0, \qquad \frac{dw_y}{dx} - \theta_z - \gamma_{xz} = 0, \qquad \frac{d\theta_z}{dx} - \kappa_z = 0. \tag{1–77}$$

The virtual internal forces are related to the virtual external loads per unit length δq_x, δq_y and δm_z via the following equations of equilibrium, cf. Eqs. (1–4a) and (1–4b):

$$\frac{d(\delta N)}{dx} + \delta q_x = 0, \qquad \frac{d(\delta Q_y)}{dx} + \delta q_y = 0, \qquad \frac{d(\delta M_z)}{dx} + \delta Q_y + \delta m_z = 0. \tag{1–78}$$

The first equation in Eq. (1–78) is multiplied with $\delta N(x)$, the second equation is multiplied with $\delta Q_y(x)$, and the third equation with $\delta M(z)$. Next, the equations are integrated from $x = 0$ to $x = l$, and the three resulting equations are added, leading to the identity

$$\int_0^l \left[\delta N \left(\frac{dw_x}{dx} - \varepsilon \right) + \delta Q_y \left(\frac{dw_y}{dx} - \theta_z - \gamma_{xy} \right) + \delta M_z \left(\frac{d\theta_z}{dx} - \kappa_z \right) \right] dx = 0 \tag{1–79}$$

Integration by parts is carried out on the first terms within the innermost parentheses, leading to

$$\left[\delta N w_x + \delta Q_y w_y + \delta M_z Q_z \right]_0^l - \int_0^l \left(\frac{d(\delta N)}{dx} w_x + \frac{d(\delta Q_y)}{dx} w_y + \frac{d(\delta M_z)}{dx} \theta_z - \delta Q_y \theta_z \right) dx$$
$$= \int_0^l \left(\delta N \varepsilon + \delta Q_y \cdot \gamma_{xy} + \delta M_z \cdot \kappa_z \right) dx. \tag{1–80}$$

Upon utilisation of Eq. (1–78), this is reduced to

$$\Big[\delta N \cdot w_x + \delta Q_y \cdot w_y + \delta M_z \cdot \theta_z\Big]_0^l + \int_0^l \Big(\delta q_x \cdot w_x + \delta q_y \cdot w_y + \delta m_z \cdot \theta_z\Big) dx$$
$$= \int_0^l \Big(\delta N \cdot \varepsilon + \delta Q_y \cdot \gamma_{xy} + \delta M_z \cdot \kappa_z\Big) dx. \tag{1–81}$$

The generalised strains on the right-hand side of Eq. (1–81) are now expressed in mechanical quantities by means of Eq. (1–74). Further, δN, δQ_y and δM_z fulfil the following boundary conditions at $x = 0$ and $x = l$, cf. Fig. 1–15,

$$\delta N(0) = -\delta N_1, \qquad \delta Q_y(0) = -\delta Q_{y,1}, \qquad \delta M_z(0) = -\delta M_{z,1}, \tag{1–82a}$$

$$\delta N(l) = \delta N_2, \qquad \delta Q_y(l) = \delta Q_{y,2}, \qquad \delta M_z(l) = \delta M_{z,2}. \tag{1–82b}$$

Equation (1–81) then obtains the following final form:

$$\sum_{j=1}^{2} \Big(\delta N_j \cdot w_{x,j} + \delta Q_{y,j} \cdot w_{y,j} + \delta M_{z,j} \cdot \theta_{z,j}\Big) + \int_0^l \Big(\delta q_x \cdot w_x + \delta q_y \cdot w_y + \delta m_z \cdot \theta_z\Big) dx$$
$$= \int_0^l \left(\frac{\delta N \cdot N}{EA} + \frac{\delta Q_y \cdot Q_y}{GA_y} + \frac{\delta M_z \cdot M_z}{EI_z}\right) dx, \tag{1–83}$$

where $w_{x,j}$, $w_{y,j}$ and $\theta_{z,j}$ denote the displacements in the x- and y-directions and the rotation in the z-direction at the end-sections, respectively. Equation (1–83) represents the principle of virtual forces. The left- and right-hand sides represent the external and internal virtual work, respectively.

The use of Eq. (1–83) in determining the displacements and rotations of a Timoshenko beam is demonstrated in Examples 1.4 and 1.5 below. Furthermore, the principle of virtual forces may be used to derive a stiffness matrix for a Timoshenko beam element as shown later.

Example 1.4 End-displacement of cantilevered beam loaded with a force at the free end

Figure A shows a plane Timoshenko beam of the length l with constant axial stiffness EA, shear stiffness GA_y and bending stiffness EI_z. The beam is fixed at the left end-section and free at the right end-section, where it is loaded with a concentrated force $Q_{y,2}$ in the y-direction. The displacement $w_{y,2}$ at the free end is searched.

The principle of virtual forces Eq. (1–83) is applied with the following external virtual loads: $\delta q_x = \delta q_y = \delta m_z = 0$, $\delta N_1 = \delta Q_{y,1} = \delta M_{z,1} = \delta N_2 = \delta M_{z,2} = 0$ and $\delta Q_{y,2} = 1$. Further $N(x) = 0$. Then, Eq. (1–83) reduces to

$$1 \cdot w_{y,2} = \int_0^l \left(\frac{\delta Q_y \cdot Q_y}{GA_y} + \frac{\delta M_z \cdot M_z}{EI_z}\right) dx. \tag{a}$$

(continued)

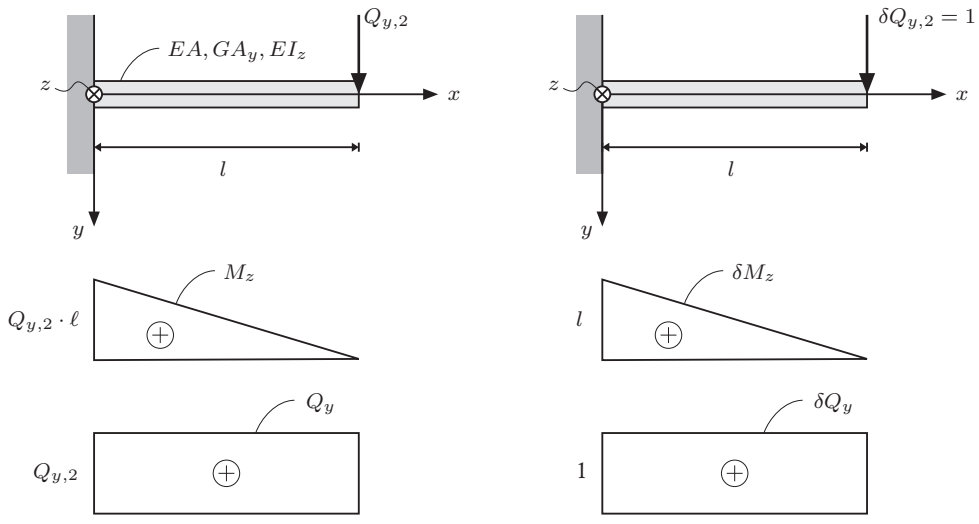

Figure A Fixed plane Timoshenko beam loaded with a concentrated force at the free end: Actual force and section forces (left) and virtual force and section forces (right).

The variation of the bending moment $M_z(x)$ and the shear force $Q_y(x)$ from the actual load $Q_{y,2}$ has been shown in Fig. A on the left. The corresponding variational moment field $\delta M_z(x)$ and shear force $\delta Q_y(x)$ from $\delta Q_{y,2} = 1$ are shown in Fig. A on the right. Insertion of these distributions in Eq. (b) provides the solution

$$w_{y,2} = \frac{Q_{y,2}l}{GA_y} + \frac{1}{3}\frac{Q_{y,2}l^3}{EI_z} = \frac{1}{12}(4 + \Phi_y) \cdot \frac{Q_{y,2}l^3}{EI_z}, \tag{b}$$

where Φ_y is given by Eq. (i) in Example 1.3. The deformation contributions from shear and bending are additive. This is a consequence of the additive nature of the flexibilities indicated by Eq. (1–83) in contribution to the fact that the beam is statically determinate, which provides the fields $M_z(x)$ and $Q_y(x)$ as well as $\delta M_z(x)$ and $\delta Q_y(x)$ directly. □

Example 1.5 End-deformations of fixed beam loaded with a moment at the free end

The beam described in Example 1.4 is considered again. However, now the free end is loaded with a concentrated moment $M_{z,2}$. The displacement $w_{y,2}$ and the rotation $\theta_{z,2}$ of the end-section is to be found.

At the determination of $w_{y,2}$ from $M_{z,2}$, the principle of virtual forces given by Eq. (1–83) is again applied with $\delta Q_{y,2} = 1$ and all other external variational loads equal to zero, leading to Eq. (a) in Example 1.4. However, $M_z(x)$ and $Q_y(x)$ are now caused by $M_{z,2}$, and are given as shown in Fig. A, whereas $\delta M_z(x)$ and $\delta Q_y(x)$ are as shown in Fig. A of Example 1.4. Then, $w_{y,2}$ becomes

$$w_{y,2} = \int_0^l \frac{\delta M_z \cdot M_z}{EI_z} dx = \frac{1}{2}\frac{M_{y,2}l^2}{EI_z}. \tag{a}$$

(continued)

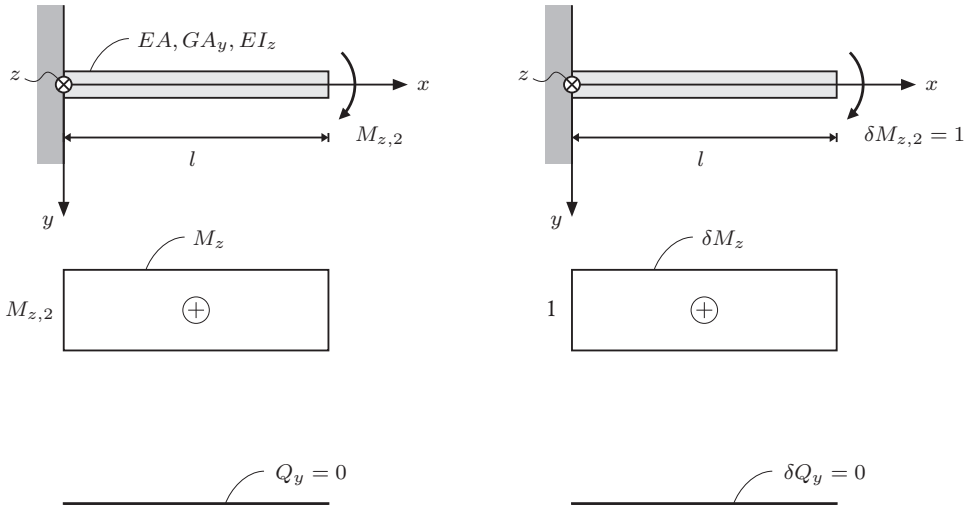

Figure A Fixed plane Timoshenko beam loaded with a moment at the free end: Actual moment and section forces (left) and virtual moment and section forces (right).

At the determination of $\theta_{z,2}$ the principle of virtual forces Eq. (1–83) is applied with the following external virtual loads $\delta q_x = \delta q_y = \delta m_z = 0$, $\delta N_1 = \delta Q_{y,1} = \delta M_{z,1} = \delta N_2 = \delta Q_{y,2} = 0$ and $\delta M_{z,2} = 1$. Then, Eq. (1–83) reduces to

$$1 \cdot \theta_{z,2} = \int_0^l \left(\frac{\delta Q_y \cdot Q_y}{GA_y} + \frac{\delta M_z \cdot M_z}{EI_z} \right) dx. \tag{b}$$

The variation of $Q_y(x)$ and $M_z(x)$ from $M_{y,2}$ has been shown in Fig. A on the left, and the variation of $\delta Q_y(x)$ and $\delta M_z(x)$ from $\delta M_{z,2} = 1$ is shown in Fig. A on the right. Then $\theta_{z,2}$ becomes

$$\theta_{z,2} = \int_0^l \frac{1 \cdot M_{z,2}}{EI_z} dx = \frac{M_{z,2} l}{EI_z}. \tag{c}$$

In the present load case, the shear force is given as $Q_y(x) = 0$. Consequently it will not induce any contributions in Eq. (a) and Eq. (c). □

1.7 Elastic beam elements

When frame structures consisting of multiple beams are to be analysed, the establishment of analytical solutions is not straightforward and instead a numerical solution must be carried out. For this purpose, a discretization of the frame structure into a number of so-called *beam elements* is necessary, eventually leading to a *finite-element model*. The aim of the present section is not to provide a full introduction to the finite-element method for the analysis of frame structures, *e.g.* tower blocks with a steel frame as the load-carrying structure. However, a formulation is given for a single beam element to be applied in such analyses. Both the Timoshenko and Bernoulli-Euler beam theories are discussed in this context, and plane as well as three-dimensional beams are touched upon.

1.7.1 A plane Timoshenko beam element

Firstly, the stiffness matrix and element load vector is derived for a plane Timoshenko beam element with constant axial stiffness EA, shear stiffness GA_y and bending stiffness EI_z, cf. Fig. 1–16. The stiffness relation is described in an (x, y)-coordinate system with origin at the left end-section and the x-axis along the bending centres.

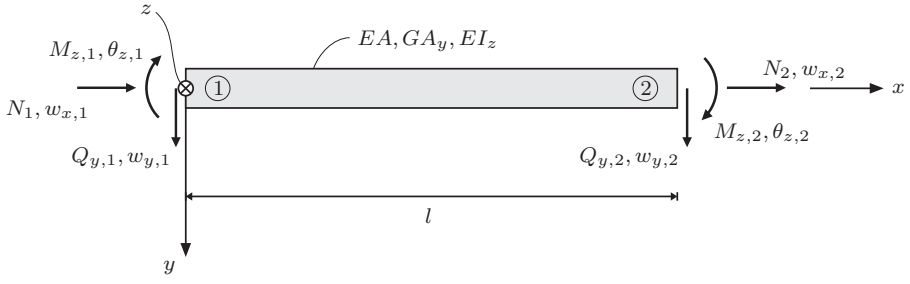

Figure 1–16 Plane Timoshenko beam element with definition of degrees of freedom and nodal reaction forces.

At the end-nodes, nodal reaction forces N_j and $Q_{y,j}$ are acting along the x- and y-directions, respectively, and reaction moments $M_{z,j}$ are applied around the z-axis. Here, $j = 1$ and $j = 2$ stand for the left-end and right-end nodes of the beam element, respectively, and the reaction forces and moments are in equilibrium with the remaining external loads on the element for arbitrary deformations of the beam.

The element has 6 degrees of freedom defining the displacements and rotations of the end-sections, cf. Fig. 1–16. These are organised in the column vector

$$\mathbf{w_e} = \begin{bmatrix} \mathbf{w_{e1}} \\ \mathbf{w_{e2}} \end{bmatrix} = \begin{bmatrix} w_{x,1} & w_{y,1} & \theta_{z,1} & w_{x,2} & w_{y,2} & \theta_{z,2} \end{bmatrix}^T \tag{1–84}$$

The sub-vector $\mathbf{w_{e}}_j$ defines the degrees of freedom related to element node j.

Similarly, the reaction forces N_j, $Q_{y,j}$ and $M_{z,j}$, $j = 1, 2$, at the end-sections, work conjugated to $w_{x,j}$, $w_{y,j}$ and $\theta_{z,j}$, are stored in the column vector

$$\mathbf{r_e} = \begin{bmatrix} \mathbf{r_{e1}} \\ \mathbf{r_{e2}} \end{bmatrix} = \begin{bmatrix} N_1 & Q_{y,1} & M_{z,1} & N_2 & Q_{y,2} & M_{z,2} \end{bmatrix}^T \tag{1–85}$$

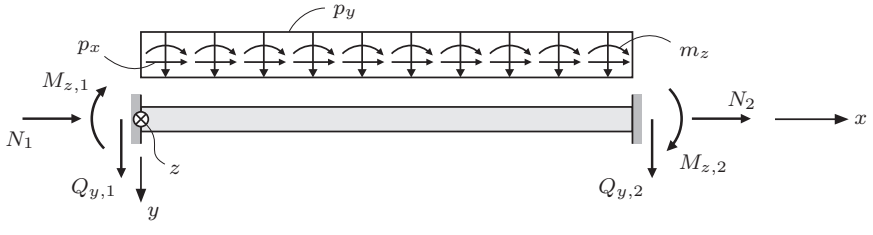

Figure 1–17 External loads and reaction forces from external loads on a plane beam element.

The equilibrium of the beam element relating the nodal reaction forces to the degrees of freedom of the element may be derived by the principle of virtual displacements as demonstrated

in a subsequent paper. The resulting equilibrium equations on matrix form may be written on the form

$$\mathbf{r_e} = \mathbf{K_e w_e} + \mathbf{f_e}. \tag{1–86}$$

The vector $\mathbf{f_e}$ in Eq. (1–86) represents the nodal reaction forces from the external element loads when $\mathbf{w_e} = \mathbf{0}$, *i.e.* when the beam is fixed at both ends as shown in Fig. 1–17. We shall merely consider constant element loads q_x and q_y per unit length in the x- and y-directions, and a constant moment load per unit length m_z in the z-direction, see Fig. 1–17. The reaction forces and reaction moments follow from Eqs. (s) and (t) in Example 1.3:

$$\mathbf{f_e} = \begin{bmatrix} -\frac{1}{2}q_x l \\ -\frac{1}{2}q_y l + m_z \\ -\frac{1}{12}q_y l^2 - \frac{1}{2}\frac{\Phi_y}{\Phi_y+1}m_z l \\ -\frac{1}{2}q_x l \\ -\frac{1}{2}q_y l - m_z \\ \frac{1}{12}q_y l^2 - \frac{1}{2}\frac{\Phi_y}{\Phi_y+1}m_z l \end{bmatrix}. \tag{1–87}$$

The matrix $\mathbf{K_e}$ in Eq. (1–86) denotes the stiffness matrix in the local (x, y, z)-coordinate system. Let w_i denote the ith component of $\mathbf{w_e}$. Then, the ith column in $\mathbf{K_e}$ represents the nodal reaction forces for $\mathbf{f_e} = \mathbf{0}$, and with $w_i = 1$ and $w_j = 0, j \neq i$. These forces are obtained following the derivations in Example 1.3 from Eq. (a) to Eq. (t) with $q_y = m_z = 0$ and with the boundary condition in Eq. (b) replaced by the indicated conditions. Because of the symmetry of the problem, only two such analyses need to be performed. Still, this is a rather tedious approach. Partly because of this, and partly in order to demonstrate an alternative approach, the stiffness matrix will be derived based on the principle of virtual forces.

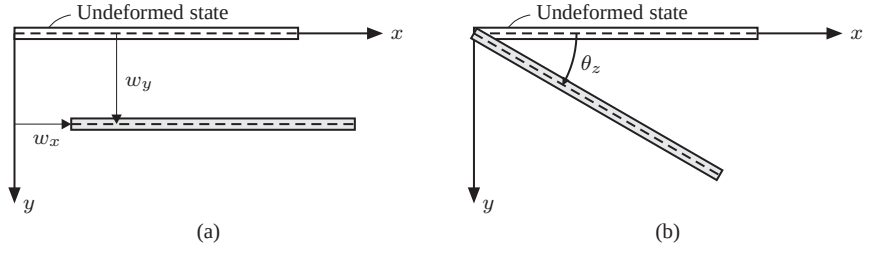

Figure 1–18 Rigid-body modes of a plane beam element: (a) Translation and (b) rotation.

The beam element has 6 degrees of freedom, by which a total of 6 linear independent modes of deformation may be defined. These consist of 3 linear independent rigid body modes and 3 linear independent elastic modes. The rigid modes may be chosen as a translation in the x-direction, a translation in the y-direction and a rotation around the z-direction as shown in Fig. 1–18. Any rigid body motion of the beam element may be obtained as a linear combination of these component modes of deformation. Obviously, the rigid body motions do not introduce stresses in the beam. Hence, the axial force N, the shear force Q_y and the bending moment M_z are all zero during such motions.

Since, axial elongations are uncoupled from bending deformations, the elastic elongation mode is uniquely defined as shown in Fig. 1–19a. The two bending deformation modes may be

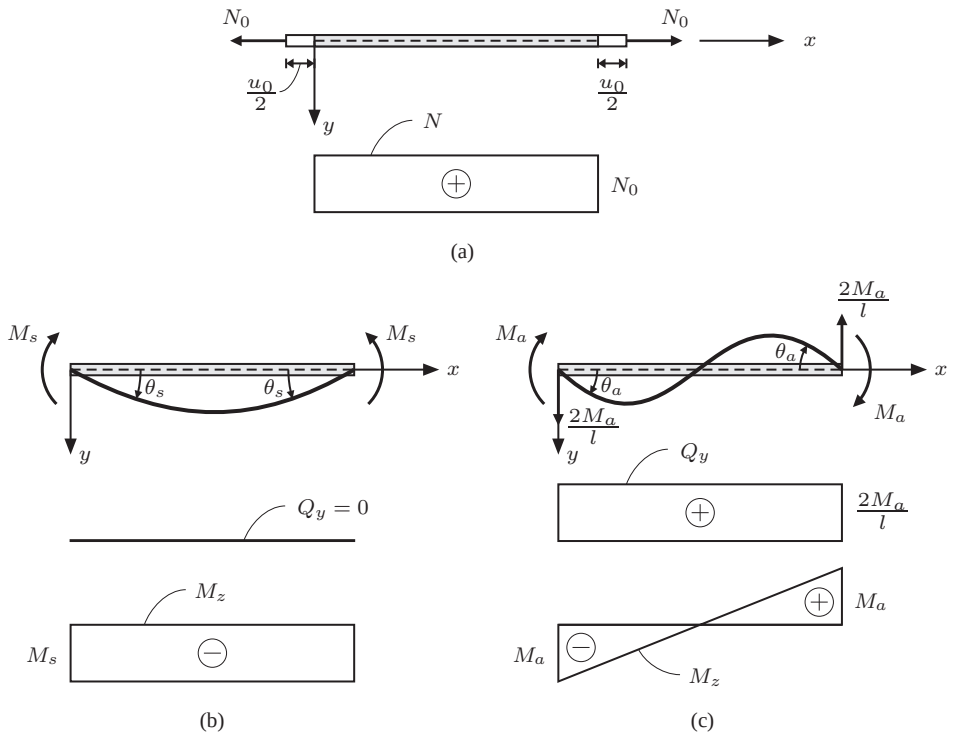

Figure 1–19 Elastic modes and related section forces in a plane beam element: (a) Axial elongation; (b) symmetric bending and (c) antisymmetric bending.

chosen in arbitrarily many ways. Typically, these are chosen by prescribing an angle of rotation at the other end-section. Following an idea by Krenk (2001), a more convenient formulation may be obtained by choice of two bending modes symmetric and anti-symmetric around the mid-point of the beam element as shown in Figs. 1–19b and 1–19c. It should be noticed that these modes also apply if the material properties of the beam are not symmetrical around the mid-point.

The axial elongation and conjugated axial force related to the axial elongation mode are denoted u_0 and N_0, respectively. The symmetric and anti-symmetric bending modes are described by the end-section rotations θ_s and θ_a defined in Figs. 1–19b and 1–19c, respectively. The conjugated moments are denoted M_s and M_a, respectively. The related distributions of the shear force $Q_y(x)$ and the bending moment $M_z(x)$ are shown in Figs. 1–19b and 1–19c.

The shear force is equal to $Q_y = 0$ in symmetric bending, because the bending moment is constant. Then, no shear deformations are related to this mode. In contrast, a constant shear force appears in the anti-symmetric bending mode. Hence, the deformations occurring in this mode are affected by bending as well as shear contributions.

At first the constitutive relations between the deformation measures and the conjugated generalised strains for the indicated elastic modes are found by means of the principle of virtual forces Eq. (1–83). In all cases, the beam element is unloaded, so $\delta q_x = \delta q_y = \delta m_z = 0$. For the axial elongation mode $N = N_0$, $Q_y = M_z = 0$, and $\delta N = 1$, $\delta N_1 = -1$, $\delta N_2 = 1$. Further,

$w_{x,1} = -\frac{1}{2}u_0$, $w_{x,2} = \frac{1}{2}u_0$, $w_{y,j} = \theta_{z,j} = 0$. Then, Eq. (1–83) reduces to

$$(-1)\cdot(-\frac{1}{2}u_0) + 1\cdot\frac{1}{2}u_0 = \int_0^l \frac{1\cdot N_0}{EA}dx \quad \Rightarrow \quad u_0 = N_0\int_0^l \frac{dx}{EA} = \frac{l}{EA}N_0. \tag{1–88}$$

The last statement holds for a beam element with constant axial stiffness EA. If EA varies, the integral in the middlemost statement must be evaluated analytically or numerically.

For the symmetric bending mode $N = Q_z = 0$, $M_z = -M_s$, $\delta M_z = -1$, $\delta M_{z,1} = 1$, and $\delta M_{z,2} = -1$. Further, $\theta_{z,1} = \theta_s$, $\theta_{z,2} = -\theta_s$ and $w_{x,j} = w_{y,j} = 0$. Then, Eq. (1–83) provides

$$1\cdot\theta_s + (-1)\cdot(-\theta_s) = \int_0^l \frac{(-1)(-M_s)}{EI_z}dx \quad \Rightarrow \quad 2\theta_s = M_s\cdot\int_0^l \frac{dx}{EI_z} = \frac{l}{EI_z}M_s. \tag{1–89}$$

Again, the last statement only applies for a homogeneous beam, whereas the middlemost statement applies for any variation of the bending stiffness EI_z along the beam.

For the anti-symmetric bending mode $N = 0$, $Q_y = 2\frac{M_a}{l}$, $M_z(x) = (-1+2x/l)M_a$, and $\delta Q_y = 2\delta M_z(x)/l = (-1+2x/l)$. Further, $\theta_{z,1} = \theta_a, \theta_{z,2} = \theta_a, w_{x,j} = w_{y,j} = 0$. Then, Eq. (1–83) provides

$$1\cdot\theta_a + 1\cdot\theta_a = \int_0^l \left(\frac{\frac{2}{l}\cdot\frac{2M_a}{l}}{GA_y} + \frac{(-1+2\frac{x}{l})(-1+2\frac{x}{l})M_a}{EI_z}\right)dx \qquad \Rightarrow$$

$$2\theta_a = M_a\left(\frac{4}{l^2}\int_0^l \frac{dx}{GA_y} + \int_0^l \frac{(-1+2\frac{x}{l})^2}{EI_z}dx\right) \qquad \Rightarrow$$

$$2\theta_a = M_a\left(4l\frac{1}{GA_yl^2} + \frac{1}{3}\frac{l}{EI_y}\right) = \frac{1}{3}\frac{l}{EI_y}(1+\Phi_y)M_a, \qquad \Phi_y = 12\frac{EI_z}{GA_yl^2}. \tag{1–90}$$

As discussed in Example 1.3, the non-dimensional parameter Φ_y defines the contribution of shear flexibility relatively to the bending flexibility.

The flexibility relations provided by Eqs. (1–88), (1–89) and (1–90) may be written in the following equivalent stiffness matrix formulation:

$$\mathbf{r}_0 = \mathbf{K}_0\mathbf{w}_0, \tag{1–91}$$

where

$$\mathbf{r}_0 = \begin{bmatrix} N_0 \\ M_s \\ M_a \end{bmatrix}, \qquad \mathbf{w}_0 = \begin{bmatrix} u_0 \\ 2\theta_s \\ 2\theta_a \end{bmatrix}, \qquad \mathbf{K}_0 = \begin{bmatrix} \frac{EA}{l} & 0 & 0 \\ 0 & \frac{EI_z}{l} & 0 \\ 0 & 0 & \frac{3}{1+\Phi_y}\frac{EI_z}{l} \end{bmatrix}. \tag{1–92}$$

The nodal reaction forces $\mathbf{r_e}$ and $\mathbf{r}_0$ in Eq. (1–85) and Eq. (1–92) are related via the transformation

$$\mathbf{r_e} = \mathbf{S}\mathbf{r}_0 = \mathbf{S}\mathbf{K}_0\mathbf{w}_0, \tag{1–93}$$

where

$$\mathbf{S} = \begin{bmatrix} -1 & 0 & 0 \\ 0 & 0 & 2/l \\ 0 & 1 & 1 \\ 1 & 0 & 0 \\ 0 & 0 & -2/l \\ 0 & -1 & 1 \end{bmatrix}. \tag{1–94}$$

Similarly, the elastic deformation measures stored in $\mathbf{w}_0$ can be expressed by the degrees of freedom of the element stored in $\mathbf{w_e}$ as follows (see Fig. 1–20):

$$u_0 = w_{x,2} - w_{x,1}, \tag{1–95}$$

$$\left.\begin{aligned} \theta_{z,1} &= \theta_a + \theta_s + \tfrac{1}{l}(w_{y,2} - w_{y,1}) \\ \theta_{z,2} &= \theta_a - \theta_s + \tfrac{1}{l}(w_{y,2} - w_{y,1}) \end{aligned}\right\} \quad \Rightarrow \quad \left\{\begin{aligned} 2\theta_a &= \theta_{z,1} + \theta_{z,2} - \tfrac{2}{l}(w_{y,2} - w_{y,1}) \\ 2\theta_s &= \theta_{z,1} - \theta_{z,2}. \end{aligned}\right. \tag{1–96}$$

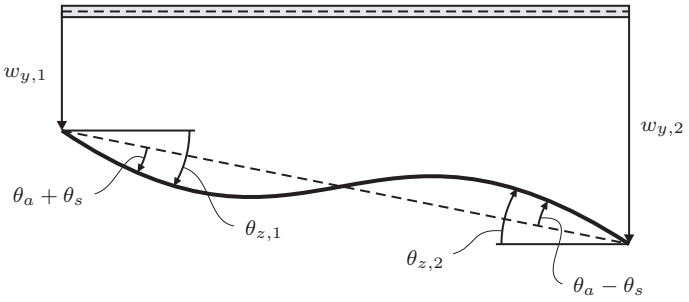

Figure 1–20 Connection between elastic deformation measures and element degrees of freedom.

Equations (1–95) and (1–96) may be rewritten in the common matrix form

$$\mathbf{w}_0 = \mathbf{S}^T \mathbf{w_e}, \tag{1–97}$$

where $\mathbf{S}$ is given by Eq. (1–94). Insertion of Eq. (1–97) into Eq. (1–93) provides upon comparison with Eq. (1–86):

$$\mathbf{r_e} = \mathbf{S}\mathbf{K}_0\mathbf{S}^T\mathbf{w_e} \qquad \Rightarrow \qquad \mathbf{K_e} = \mathbf{S}\mathbf{K}_0\mathbf{S}^T. \tag{1–98}$$

Insertion of $\mathbf{K}_0$ and $\mathbf{S}$ as given by Eq. (1–92) and Eq. (1–94) provides the following explicit solution for $\mathbf{K_e}$:

$$\mathbf{K_e} = \frac{E}{l^3}\begin{bmatrix} Al^2 & 0 & 0 & -Al^2 & 0 & 0 \\ 0 & \frac{12}{1+\Phi_y}I_z & \frac{6}{1+\Phi_y}I_z l & 0 & -\frac{12}{1+\Phi_y}I_z & \frac{6}{1+\Phi_y}I_z l \\ 0 & \frac{6}{1+\Phi_y}I_z l & \frac{4+\Phi_y}{1+\Phi_y}I_z l^2 & 0 & -\frac{6}{1+\Phi_y}I_z l & \frac{2-\Phi_y}{1+\Phi_y}I_z l^2 \\ -Al^2 & 0 & 0 & Al^2 & 0 & 0 \\ 0 & -\frac{12}{1+\Phi_y}I_z & -\frac{6}{1+\Phi_y}I_z l & 0 & \frac{12}{1+\Phi_y}I_z & -\frac{6}{1+\Phi_y}I_z l \\ 0 & \frac{6}{1+\Phi_y}I_z l & \frac{2-\Phi_y}{1+\Phi_y}I_z l^2 & 0 & -\frac{6}{1+\Phi_y}I_z l & \frac{4+\Phi_y}{1+\Phi_y}I_z l^2 \end{bmatrix}. \tag{1–99}$$

The corresponding result for a plane Bernoulli-Euler beam element is obtained simply by setting $\Phi_y = 0$. The equivalent element relations for a three-dimensional beam formulated in a (x, y, x) principal axes coordinate system are given in the next section.

Example 1.6 Deformations of a plane Timoshenko beam structure

Figure A shows a plane beam structure ABC consisting of two Timoshenko beam elements AB and BC of the lengths l and $l/2$, respectively. The loads on the structure and the resulting displacements are described in the indicated (x, y)-coordinate system. The shear stiffness GA_y and the bending stiffness EI_z are constant and the same in both beam elements. The structure is fixed at point A, free at point C, and simply supported at point B. Both beam elements are loaded with a constant load per unit length q_y. Additionally, beam BC is loaded with a concentrated load $P_y = q_y l$ at the free end C.

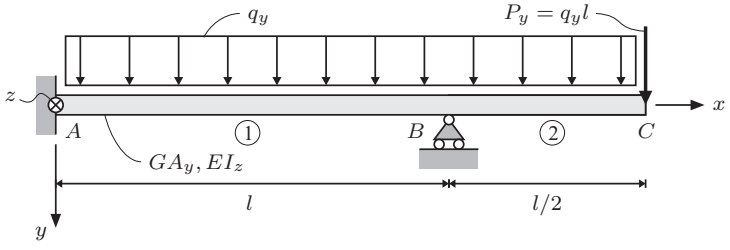

Figure A Plane Timoshenko beam structure consisting of two beam elements.

We want to determine the displacement of point C in the y-direction, and the reaction forces and moments at the support points A and B. The calculations are performed with the shear stiffness given as

$$GA_y = 120\frac{EI_z}{l^2}. \tag{a}$$

We shall refer to the beam elements AB and BC with the index $e = 1$ and $e = 2$, respectively. With reference to Eq. (i) in Example 1.3, the shear flexibility parameters for the two beam elements become:

$$\Phi_{y1} = \frac{12EI_z}{GA_y l^2} = 0.1, \qquad \Phi_{y2} = \frac{12EI_z}{GA_y (l/2)^2} = 0.4. \tag{b}$$

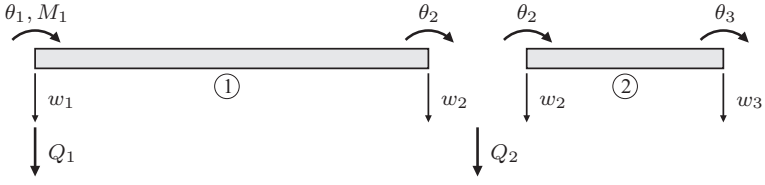

Figure B Global degrees of freedom and reaction forces in the plane Timoshenko beam structure.

Since, the axial deformations are disregarded, each element has 4 degrees of freedom out of which two are common, namely the displacement and rotation at point B. The related global degrees of freedom have been defined in Fig. B. The element stiffness matrices follow from Eq. (1–99) and Eq. (b):

$$\mathbf{K_1} = \frac{EI_z}{1.1l^3}\begin{bmatrix} 12 & 6l & -12 & 6l \\ 6l & 4.1l^2 & -6l & 1.9l^2 \\ -12 & -6l & 12 & -6l \\ -6l & 1.9l^2 & -6l & 4.1l^2 \end{bmatrix}, \quad \mathbf{K_2} = \frac{8EI_z}{1.4l^3}\begin{bmatrix} 12 & 3l & -12 & 3l \\ 3l & 1.1l^2 & -3l & 0.4l^2 \\ -12 & -3l & 12 & -3l \\ 3l & 0.4l^2 & -3l & 1.1l^2 \end{bmatrix}. \tag{c}$$

(continued)

The corresponding element loads become, cf. Eq. (1–87):

$$\mathbf{f_1} = \begin{bmatrix} -\frac{1}{2}q_y l \\ -\frac{1}{12}q_y l^2 \\ -\frac{1}{2}q_y l \\ \frac{1}{12}q_y l^2 \end{bmatrix} = -\frac{1}{12}q_y l \begin{bmatrix} 6 \\ l \\ 6 \\ -l \end{bmatrix}, \quad \mathbf{f_2} = \begin{bmatrix} -\frac{1}{2}q_y \cdot \frac{l}{2} \\ -\frac{1}{12}q_y(\frac{l}{2})^2 \\ -\frac{1}{2}q_y \frac{l}{2} + P_y \\ \frac{1}{12}q_y(\frac{l}{2})^2 \end{bmatrix} = -\frac{1}{48}q_y l \begin{bmatrix} 12 \\ l \\ 60 \\ -l \end{bmatrix}. \tag{d}$$

The global equilibrium equation, made up of contributions from both elements, has the structure

$$\mathbf{r} = \mathbf{K}\mathbf{w} + \mathbf{f}, \tag{e}$$

where

$$\mathbf{r} = \begin{bmatrix} \ulcorner \quad \urcorner \\ | \ \mathbf{r_1} \ | \\ | \ \ulcorner \ | \ \urcorner \\ \llcorner \ | \ \lrcorner \ | \\ | \ \mathbf{r_2} \ | \\ \llcorner \quad \lrcorner \end{bmatrix} = \begin{bmatrix} Q_1 \\ M_1 \\ Q_2 \\ 0 \\ 0 \\ 0 \end{bmatrix}, \quad \mathbf{w} = \begin{bmatrix} w_1 \\ \theta_1 \\ w_2 \\ \theta_2 \\ w_3 \\ \theta_3 \end{bmatrix}, \quad \mathbf{f} = \begin{bmatrix} \ulcorner \quad \urcorner \\ | \ \mathbf{f_1} \ | \\ | \ \ulcorner \ | \ \urcorner \\ \llcorner \ | \ \lrcorner \ | \\ | \ \mathbf{f_2} \ | \\ \llcorner \quad \lrcorner \end{bmatrix} = -\frac{1}{48}q_y l \begin{bmatrix} 24 \\ 4l \\ 36 \\ -3l \\ 60 \\ l \end{bmatrix}, \tag{f}$$

$$\mathbf{K} = \begin{bmatrix} \ulcorner \quad \urcorner \\ | \ \mathbf{K_1} \ | \\ | \ \ulcorner \ \urcorner \\ \llcorner \ | \ \lrcorner \ | \\ | \ \mathbf{K_2} \ | \\ \llcorner \quad \lrcorner \end{bmatrix}$$

$$= \frac{EI_z}{l^2} \begin{bmatrix} \frac{12}{1.1} & \frac{6}{1.1}l & -\frac{12}{1.1} & \frac{6}{1.1}l & 0 & 0 \\ \frac{6}{1.1}l & \frac{4.1}{1.1}l^2 & -\frac{6}{1.1}l & \frac{1.9}{1.1}l^2 & 0 & 0 \\ -\frac{12}{1.1} & -\frac{6}{1.1}l & \frac{12}{1.1}+\frac{96}{1.4} & \left(-\frac{6}{1.1}+\frac{24}{1.4}\right)l & -\frac{96}{1.4} & \frac{24}{1.4}l \\ \frac{6}{1.1}l & \frac{1.9}{1.1}l^2 & \left(-\frac{6}{1.1}+\frac{24}{1.4}\right)l & \left(\frac{4.1}{1.1}+\frac{8.8}{1.4}\right)l^2 & -\frac{24}{1.4}l & \frac{3.2}{1.4}l^2 \\ 0 & 0 & -\frac{96}{1.4} & -\frac{24}{1.4}l & \frac{96}{1.4} & -\frac{24}{1.4}l \\ 0 & 0 & \frac{24}{1.4}l & \frac{3.2}{1.4}l^2 & -\frac{24}{1.4}l & \frac{8.8}{1.4}l^2 \end{bmatrix}. \tag{g}$$

The details in the derivation of the matrix equation Eq. (e), including the formation of the column vectors $\mathbf{r}$ and $\mathbf{f}$ and the global stiffness matrix $\mathbf{K}$ by adding contribution from element components, will be explained in a later chapter.

The displacement degrees of freedom w_1 and w_2 at the nodes A and C are both equal to zero. Similarly, the rotation θ_1 at the fixed support at A is zero. When these values are introduced in $\mathbf{w}_0$, Eq. (e) provides the values of the reaction components Q_1, M_1 and Q_2 if the remaining unconstrained degrees of freedom θ_2, w_3 and θ_3 are inserted. These are determined from the corresponding equations in Eq. (e) using $w_1 = \theta_1 = w_2 = 0$, leading to

$$\frac{EI}{l^3} \begin{bmatrix} (\frac{4.1}{1.1}+\frac{8.8}{1.4})l^2 & -\frac{24}{1.4}l & \frac{3.2}{1.4}l^2 \\ -\frac{24}{1.4}l & \frac{96}{1.4} & -\frac{24}{1.4}l \\ \frac{3.2}{1.4}l^2 & -\frac{24}{1.4}l & \frac{8.8}{1.4}l^2 \end{bmatrix} \begin{bmatrix} \theta_2 \\ w_3 \\ \theta_3 \end{bmatrix} - \frac{1}{48}q_y l \begin{bmatrix} -3l \\ 60 \\ -l \end{bmatrix} = \begin{bmatrix} 0 \\ 0 \\ 0 \end{bmatrix} \quad \Rightarrow$$

$$\begin{bmatrix} \theta_2 l \\ w_3 \\ \theta_3 l \end{bmatrix} = \frac{q_y l^4}{EI_z} \begin{bmatrix} 0.1453 \\ 0.1274 \\ 0.2912 \end{bmatrix}. \tag{h}$$

Insertion of Eq. (h) along with $w_1 = \theta_1 = w_2 = 0$ into the remaining equation (e) provides the following solution for the reaction components Q_1, M_1 and Q_2: *(continued)*

$$\begin{bmatrix} Q_1 \\ M_1 \\ Q_2 \end{bmatrix} = \frac{EI_z}{l^3} \begin{bmatrix} \frac{6}{1.1}l & 0 & 0 \\ \frac{1.9}{1.1}l^2 & 0 & 0 \\ (-\frac{6}{1.1}+\frac{24}{1.4})l & -\frac{96}{1.4} & \frac{24}{1.4}l \end{bmatrix} - \frac{q_y l^4}{EI_z} \begin{bmatrix} 0.1453/l \\ 0.1274 \\ 0.2912/l \end{bmatrix} - \frac{1}{48} q_y l \begin{bmatrix} 24 \\ 4l \\ 36 \end{bmatrix} \quad \Rightarrow$$

$$\begin{bmatrix} Q_1 l \\ M_1 \\ O_2 l \end{bmatrix} = q_y l^2 \begin{bmatrix} 0.2927 \\ 0.1677 \\ -2.7927 \end{bmatrix}. \tag{i}$$

In case of Bernoulli-Euler kinematics, corresponding to $\Phi_{y1} = \Phi_{y2} = 0$, the corresponding solutions become:

$$\begin{bmatrix} \theta_1 l \\ w_3 \\ \theta_2 l \end{bmatrix} = \frac{q_y l^4}{EI} \begin{bmatrix} 0.1354 \\ 0.1172 \\ 0.2812 \end{bmatrix} \tag{j}$$

$$\begin{bmatrix} Q_1 l \\ M_1 \\ Q_2 l \end{bmatrix} = q_y l^2 \begin{bmatrix} 0.3125 \\ 0.1875 \\ -2.8125 \end{bmatrix} \tag{k}$$

Comparison of Eqs. (h) and (j) reveals that the displacement w_3 as well as the rotations θ_1 and θ_3 are increased by the shear flexibility. This is so because bending and shear deformations in general are coupled for statical indeterminate structures. At the same time, a comparison of Eqs. (i) and (k) shows that Bernoulli-Euler beam kinematics lead to higher stresses than Timoshenko beam theory, which is due to the fact that the shear stiffness in the Bernoulli-Euler beam is infinite. □

1.7.2 A three-dimensional Timoshenko beam element

The formulation of the beam-element stiffness matrix is now extended to three dimensions. This involves flexural displacements in two directions, axial displacements and, in addition to this, twist of the beam. It is assumed that the beam element is straight, of the length l and with constant cross-section. The element relation is described in a principal axes (x, y, z)-coordinate system with origin at the left end-section and the x-axis placed along the bending centres of the cross-sections. Only St. Venant torsion is taken into consideration. The axial stiffness EA, the shear stiffnesses GA_y and GA_z in the y- and z-directions, respectively, the torsional stiffness GK, and the principal inertial bending stiffnesses EI_y and EI_z around the y- and z-axes are all constant along the beam element.

The degrees of freedom of the element are made up by the 6 components $w_{x,j}$, $w_{y,j}$ and $w_{z,j}$, $j = 1, 2$, providing the displacements of the bending centres, and the 6 components $\theta_{x,j}$, $\theta_{y,j}$ and $\theta_{z,j}$ defining the rotation of the end-sections. Again, $j = 1$ and $j = 2$ refer to the left and right end-sections, respectively. The nodal reaction forces conjugated to the indicated degrees of freedom consist of the axial forces $Q_{y,j}$ and $Q_{z,j}$ in the y- and z-directions, respectively, the torsional moments $M_{x,j}$ and the bending moment components $M_{y,j}$ and $M_{z,j}$ in the y- and z-directions. Finally, the element loadings consist of constant loads per unit length $\{q_x, q_y, q_z\}$ and constant moment loads per unit length $\{m_x, m_y, m_z\}$ in the x-, y- and z-directions. No concentrated element forces or moments are considered. The loads q_y and q_z as well as the shear forces $Q_{y,j}$ and $Q_{z,j}$ are assumed to act through the so-called *shear centre*, leading to an uncoupling of the flexural and torsional deformations. The definition of the shear centre and further details about uncoupling of torsional and flexural displacements are given in Chapter 2.

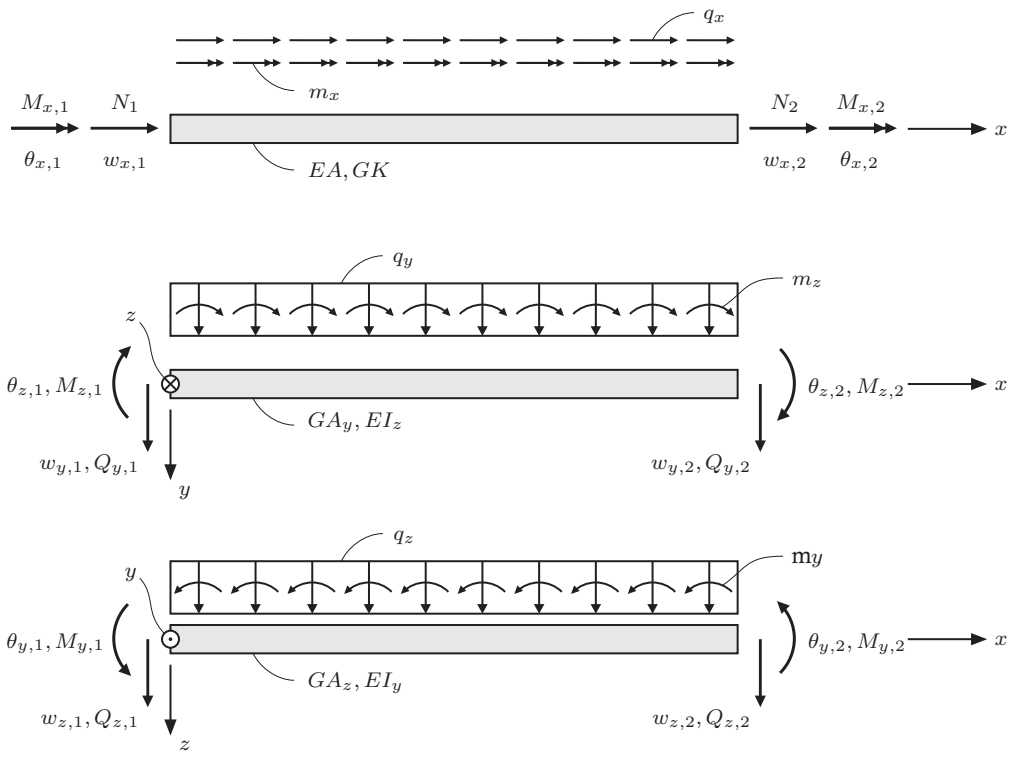

Figure 1–21 Three-dimensional Timoshenko beam element with definition of degrees of freedom, nodal reaction forces, element loads and sectional properties.

The element equilibrium equations may be expressed on the matrix form, cf. Eq. (1–86),

$$\mathbf{r_e} = \mathbf{K_e w_e} + \mathbf{f_e} \tag{1–100}$$

Here, $\mathbf{r_e}$ and $\mathbf{w_e}$ are 12-dimensional column vectors storing the reaction forces and the element degrees of freedom, respectively, cf. Eqs. (1–84) and (1–85),

$$\mathbf{r_e} = \begin{bmatrix} \mathbf{r_{e}}1 \\ \mathbf{r_{e}}2 \end{bmatrix} = \begin{bmatrix} N_1 \\ Q_{y,1} \\ Q_{z,1} \\ M_{x,1} \\ M_{y,1} \\ M_{z,1} \\ N_2 \\ Q_{y,2} \\ Q_{z,2} \\ M_{x,2} \\ M_{y,2} \\ M_{z,2} \end{bmatrix}, \qquad \mathbf{w_e} = \begin{bmatrix} \mathbf{w_{e}}1 \\ \mathbf{w_{e}}2 \end{bmatrix} = \begin{bmatrix} w_{x,1} \\ w_{y,1} \\ w_{z,1} \\ \theta_{x,1} \\ \theta_{y,1} \\ \theta_{z,1} \\ w_{x,2} \\ w_{y,2} \\ w_{z,2} \\ \theta_{x,2} \\ \theta_{y,2} \\ \theta_{z,2} \end{bmatrix}. \tag{1–101}$$

Likewise, $\mathbf{f_e}$ is 12-dimensional column vector storing the contributions to the reaction forces

from the element loads, given as, cf. Eq. (1–87),

$$\mathbf{f_e} = \begin{bmatrix} \mathbf{f_{e1}} \\ \mathbf{f_{e2}} \end{bmatrix} = \begin{bmatrix} -\frac{1}{2}q_x l \\ -\frac{1}{2}q_y l + m_z \\ -\frac{1}{2}q_z l - m_y \\ -\frac{1}{2}m_x l \\ \frac{1}{12}q_z l^2 - \frac{1}{2}\frac{\Phi_z}{1+\Phi_z}m_y l \\ -\frac{1}{12}q_y l^2 - \frac{1}{2}\frac{\Phi_y}{1+\Phi_y}m_z l \\ -\frac{1}{2}q_x l \\ -\frac{1}{2}q_y l - m_z \\ -\frac{1}{2}q_z l + m_y \\ -\frac{1}{2}m_x l \\ -\frac{1}{12}q_z l^2 - \frac{1}{2}\frac{\Phi_z}{1+\Phi_z}m_y l \\ \frac{1}{12}q_y l^2 - \frac{1}{2}\frac{\Phi_y}{1+\Phi_y}m_z l \end{bmatrix}, \tag{1–102}$$

where Φ_y and Φ_z are given as, cf. Eq. (i) in Example 1.3,

$$\Phi_y = 12\frac{EI_z}{GA_y l^2}, \qquad \Phi_z = 12\frac{EI_y}{GA_z l^2}. \tag{1–103}$$

Finally, $\mathbf{K_e}$ specifies the element stiffness given as, cf. Eq. (1–99),

$$\mathbf{K_e} = \begin{bmatrix} \frac{EA}{l} & 0 & 0 & 0 & 0 & 0 & -\frac{EA}{l} & 0 & 0 & 0 & 0 & 0 \\ 0 & k_{11}^z & 0 & 0 & 0 & k_{12}^z & 0 & k_{13}^z & 0 & 0 & 0 & k_{14}^z \\ 0 & 0 & k_{11}^y & 0 & k_{12}^y & 0 & 0 & 0 & k_{13}^y & 0 & k_{14}^y & 0 \\ 0 & 0 & 0 & \frac{GK}{l} & 0 & 0 & 0 & 0 & 0 & -\frac{GK}{l} & 0 & 0 \\ 0 & 0 & k_{12}^y & 0 & k_{22}^y & 0 & 0 & 0 & k_{23}^y & 0 & k_{24}^y & 0 \\ 0 & k_{12}^z & 0 & 0 & 0 & k_{22}^z & 0 & k_{23}^z & 0 & 0 & 0 & k_{24}^z \\ -\frac{EA}{l} & 0 & 0 & 0 & 0 & 0 & \frac{EA}{l} & 0 & 0 & 0 & 0 & 0 \\ 0 & k_{13}^z & 0 & 0 & 0 & k_{23}^z & 0 & k_{33}^z & 0 & 0 & 0 & k_{34}^z \\ 0 & 0 & k_{13}^y & 0 & k_{23}^y & 0 & 0 & 0 & k_{33}^y & 0 & k_{34}^y & 0 \\ 0 & 0 & 0 & -\frac{GK}{l} & 0 & 0 & 0 & 0 & 0 & \frac{GK}{l} & 0 & 0 \\ 0 & 0 & k_{14}^y & 0 & k_{24}^y & 0 & 0 & 0 & k_{34}^y & 0 & k_{44}^y & 0 \\ 0 & k_{14}^z & 0 & 0 & 0 & k_{24}^z & 0 & k_{34}^z & 0 & 0 & 0 & k_{44}^z \end{bmatrix}, \tag{1–104}$$

where

$$\begin{bmatrix} k_{11}^z & k_{12}^z & k_{13}^z & k_{14}^z \\ & k_{22}^z & k_{23}^z & k_{24}^z \\ & & k_{33}^z & k_{34}^z \\ & & & k_{44}^z \end{bmatrix} = \frac{EI_z}{(1+\Phi_y)l^2} \begin{bmatrix} 12 & 6l & -12 & 6l \\ & (4+\Phi_y)l^2 & -6l & (2-\Phi_y)l^2 \\ & & 12 & -6l \\ & & & (4+\Phi_y)l^2 \end{bmatrix}, \tag{1–105}$$

$$\begin{bmatrix} k_{11}^y & k_{12}^y & k_{13}^y & k_{14}^y \\ & k_{22}^y & k_{23}^y & k_{24}^y \\ & & k_{33}^y & k_{34}^y \\ & & & k_{44}^y \end{bmatrix} = \frac{EI_y}{(1+\Phi_z)l^2} \begin{bmatrix} 12 & -6l & -12 & -6l \\ & (4+\Phi_z)l^2 & 6l & (2-\Phi_z)l^2 \\ & & 12 & 6l \\ & & & (4+\Phi_z)l^2 \end{bmatrix}. \tag{1–106}$$

The element equilibrium relation provided by Eq. (1–100) presumes that only St. Venant torsion is taken into consideration, corresponding to the torsional equilibrium equations

$$\begin{bmatrix} M_{x,1} \\ M_{x,2} \end{bmatrix} = \frac{GK}{l} \begin{bmatrix} 1 & -1 \\ -1 & 1 \end{bmatrix} \begin{bmatrix} \theta_{x,1} \\ \theta_{x,2} \end{bmatrix} - \frac{1}{2} m_x l \begin{bmatrix} 1 \\ 1 \end{bmatrix}. \tag{1–107}$$

The torsional constant K is determined in the next chapter. It will be shown that the inclusion of Vlasov torsion requires the introduction of two extra degrees of freedom $\frac{d\theta_{x,1}}{dx}$ and $\frac{d\theta_{x,2}}{dx}$. The conjugated generalised stresses are the so-called bimoments. Hence, a Timoshenko beam element, where both St. Venant and Vlasov torsion are taken into consideration, is described by a total of 14 degrees of freedom.

1.8 Summary

In this chapter, the basic theory of Timoshenko and Bernoulli-Euler beams in three-dimensional space has been presented. Some of the main topics covered are summarised below.

Beams are one-dimensional structures that may carry loads in three dimensions including axial forces, shear forces in two orthogonal directions and moments around three directions.

Bernoulli-Euler beam kinematics assume that cross-sections remain orthogonal to the beam axis during deformation. Hence, no shear deformation occurs.

Timoshenko beam kinematics include shear flexibility, but still a cross-section remains plane during deformation. Hence, shear strains and stresses are homogeneous over the beam height.

The bending centre of a beam cross-section is defined as the point of attack of an axial force not producing a bending moment.

The principal axes of a beam cross-section are defined as the axes around which a bending moment will neither produce an axial force nor flexural displacements in the other direction.

The principle of virtual forces can by applied to the analysis of deformations in a beam. In the case of Timoshenko beam theory, both shear and bending deformation occurs, whereas only bending deformation is present in a Bernoulli-Euler beam.

Plane beam elements have six degrees of freedom with three at either end, *i.e.* two displacements and one in-plane rotation. In the general case, the rotations and the axial displacements are coupled, but in a principle-axes description, they become uncoupled.

Spatial beam elements have 12 degrees of freedom, that is three displacements and three rotations at either end. Generally, the displacements and rotations are coupled, but an uncoupling can be achieved by a proper choice of coordinate system.

Thus, a detailed description has been given of the lateral and flexural deformations in a beam. However, in this chapter only a brief introduction has been given to twist and torsion of a beam. A thorough explanation and analysis of these phenomena will be the focus of the next chapter.

CHAPTER 2
Shear stresses in beams due to torsion and bending

In this chapter, a theoretical explanation is given for the shear forces in beams stemming from bending as well as torsion. In this regard, the coupling of torsion and bending is discussed, and the so-called shear centre is introduced. The derivations are confined to homogeneous torsion, or St. Venant torsion. Later, the strains and stresses provided in the case of non-homogeneous torsion, or Vlasov torsion, will be dealt with.

2.1 Introduction

When the beam is exposed to the loads per unit length q_y and q_z, the beam will generally deform with bending deformations $\{u_y, \theta_z\}$ and $\{u_z, \theta_y\}$, respectively. Depending on the line of action of these loads, the bending deformations will be combined with a torsional rotation θ_x around the x-axis as illustrated in Fig. 2–1a and Fig. 2–1c. Under certain conditions, the bending of the beam is not associated with a torsional deformation. This happens if the loads per unit length q_y and q_z, the reaction forces at the ends of the beam as well as the shear forces Q_y and Q_z are acting through a special point S, known as the *shear centre*, as illustrated in Fig. 2–1b.

When this is the case, torsion is caused solely by the moment load m_x per unit length, which in part includes contributions from the translation of q_y and q_z to S. These torsional deformations take place without bending deformation as illustrated in Fig. 2–1d. Hence, bending and torsion can be analysed independently.

The position of the shear centre depends on the geometry of the cross-section and is generally different from the position of the bending centre B. However, for double-symmetric cross-sections, the positions of the bending and torsion centres will coincide.

The shear forces Q_y and Q_z as well as the torsional moment M_x bring about shear stresses σ_{xy} and σ_{xz} on the beam section. In what follows these will be determined independently for the two deformation mechanisms. Hence, q_y and q_z are presumed to be referred to the shear centre. The shear stresses caused by the torsional moment M_x are statically equivalent to the shear forces $Q_y = Q_z = 0$. The position of the shear centre has no influence on the distribution of shear stresses in this case.

Likewise, in the decoupled bending problem, in which the cross-section is exposed to the shear forces Q_y and Q_z, the position of the shear centre is determined from the requirement that the resulting shear stresses are statically equivalent to Q_y and Q_z, and produce the torsional moment $M_x = 0$ around S.

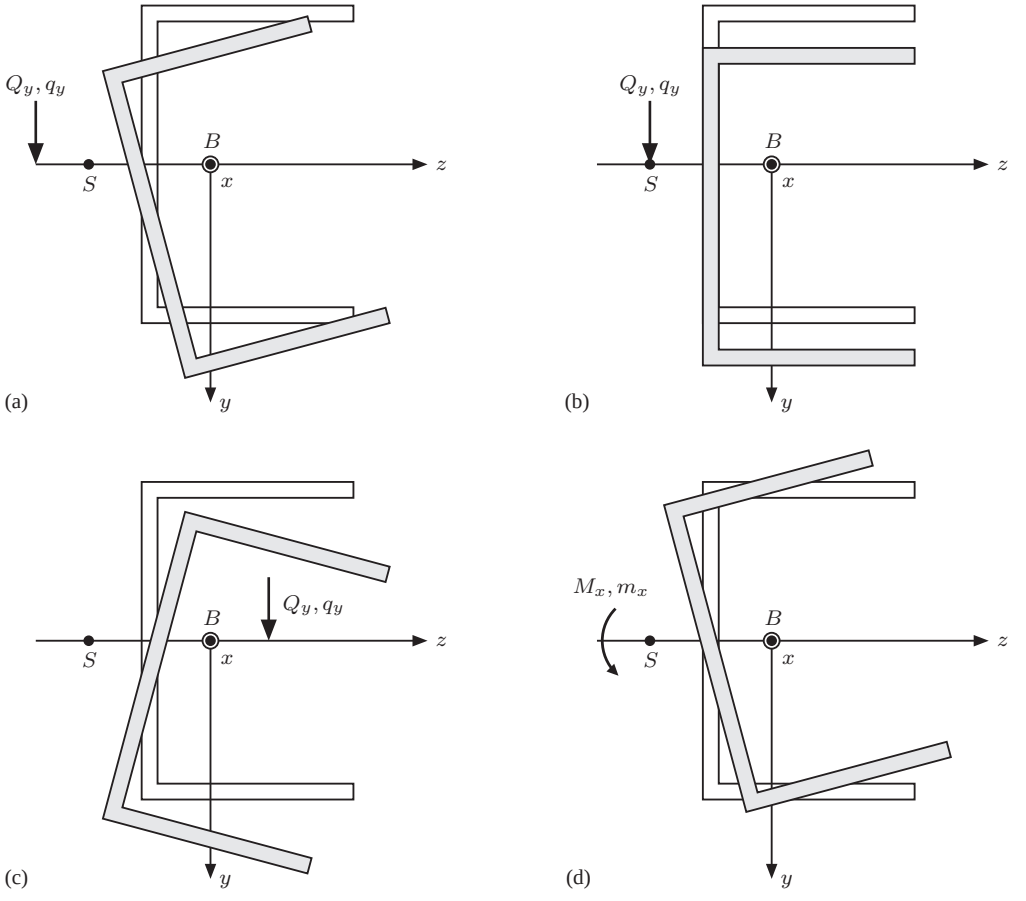

Figure 2–1 Coupled and uncoupled bending and torsion. Coupling exists in cases (a) and (c), whereas cases (b) and (d) involve no coupling.

2.2 Homogeneous torsion (St. Venant torsion)

It is assumed that the torsional moment M_x and the incremental twist per unit length $d\theta_x/dx$ and the warping of the cross-sections remain unchanged along the beam. Then all cross-sections of the beam are exposed to the same distribution of the shear stresses σ_{xy} and σ_{xz}. For this reason, this case is referred to as *homogeneous torsion*. Since the solution of the problem was given by St. Venant (ref.), the case is also called *St. Venant torsion*. Inhomogeneous torsion refers to the case, where either M_x or the material properties vary along the beam. Then $d\theta_x/dx$ or the warping will vary as well.

Figure 2–2a shows a cross-section of a cylindrical beam of the length l. The cross-sectional area is A. The curve along the outer periphery is denoted Γ_0. The cross-section may have a number N of holes determined by the boundary curves Γ_j, $j = 1, 2, \ldots, N$. At the boundary curves arc-length coordinates $s_0, s_1, \ldots, s_N$ are defined. The arc-length coordinate s_0 along Γ_0 is orientated in the anti clock-wise direction, whereas $s_1, s_2, \ldots, s_N$, related to the interior boundaries $\Gamma_1, \Gamma_2, \ldots, \Gamma_N$, are orientated in the clock-wise direction. The outward directed unit

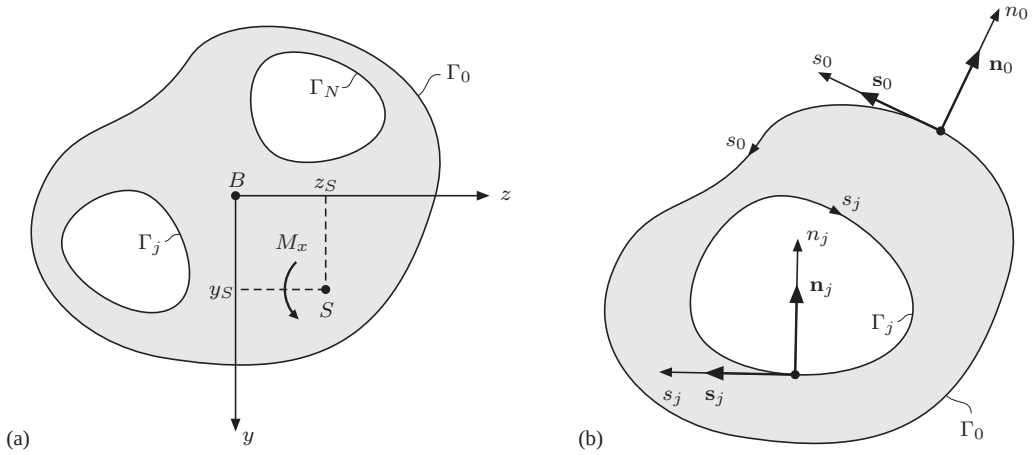

Figure 2–2 Cross-section with holes: (a) Interior and exterior edges; (b) definition of local (x, n_j, s_j)-coordinate systems.

vector on a point of the exterior or interior boundaries Γ_j is denoted $\mathbf{n}_j$, $j = 0, 1, \ldots, N$. The unit tangential vector to a boundary curve is denoted $\mathbf{s}_j$ and is co-directional to the arc-length coordinate s_j, see Fig. 2–2b. Thus, a local (x, n_j, s_j)-coordinate system may be defined with the base unit vectors $\{\mathbf{i}, \mathbf{n}_j, \mathbf{s}_j\}$. The indicated orientation of the exterior and interior arc-length coordinates s_j, $j = 0, 1, \ldots, N$, insures that the related (x, n_j, s_j)-coordinate system forms a right-hand coordinate system.

The beam material is assumed to be homogeneous, isotropic linear elastic with the shear modulus G. In homogeneous torsion, only shear stresses are present for which reason G is the only needed elasticity constant.

2.2.1 Basic assumptions

For convenience the index x is omitted on the twist θ_x (the rotation angle around the x-axis), *i.e.* $\theta \sim \theta_x$. Figure 2–3 shows a differential beam element of the length dx. Both end-sections of the element are exposed to the torsional moment M_x, so the element is automatically in equilibrium. On the left and right end-sections the twists are θ and $\theta + d\theta$, respectively. The increment $d\theta$ may be written as

$$d\theta = \frac{d\theta}{dx} dx. \tag{2–1}$$

Since M_x and the material properties are the same in all cross-sections, $d\theta/dx$ must be constant along the beam. Further, the warping must be the same in all cross-sections, *i.e.* $u_x = u_x(y, z)$. This implies that the warping in homogeneous torsion does not induce normal strains, *i.e.*

$$\varepsilon_{xx} = \frac{\partial u_x}{\partial x} = 0. \tag{2–2}$$

In turn this means that the normal stress becomes $\sigma_{xx} = E\varepsilon_{xx} = 0$. Hence, only the shear stresses σ_{xy} and σ_{xz} are present on a cross-section in homogeneous torsion.

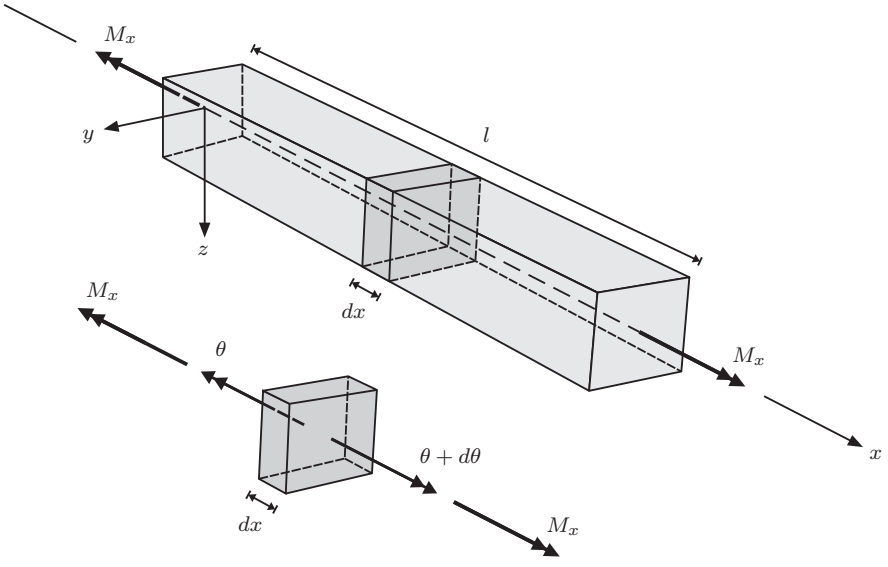

Figure 2–3 Beam and differential beam element subjected to homogeneous torsion.

The only deformation measure of the problem is the twist gradient $d\theta/dx$. Then, due to the linearity assumptions, the torsional moment M_x must depend linearly on $d\theta/dx$. Further, σ_{xy} and σ_{xz} (and hence M_x) depend linearly on G. This implies the following relation:

$$M_x = GK\frac{d\theta}{dx}. \tag{2–3}$$

The proportionality constant K with the dimension [unit of length]^4 is denoted the *torsional constant*. The determination of this constant is a part of the solution of the torsion problem.

2.2.2 Solution of the homogeneous torsion problem

As for all beam theories, the shape of the cross-section is assumed to be preserved during the deformation. Then, the displacements in the (y, z)-plane are caused merely by the rotation θ around the shear centre S. The warping displacements u_x must also be linearly dependent on the strain measure $d\theta/dx$, corresponding to the last term in Eq. (1–13). This implies the displacement components

$$u_x = u_x(y, z) = \omega(y, z)\frac{d\theta}{dx}, \qquad u_y = -(z - z_s)\theta, \qquad u_z = (y - y_s)\theta. \tag{2–4}$$

Here $\omega(y, z)$ is the so-called *warping function* as discussed in Section 1.2.2, and its determination constitutes the basic part of the solution of the homogeneous torsion problem.

Similarly to Eq. (1–14), it follows from Eq. (2–4) that the components of the strain tensor become:

$$\varepsilon_{xx} = \frac{\partial u_x}{\partial x} = 0, \qquad \varepsilon_{yy} = \frac{\partial u_y}{\partial y} = 0, \qquad \varepsilon_{zz} = \frac{\partial u_z}{\partial z} = 0, \tag{2–5a}$$

$$\varepsilon_{yz} = \frac{1}{2}\left(\frac{\partial u_y}{\partial z} + \frac{\partial u_z}{\partial y}\right) = \frac{1}{2}(-\theta + \theta) = 0, \tag{2–5b}$$

$$\varepsilon_{xy} = \frac{1}{2}\left(\frac{\partial u_x}{\partial y} + \frac{\partial u_y}{\partial x}\right) = \frac{1}{2}\left(\frac{\partial \omega}{\partial y} - (z - z_s)\right)\frac{d\theta}{dx}, \tag{2–5c}$$

$$\varepsilon_{xz} = \frac{1}{2}\left(\frac{\partial u_x}{\partial z} + \frac{\partial u_z}{\partial x}\right) = \frac{1}{2}\left(\frac{\partial \omega}{\partial z} + (y - y_s)\right)\frac{d\theta}{dx}. \tag{2–5d}$$

As seen only ε_{xy} and ε_{xz} are non-vanishing. Correspondingly, all components of the Cauchy stress tensor become equal to zero, save the shear stresses σ_{xy} and σ_{xz}. These are given as

$$\sigma_{xy} = \sigma_{xy}(y,z) = 2G\varepsilon_{xy} = G\left(\frac{\partial \omega}{\partial y} - (z - z_s)\right)\frac{d\theta}{dx}, \tag{2–6a}$$

$$\sigma_{xz} = \sigma_{xz}(y,z) = 2G\varepsilon_{xz} = G\left(\frac{\partial \omega}{\partial z} + (y - y_s)\right)\frac{d\theta}{dx}. \tag{2–6b}$$

Ignoring the volume loads, the equilibrium equations read

$$\frac{\partial \sigma_{xx}}{\partial x} + \frac{\partial \sigma_{xy}}{\partial y} + \frac{\partial \sigma_{xz}}{\partial z} = 0, \tag{2–7a}$$

$$\frac{\partial \sigma_{xy}}{\partial x} + \frac{\partial \sigma_{yy}}{\partial y} + \frac{\partial \sigma_{yz}}{\partial z} = 0, \tag{2–7b}$$

$$\frac{\partial \sigma_{xz}}{\partial x} + \frac{\partial \sigma_{yz}}{\partial y} + \frac{\partial \sigma_{zz}}{\partial z} = 0. \tag{2–7c}$$

With $\sigma_{xx} = \sigma_{yy} = \sigma_{zz} = \sigma_{yz} = 0$, and σ_{xy} and σ_{xz} only dependent on y and z, the two last equations are identically fulfilled, and the first equation reduces to

$$\frac{\partial \sigma_{xy}}{\partial y} + \frac{\partial \sigma_{xz}}{\partial z} = 0. \tag{2–8}$$

Equation (2–8) may be formulated at a point on the boundary curve Γ_j, $j = 0, 1, \ldots, N$, in the related local (x, n_j, s_j)-coordinate system. Ignoring the index j, the non-trivial equilibrium equation then reads

$$\frac{\partial \sigma_{xn}}{\partial n} + \frac{\partial \sigma_{xs}}{\partial s} = 0, \tag{2–9}$$

where σ_{xn} and σ_{xs} denote the shear stresses along the local n- and s-axes. According to Cauchy's boundary condition (ref.), σ_{xn} can be expressed in terms of the shear stress components σ_{xy} and σ_{xz} as

$$\sigma_{xn} = \sigma_{xy} n_y + \sigma_{xz} n_z. \tag{2–10}$$

Here n_y and n_z denote the components of the unit normal vector $\mathbf{n}$ along the y- and z-axes.

The symmetry of the stress tensor implies that $\sigma_{xn} = \sigma_{nx}$. Further, since the exterior and all interior surfaces are free of surface traditions, corresponding to $\sigma_{nx} = 0$, it follows that $\sigma_{xn} = 0$ (see Fig. 2–4). Then, Eq. (2–10) reduces to

$$\sigma_{xy} n_y + \sigma_{xz} n_z = 0. \tag{2–11}$$

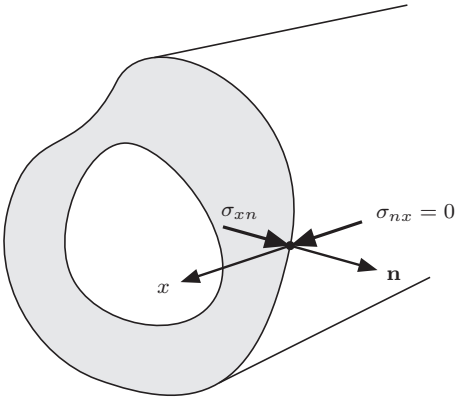

Figure 2–4 Shear stress in the normal direction at an exterior or interior boundary.

Finally, insertion of Eq. (2–6) into Eq. (2–11) provides the following boundary condition formulated in the warping function

$$\frac{\partial \omega}{\partial y} n_y + \frac{\partial \omega}{\partial z} n_y - (z - z_s) n_y + (y - y_s) n_z = 0 \qquad \Rightarrow$$
$$\frac{\partial \omega}{\partial n} = (z - z_s) n_y - (y - y_s) n_z, \tag{2–12}$$

where $\partial\omega/\partial n$ denotes the partial derivative of ω in the direction of the outward directed unit normal.

Equation (2–12) must be fulfilled at the exterior and all interior boundaries. The partial differential for ω to be fulfilled in the interior A of the profile follows from insertion of Eq. (2–6) into the equilibrium equation (2–8), leading to

$$\frac{\partial^2 \omega}{\partial y^2} + \frac{\partial^2 \omega}{\partial z^2} = 0. \tag{2–13}$$

If a solution to Eq. (2–13) with the boundary conditions (2–12) is obtained, the shear stresses are subsequently determined from Eq. (2–10). Equation (2–13) is Laplace's differential equation, and the boundary conditions Eq. (2–13) are classified as the so-called Neumann boundary conditions. Notice that the solution to Eqs. (2–12) and (2–13) is not unique. Actually, if $\omega(y, z)$ is a solution, then $\omega(y, z) + \omega_0$ will be a solution as well, where ω_0 is an arbitrary constant. Since the shear stresses are determined by partial differentiation of the of the warping function, all these solutions lead to the same stresses. The boundary value problem for the warping function has been summarised in Box 2.1.

Box 2.1 Boundary value problem for the warping function

The differential equation, representing the non-trivial equation of equilibrium, reads:

$$\frac{\partial^2\omega}{\partial y^2}+\frac{\partial^2\omega}{\partial z^2}=0, \qquad (y,z)\in A. \tag{2–14a}$$

The Neumann boundary condition, representing the relevant Cauchy boundary condition, reads:

$$\frac{\partial\omega}{\partial n}=(z-z_s)n_y-(y-y_s)n_z, \qquad (y,z)\in\Gamma_0\cup\Gamma_1\cup\cdots\cup\Gamma_N. \tag{2–14b}$$

An alternative formulation for the solution of the problem can be obtained by the introduction of the so-called *Prandtl's stress function* S with the defining properties

$$\sigma_{xy}=\frac{\partial S}{\partial z}, \qquad \sigma_{xz}=-\frac{\partial S}{\partial y}. \tag{2–15}$$

Upon insertion of Eq. (2–15) into Eq. (2–9), the equilibrium equation is seen to be identical fulfilled, *i.e.*

$$\frac{\partial\sigma_{xy}}{\partial y}+\frac{\partial\sigma_{xz}}{\partial z}=\frac{\partial^2 S}{\partial y\partial z}-\frac{\partial^2 S}{\partial z\partial y}\equiv 0. \tag{2–16}$$

From Eq. (2–6) follows

$$\frac{\partial\sigma_{xy}}{\partial z}-\frac{\partial\sigma_{xz}}{\partial y}=\left(\frac{\partial^2\omega}{\partial z\partial y}-1\right)G\frac{d\theta}{dx}-\left(\frac{\partial^2\omega}{\partial y\partial z}+1\right)G\frac{d\theta}{dx}=-2G\frac{d\theta}{dx}. \tag{2–17}$$

Then, the differential equation for S is obtained by insertion of Eq. (2–15) on the left-hand side of Eq. (2–17), leading to

$$\frac{\partial^2 S}{\partial y^2}+\frac{\partial^2 S}{\partial z^2}=-2G\frac{d\theta}{dx}. \tag{2–18}$$

Equation (2–18) is a compatibility condition for S in order that the kinematical conditions (2–6) are fulfilled.

The boundary condition for S follow upon insertion of Eq. (2–15) into Eq. (2–11), *i.e.*

$$\frac{\partial S}{\partial z}n_y-\frac{\partial S}{\partial y}n_z=0 \tag{2–19}$$

The tangential unit vector is given as $\mathbf{s}^T=[s_y,s_z]=[-n_z,n_y]$, cf. Fig. 2–2b, where $\{n_y,n_z\}$ denotes the Cartesian components of the outward directed unit normal vector at any of the boundary curves Γ_j, $j=0,1,\ldots,N$, cf. Fig. 2–2b. Then, Eq. (2–19) may be written as

$$\frac{\partial S}{\partial y}s_y+\frac{\partial S}{\partial z}s_z=\frac{\partial S}{\partial s}=0. \tag{2–20}$$

where $\partial S/\partial s$ denotes the directional derivative of S in the direction of the tangential unit vector $\mathbf{s}$. Equation (2–20) implies that S is constant along the exterior and the interior boundary curves, *i.e.*

$$S=S_j, \qquad j=0,1,\ldots,N. \tag{2–21}$$

Equation (2–18) is a Poisson differential equation (inhomogeneous Laplace equation), and the boundary conditions Eq. (2–21) are classified as the so-called Dirichlet boundary conditions. In principle, the solution to the indicated boundary value problem is unique. The problem is that the constant values S_j of the stress function along the boundary curves are unknown. The determination of these is a part of the problem. For profiles with interior holes this is only possible by the introduction of additional geometric conditions. The boundary value problem for the Prandtl stress function has been summarised in Box 2.2. The formulation in terms of Prandtl's stress function is especially useful in relation to homogeneous torsion of thin-walled profiles and will be utilised in a number of examples below.

Box 2.2 Boundary value problem for the Prandtl stress function

The equilibrium equation is automatically fulfilled. The compatibility condition is represented by the following differential equation:

$$\frac{\partial^2 S}{\partial y^2} + \frac{\partial^2 S}{\partial z^2} = -2G\frac{d\theta}{dx}, \qquad (x,y) \in A. \tag{2–22a}$$

The Dirichlet boundary condition, representing the Cauchy boundary condition, reads:

$$S = S_j, \qquad j = 0, 1, \ldots, N, \qquad (x,y) \in \Gamma_0 \cup \Gamma_1 \cup \cdots \cup \Gamma_N. \tag{2–22b}$$

The shear stresses σ_{xy} and σ_{xz} must be statically equivalent to the shear forces $Q_y = Q_z = 0$ and the torsional moment M_x. Application of Gauss's theorem on the vector field $\mathbf{v}^T = [v_y, v_z] = [0, S]$ provides,

$$Q_y = \int_A \sigma_{xy} dA = \int_A \left(\frac{\partial 0}{\partial y} + \frac{\partial S}{\partial z}\right) dA = \sum_{j=0}^{N} \oint_{\Gamma_j} (0 \cdot dz - S \cdot dy) = -\sum_{j=0}^{N} S_j \oint_{\Gamma_j} dy, \tag{2–23}$$

where the circulation is taken anticlockwise along Γ_0 and clockwise along $\Gamma_j, j = 1, \cdots, N$. Further it has been used that S_j is constant along the boundary curve, and hence may be transferred outside the circulation integral. Now, $\oint_{\Gamma_j} dy = 0$. Hence, it follows that any solution to the boundary value problem defined by Eqs. (2–22a) and (2–22b) automatically provides a solution fulfilling $Q_y = 0$. Using $\mathbf{v}^T = [S, 0]$ it can in the same way be shown that

$$Q_z = \int_A \sigma_{xz} dA = -\int_A \left(\frac{\partial S}{\partial y} + \frac{\partial 0}{\partial z}\right) dA \qquad \Rightarrow$$
$$Q_z = -\sum_{j=0}^{N} \oint_{\Gamma_j} (S \cdot dz - 0 \cdot dy) = -\sum_{j=0}^{N} S_j \oint_{\Gamma_j} dz = 0. \tag{2–24}$$

The torsional moment M_x must be statically equivalent to the moment of the shear stresses around S, *i.e.*

$$M_x = \int_A \left((y - y_S)\sigma_{xz} - (z - z_S)\sigma_{xy}\right) dA = \int_A (y\sigma_{xz} - z\sigma_{xy}) dA, \tag{2–25}$$

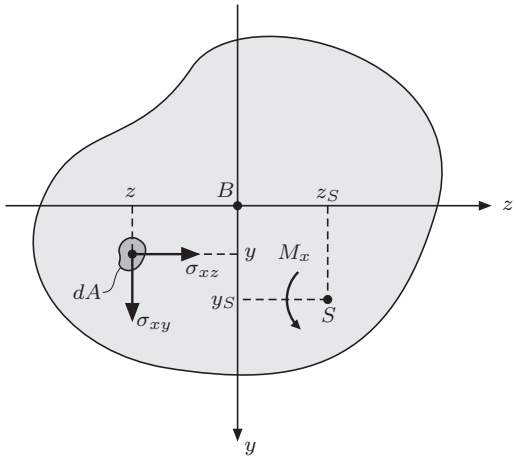

Figure 2–5 Static equivalence of torsional moment to shear stresses.

where it has been used that $\int_A \sigma_{xy} dA = \int \sigma_{xz} dA = 0$. Next, insertion of Eq. (2–15) provides

$$M_x = -\int_A \left(y\frac{\partial S}{\partial y} + z\frac{\partial S}{\partial z} \right) dA = -\int_A \left(\frac{\partial}{\partial y}(yS) + \frac{\partial}{\partial z}(zS) \right) dA + 2\int_A S dA. \tag{2–26}$$

The divergence theorem with $\mathbf{v}^T = [yS, zS]$ provides

$$\int_A \left(\frac{\partial}{\partial y}(yS) + \frac{\partial}{\partial z}(zS) \right) dA = \sum_{j=0}^{N} \oint_{\Gamma_j} (yS dz - zS dy) = \sum_{j=0}^{N} S_j \oint_{\Gamma_j} (y dz - z dy). \tag{2–27}$$

Let A_0 and A_j denote the area inside the boundary curves Γ_0 and Γ_j. Then, use of Eq. (1–4a) in Eq. (2–27) provides

$$\int_A \left(\frac{\partial}{\partial y}(yS) + \frac{\partial}{\partial z}(zS) \right) dA = 2A_0 S_0 - \sum_{j=1}^{N} 2A_j S_j. \tag{2–28}$$

The negative sign of the last term is because the circulation on the interior boundaries is taken clockwise, cf. the discussion subsequent to Eq. (1–4a). Insertion of Eq. (2–28) gives the following final result:

$$M_x = -2A_0 S_0 + 2\int_A S dA + 2\sum_{j=1}^{N} A_j S_j. \tag{2–29}$$

The shear stresses remain unchanged if an arbitrary constant is added to S. Then, without restriction one can choose $S_0 = 0$, which is assumed in what follows.

Let the domain of definition for $S(y, z)$ be extended to the interior of the holes, where $S(y, z)$ is given the same value S_j as the boundary value along the holes. With $S_0 = 0$, Eq. (2–29) determines M_x as twice the volume below $S(y, z)$. Further, with $S(x, y)$ determined along with

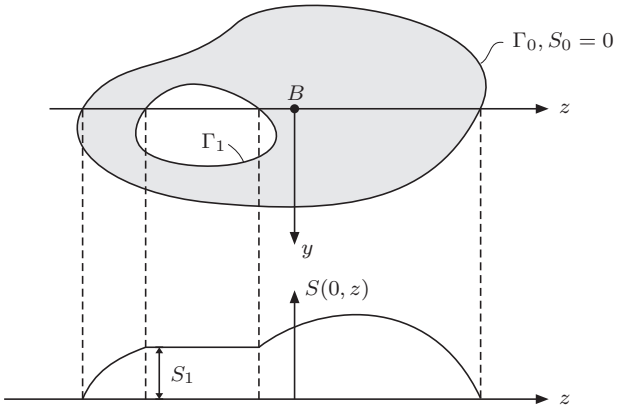

Figure 2–6 Variation of Prandtl's stress function over a cross-section with a hole.

the boundary values S_j, $j = 1, 2, \ldots, N$, the torsional constant K can next be determined upon comparison of Eqs. (2–3) and (2–29). This is illustrated by examples below.

It is remarkable that no reference is made to the position of the shear centre, neither in the boundary value problem (2–22), for the Prandtl stress function, nor in the expression (2–25) for the torsional moment. In contrast, the coordinates of the shear centre enter the boundary value problem (2–14) for the warping function.

Defining the same homogeneous torsion problem, the warping function and Prandtl's stress function cannot be independent function. The relation follows from a comparison of Eqs. (2–6) and (2–15):

$$\frac{\partial S}{\partial z} = \left(\frac{\partial \omega}{\partial y} - (z - z_s) \right) G \frac{d\theta}{dx}, \tag{2–30a}$$

$$-\frac{\partial S}{\partial y} = \left(\frac{\partial \omega}{\partial z} + (y - y_s) \right) G \frac{d\theta}{dx}, \tag{2–30b}$$

where it is recalled that $\theta \sim \theta_x$.

Example 2.1 Homogeneous torsion of infinitely long rectangular cross-section

Figure A shows an infinitely long rectangular cross-section with the thickness t exposed to a torsional moment M_x. The torsional moment is carried by shear stresses uniformly distributed in the y-direction. Then, $S = S(z)$ is independent of y, and the boundary value problem (2–22) reduces to

$$\frac{d^2 S}{dz^2} = -2G \frac{d\theta}{dx}, \qquad S(-t/2) = S(t/2) = 0 \tag{a}$$

with the solution

$$S(z) = -\frac{1}{4}(4z^2 - t^2) G \frac{d\theta}{dx}. \tag{b}$$

(continued)

The shear stresses follow from Eq. (2–15):

$$\sigma_{xy} = \frac{\partial S}{\partial z} = -2zG\frac{d\theta}{dx}, \qquad \sigma_{xz} = 0. \tag{c}$$

The shear stresses are linearly distributed in the thickness direction, and has been illustrated in Fig. A.

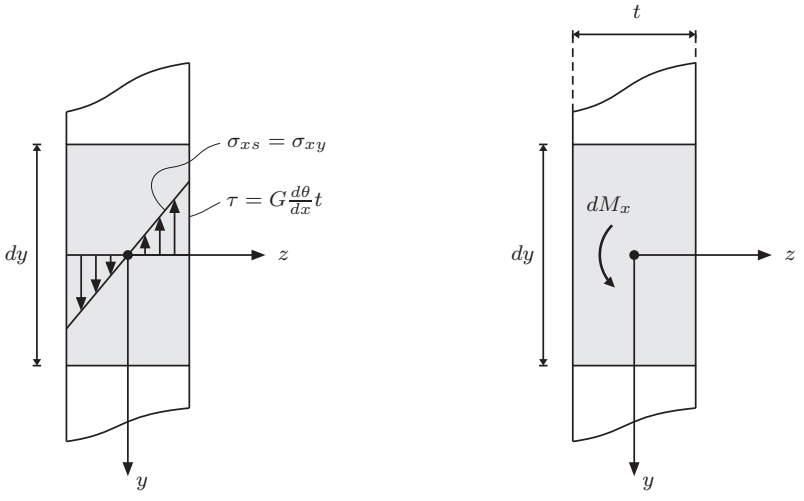

Figure A Torsion of a infinitely long rectangular cross-section: Distribution of shear stresses (left); torsional moment on differential cross-sectional segment (right).

Due to the independence of the shear stresses on y, the torsional problem can be analysed by merely considering a differential cross-sectional segment of the length dy exposed to the torsional moment dMx, see Fig. A. The increment dMx is related to the stress function by Eq. (2–28), *i.e.*

$$dM_x = 2\int_{-t/2}^{t/2} S(z)dzdy = \frac{1}{2}dyG\frac{d\theta}{dx}, \quad \int_{-t/2}^{d/2}(4z^2 - t^2)dz = \frac{1}{3}t^3 dyG\frac{d\theta}{dx}. \tag{d}$$

At the same time $dM_x = GdKd\theta/dx$, where dK denotes the torsional constant related to the differential segment. As seen from Eq. (d), this is given as

$$dK = \frac{1}{3}d^3dy. \tag{e}$$

The value dK of the torsional constant for the differential segment will be applied below. □

Example 2.2 Homogeneous torsion of a solid ellipsoidal cross-section

Figure A shows an ellipsoidal cross-section without holes with semi-axes a and b, exposed to a torsional moment M_x. At first, it is verified that the Prandtl's stress-function of this problem is given as

$$S(y,z) = -\frac{a^2b^2}{a^2+b^2}\left(\frac{y^2}{a^2} + \frac{z^2}{b^2} - 1\right)G\frac{d\theta}{dx}. \tag{a}$$

(continued)

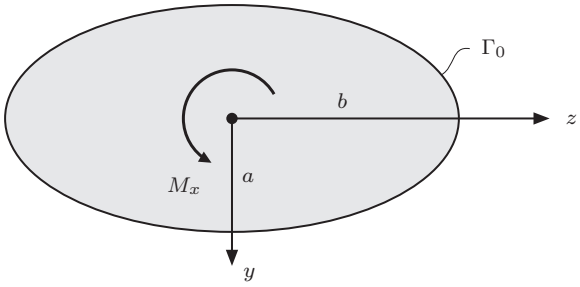

Figure A Ellipsoidal cross-section.

The boundary curve Γ_0 is described by the ellipsis

$$\frac{y^2}{a^2}+\frac{z^2}{b^2}=1. \tag{b}$$

Hence, $S(x,y)=0$ for $(y,z)\in\Gamma_0$, so the boundary condition (2–22b) is fulfilled by Eq. (a). The Laplacian of $s(y,z)$ becomes

$$\frac{\partial^2 S}{\partial y^2}+\frac{\partial^2 S}{\partial z^2}=-\frac{a^2b^2}{a^2+b^2}\left(\frac{2}{a^2}+\frac{2}{b^2}\right)G\frac{d\theta}{dx}=-2G\frac{d\theta}{dx}. \tag{c}$$

Then, also the differential equation (2–22a) is fulfilled, from which is concluded that Eq. (a) is indeed the solution to the homogeneous torsion problem.

From Eq. (2–29) follows that

$$M_x=2\int_A S\,dA=-2\frac{a^2b^2}{a^2+b^2}G\frac{d\theta}{dx}\int_A\left(\frac{y^2}{a^2}+\frac{z^2}{b^2}-1\right)dA=\pi\frac{a^3b^3}{a^2+b^2}G\frac{d\theta}{dx}, \tag{d}$$

where the following result has been utilised:

$$\int_A\left(\frac{y^2}{a^2}+\frac{z^2}{b^2}-1\right)dA=-\frac{\pi}{2}ab. \tag{e}$$

From Eq. (2–3) and Eq. (d) follows that the torsional constant for an ellipsoidal cross-section becomes:

$$K=\pi\frac{a^3b^3}{a^2+b^2}. \tag{f}$$

$Gd\theta/dx$ follows from Eq. (d), *i.e.*

$$G\frac{d\theta}{dx}=\frac{1}{\pi}\frac{a^2+b^2}{a^3b^3}M_x. \tag{g}$$

Then, the shear stresses become, cf. Eqs. (2–15) and (a):

$$\sigma_{xy}=\frac{\partial S}{\partial z}=-\frac{2z}{b^2}\frac{a^2b^2}{a^2+b^2}\cdot\frac{1}{\pi}\frac{a^2+b^2}{a^3b^3}M_x=-\frac{2}{\pi}\frac{M_x}{ab^3}z, \tag{h}$$

$$\sigma_{xz}=-\frac{\partial S}{\partial y}=\frac{2y}{a^2}\frac{a^2b^2}{a^2+b^2}\cdot\frac{1}{\pi}\frac{a^2+b^2}{a^3b^3}M_x=\frac{2}{\pi}\frac{M_x}{a^3b}y. \tag{i}$$

(continued)

The warping of the cross-section is given by Eq. (2–4). Due to the symmetry of the cross-section, it is observed that $y_s = z_s = 0$, *i.e.* the shear centre coincides with the bending centre. Then, the warping function is determined from, cf. Eq. (2–30):

$$\frac{\partial \omega}{\partial y} = \frac{1}{Gd\theta/dx}\frac{\partial S}{\partial z} + z = -\frac{2a^2}{a^2+b^2}z + z = \frac{b^2-a^2}{b^2+a^2}z, \tag{j}$$

$$\frac{\partial \omega}{\partial z} = -\frac{1}{Gd\theta/dx}\frac{\partial S}{\partial y} - y = \frac{2b^2}{a^2+b^2}y - y = \frac{b^2-a^2}{b^2+a^2}y. \tag{k}$$

The solution to Eqs. (j) and (k) is given as

$$\omega(y,z) = \frac{b^2-a^2}{b^2+a^2}yz. \tag{l}$$

It is left as an exercise to prove that Eq. (l) fulfils the boundary value problem (2–14).

The warping follows from Eq. (2–4), Eq. (g) and Eq. (l)

$$u_x(y,z) = \omega(y,z)\frac{d\theta}{dx} = \frac{b^2-a^2}{a^2+b^2}yz \cdot \frac{1}{\pi}\frac{a^2+b^2}{a^3b^3}\frac{M_x}{G} \frac{1}{\pi}\frac{b^2-a^2}{a^3b^3}yz\frac{M_x}{G}. \tag{m}$$

The solution (l) has been chosen so that the warping from torsion provided by Eq. (m) is zero at the bending centre. This will generally be presumed in what follows. Then, the displacement of the bending centre in the x-direction is caused entirely by the axial force N. Finally, it is noted that, especially for a circular profile with $a = b$, the warping vanishes everywhere on the profile. □

2.2.3 Homogeneous torsion of open thin-walled cross-sections

Figure 2–7 shows an open cross-section of a cylindrical beam. An arc-length coordinate s is defined along the midpoints of the profile wall, where $s = 0$ is chosen at one of the free ends, and $s = L$ at the other free. Further, L specifies the total length of the profile wall, and the wall thickness at arc-length coordinate s is denoted $t(s)$.

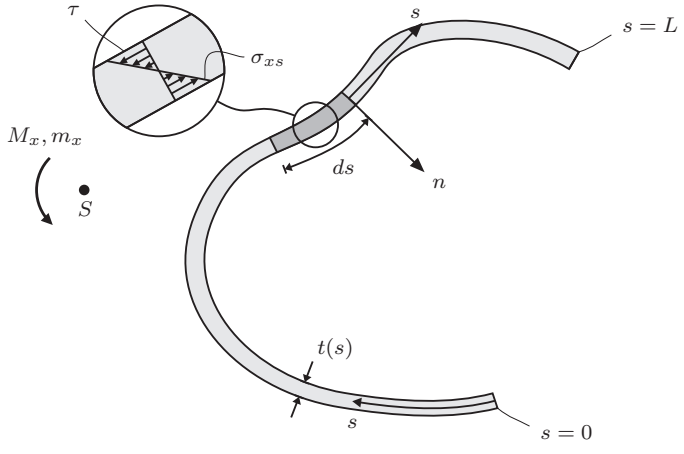

Figure 2–7 Open thin-walled cross-section of cylindrical beam exposed to homogeneous torsion.

For thin-walled cross-sections it is assumed that $t(s) \ll L$. Then, the profile can be considered as built-up of differential rectangles of the length ds, similar to those considered in Example 2.2. Each has the torsional constant $dK = \frac{1}{3}t^3(s)ds$, cf. Eq. (e) in Example 2.2. Hence, the torsional constant for the whole profile is given as

$$K = \frac{1}{3}\int_L t^3(s)ds, \tag{2–33}$$

where the index L indicates that the line integral is extended over the whole length of the profile measured along the profile wall.

The shear stresses are specified in a local (x, n, s)-coordinate system as shown in Fig. 2–7. These coordinates follow from Eq. (c) upon replacing y with s and z with w. Then,

$$\sigma_{xs} = 2nG\frac{d\theta}{dx}, \qquad \sigma_{xn} = 0. \tag{2–34}$$

Finally, using $Gd\theta/dx = M_x/K$, the maximum shear stresses for $n = t(s)/2$ becomes

$$\tau = G\frac{d\theta}{dx}t(s) = \frac{M_x}{K}t(s). \tag{2–35}$$

The computation of the shear stress in a U-profile is considered in the example below.

Example 2.3 Homogeneous torsion of a U-profile

Figure A shows a U-profile exposed to homogeneous torsion from the torsional moment M_x. With the thin-wall approximation $t \ll a$, the position of the bending centre is as shown in the figure. Further, the cross-sectional area and the bending moments of inertia around the y- and z-axes become

$$A = 10at, \qquad I_y = \frac{64}{15}a^3t, \qquad I_z = \frac{26}{3}a^3t, \tag{a}$$

where the single indices y and z indicate that the corresponding axes are principal axes. The cross-sectional constants given in Eq. (a) have been calculated for later use. With reference to Eq. (2–33), the torsional constant becomes:

$$K = \frac{2}{3}2a(2t)^3 + \frac{1}{3}2at^3 = \frac{34}{5}a^3t. \tag{b}$$

(continued)

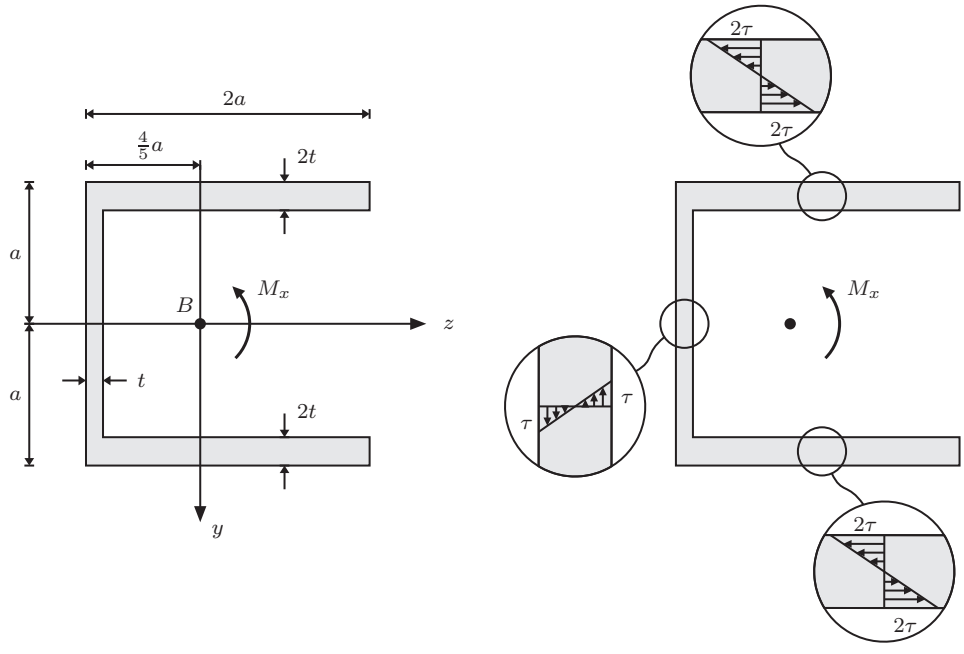

Figure A Homogeneous torsion of U-profile: Dimensions (left) and shear stresses (right).

The distribution of shear stresses follows from Eq. (2–35). The maximum shear becomes τ and 2τ, respectively, where τ is given as

$$\tau = \frac{M_x}{K}t = \frac{3}{34}\frac{M_x}{at^2}. \tag{c}$$

Hence, in the present case, the shear stresses in the flanges are higher than those in the web. □

2.2.4 Homogeneous torsion of closed thin-walled cross-sections

The boundary value problem for the warping function $\omega(y, z)$, defined by Eq. (2–14), has a unique solution (save an arbitrary additive constant) no matter if the profile has an interior hole or not. Although an analytical solution is seldom obtainable, a numerical solution can always be achieved by a discretization of the Laplace operator by a finite-difference or a finite-element approach.

In contrast to this, the boundary value problem defined by Eq. (2–22) for Prandtl's stress function cannot immediately be solved, because the boundary values S_j, $j = 1, 2, \ldots, N$, are not known. The determination of these values requires the formulation of additional geometrical conditions which express that the warping function $\omega(y, z)$ shall be continuous along the

boundary curves Γ_j. This may be formulated as

$$\oint_{\Gamma_j} d\omega = \oint_{\Gamma_j} \left(\frac{\partial \omega}{\partial y} dy + \frac{\partial \omega}{\partial z} dz \right) = 0, \qquad j = 1, 2, \ldots, N. \tag{2–37}$$

Equation (2–37) can be expressed in the stress function by use of Eq. (2–30):

$$\oint_{\Gamma_j} \left(\frac{\partial S}{\partial z} dy - \frac{\partial S}{\partial y} dz \right) + G \frac{d\theta}{dx} \oint_{\Gamma_j} ((z - z_s) dy - (y - y_s) dz) = 0. \tag{2–38}$$

It can be shown that the integrand of the first integral can be rewritten in terms of the coordinates s and n by the substitution

$$\frac{\partial S}{\partial z} dy - \frac{\partial S}{\partial y} dz = -\frac{\partial S}{\partial n} ds. \tag{2–39}$$

The second integral in Eq. (2–38) may be recast as

$$\oint_{\Gamma_j} ((z - z_s) dy - (y - y_s) dz) = -\oint_{\Gamma_j} (y dz - z dy) = 2A_j. \tag{2–40}$$

The change of sign in Eq. (2–40) is because all circulations are taken clockwise. Further, it has utilised that $\oint_{\Gamma_j} y_s dz = y_s \oint_{\Gamma_j} dz = 0$ and $\oint_{\Gamma_j} z_s dy = 0$. Insertion of Eqs. (2–39) and (2–40) into Eq. (2–38) provides the following form for the geometrical conditions:

$$\oint_{\Gamma_j} \frac{\partial S}{\partial n} ds = 2A_j G \frac{d\theta}{dx}. \tag{2–41}$$

Only thin-walled cross-sections are considered. At first a cross-section with a single cell is considered as shown in Fig. 2–8. An arc-length coordinate is introduced, orientated in the clockwise direction. Correspondingly, a local (x, n, s)-coordinate system is defined at each point of the boundary curve with the n-axis orientated inward into the cavity, whereas the s-axis is tangential to the boundary curve and unidirectional to the arc-length coordinate. Then, the shear stresses along the n- and s-directions become, cf. Eq. (2–15),

$$\sigma_{xn} = \frac{\partial S}{\partial s}, \qquad \sigma_{xs} = -\frac{\partial S}{\partial n}. \tag{2–42}$$

Here, S is constant along the exterior and interior boundary curve of the wall, given as $S = S_0 = 0$ and $S = S_1$, respectively. Hence, $\sigma_{xn} = 0$ along these boundaries. If the thickness $t(s)$ of the wall is small compared to a characteristic diameter of the profile, it then follows from continuity that σ_{xn} is ignorable in the interior of the wall, *i.e.*

$$\sigma_{xn} \simeq 0. \tag{2–43}$$

The stress function decreases from $S = S_1$ at the inner side of the wall to $S = S_0 = 0$ at the outer side. If $t(s)$ is small, the variation of $S(n, s)$ must vary approximately linearly over the wall thickness $t(s)$, see Fig. 2–8. This implies the following approximation

$$\sigma_{xs} = -\frac{\partial S}{\partial n} \simeq -\frac{S_1 - S_0}{t(s)} = -\frac{S_1}{t(s)}. \tag{2–44}$$

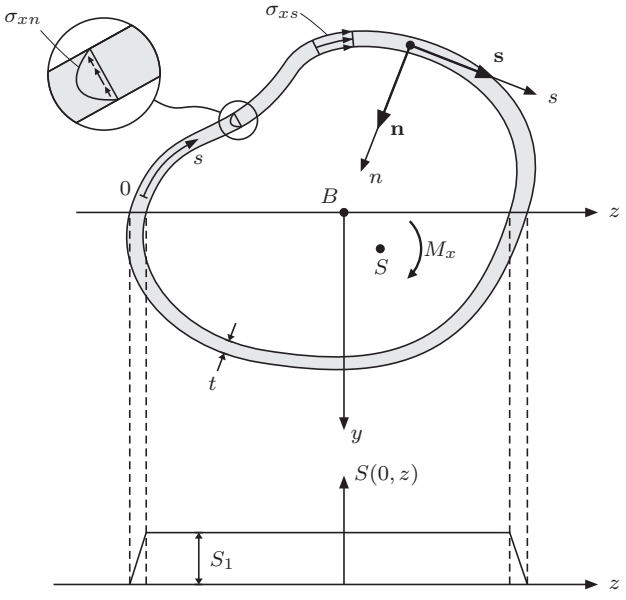

Figure 2–8 Closed thin-walled cross section of a cylindrical beam exposed to homogeneous torsion.

Then, the geometrical condition Eq. (2–41) may be written as

$$S_1 \oint_{\Gamma_1} \frac{ds}{t(s)} = 2A_1 G \frac{d\theta}{dx}, \tag{2–45}$$

where A_1 is area of the cavity.

The torsional moment is given by Eqs. (2–3) and (2–29):

$$M_x = GK\frac{d\theta}{dx} = 2A_1 S_1 \tag{2–46}$$

Combining Eq. (2–45) and Eq. (2–46) provides the following result for the torsional constant:

$$K = 2A_1 \frac{S_1}{Gd\theta/dx} = \frac{4A_1^2}{J}, \qquad J = \oint_{\Gamma_1} \frac{ds}{t(s)}. \tag{2–47}$$

Equation (2–47) is known as *Bredt's formula*.

The shear stresses follow from Eqs. (2–44) and (2–46):

$$\sigma_{xs}(s) = -\frac{S_1}{t(s)} = -\frac{M_x}{2A_1 t(s)}. \tag{2–48}$$

Notice, that the shear stress $\sigma_{xs}(s)$ is uniformly distributed over the wall-thickness as shown in Fig. 2–8. This is in contrast to an open section, where a linear variation was obtained, as given by Eq. (2–34) .

Example 2.4 Homogeneous torsion of a closed thin-walled cross-section

Figure A shows the cross-section of a beam with a single cell exposed to homogeneous torsion. The thin-wall approximation $t \ll a$ is assumed to be valid.

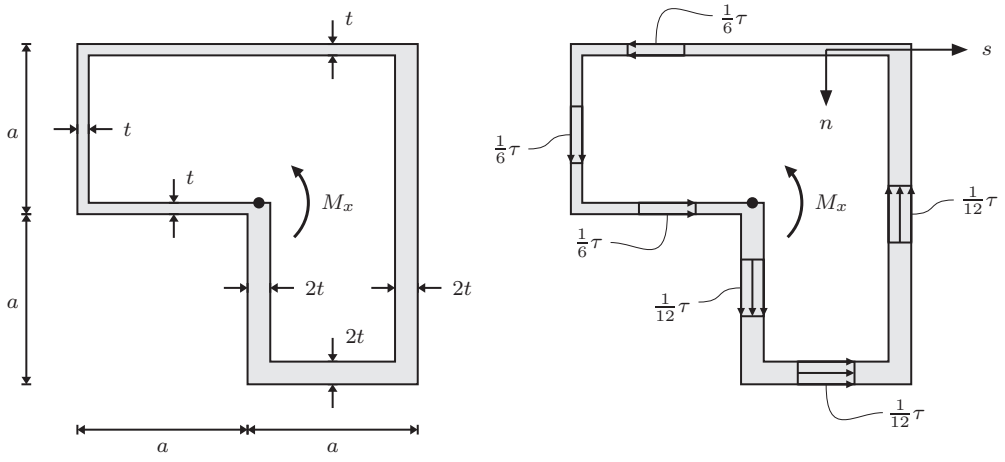

Figure A Homogeneous torsion of a closed thin-walled cross-section: Geometry (left) and distribution of shear stresses with $\tau = M_x/(a^2 t)$ (right).

The area of the cavity and the line integral entering Eqs. (2–45) and (2–47) become

$$A_1 = 3a^2, \qquad \oint_{\Gamma_1} \frac{ds}{t(s)} = \frac{4a}{t} + \frac{4a}{2t} = \frac{6a}{t}. \tag{a}$$

Then, the torsional constant becomes, cf. Eq. (2–47),

$$K = \frac{4(3a^2)^2}{6a/t} = 6a^3 t. \tag{b}$$

The shear stresses follow from Eq. (2–48):

$$\sigma_{xs} = -\frac{M_x}{6a^2 t(s)}. \tag{c}$$

The distribution has been shown in Fig. A along with the direction of action. Note that $\tau = M_x/(a^2 t)$ has been introduced as a normalisation quantity. □

Example 2.5 Comparison of homogeneous torsion of open and closed profiles

Figure A shows two cylindrical beams, both with a cylindrical thin-walled cross-section with the side length a and the thickness t. In one case, the cross-section is closed, whereas the cross-section in the other case has been made open by a cut along a developer. The rotation gradient $d\theta/dx$ and the shear stresses in two beams due to homogeneous torsion are compared below. *(continued)*

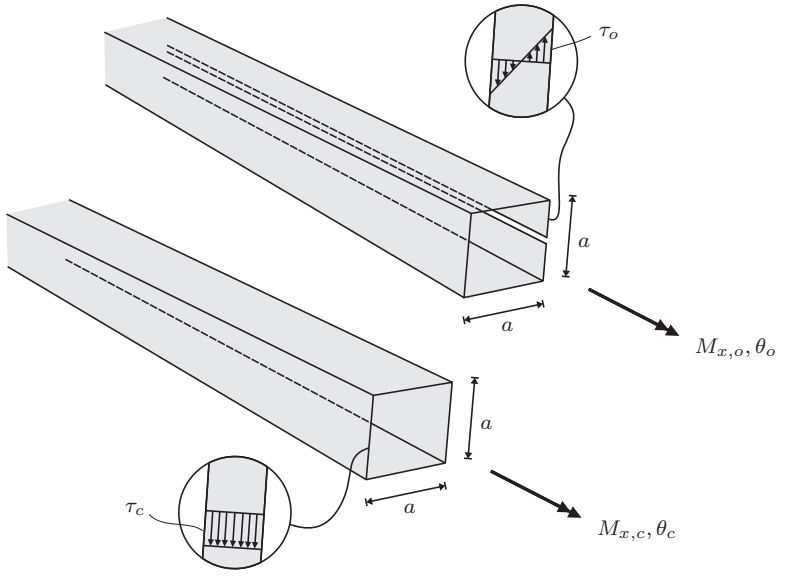

Figure A Homogeneous torsion of open and closed cross-sections.

According to Eqs. (2–33) and (2–47), the torsional constants K_o and K_c for the beams with open and closed cross-sections are given as

$$K_o = \frac{1}{3}\int t^3(s)ds = \frac{4}{3}at^3, \tag{a}$$

$$K_c = \frac{4A^2}{\oint \frac{ds}{t}} = \frac{4a^4}{4a/t} = a^3 t. \tag{b}$$

If the two beams are exposed to the same torsional moment M_x, it follows from Eq. (2–3) that the rotation gradients $d\theta_o/dx$ and $d\theta_c/dx$ for the open and closed sections are related as

$$\frac{d\theta_o/dx}{d\theta_c/dx} = \frac{K_c}{K_o} = \frac{4}{3}\frac{a^2}{t^2}. \tag{c}$$

Next, assume that both cross-sections are fully stressed, *i.e.* the maximum shear stress $\tau_o = \tau_c$ is in both cases equal to the yield shear stress τ_y. The corresponding torsional moments that can be carried by the profiles are denoted $M_{x,o}$ and $M_{x,c}$, respectively. With reference to Eqs. (2–35) and (2–48), these torsional moment are related as

$$\frac{M_{x,o}}{M_{x,c}} = \frac{K_o\tau_y/t}{2a^2t\tau_y} = \frac{2}{3}\frac{a}{t}. \tag{d}$$

Hence, whereas the deformations of the two beams depend on the fraction a^2/t^2, the torsional moment which can be carried depends on a/t. In conclusion, open sections are extremely ill-conditioned to carry torsional moments in homogeneous torsion compared to closed sections. However, in many cases another mechanics is active, which involves inhomogeneous torsion. This substantially increases the torsional properties of open sections. □

As illustrated by Example 2.5, closed thin-walled cross-sections, *e.g.* tubes and box girders, have a much higher torsional strength and stiffness than open thin-walled cross-section. A mechanical explanation for the highly increased stiffness obtained for a closed cross-section compared with the open cross-section is the fact that warping is hindered by the fact that the displacements in the axial direction must be continuous along the s-direction, *i.e.* along the wall. Especially, for a circular tube no warping is achieved in homogeneous torsion, making this profile particularly useful for structural elements with the primary function of carrying torsional loads.

Next, consider a thin-walled cellular cross-section with a total of N cavities as illustrated in Fig. 2–9. Each cavity has the cross-sectional area A_j, $j = 1, 2, \ldots, N$, and the boundary of the cell is denoted Γ_j. In each cell, a local (x, n_j, s_j)-coordinate system is defined with the n_j-axis oriented into the cavity as illustrated in Fig. 2–9. The local arc-length coordinate s_j is defined along the cell boundary in the clockwise direction, and the wall-thickness is $t(s_j)$.

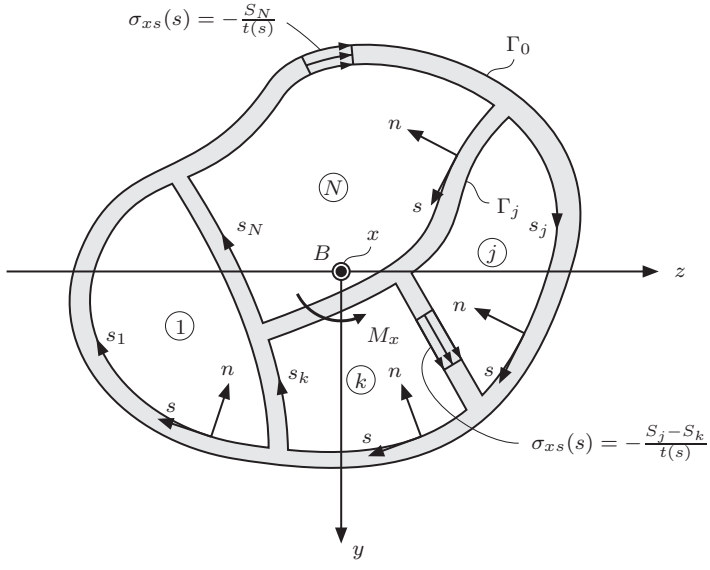

Figure 2–9 Cellular thin-walled cross section of a cylindrical beam exposed to homogeneous torsion.

As discussed in Subsection 2.2.2 and illustrated in Fig. 2–6, Prandtl's stress function S is constant along each interior boundary. Hence, on the cell boundary Γ_j, S has the constant value S_j, $j = 1, 2, \ldots, N$. However, different values of Prandtl's stress function are generally present on either side of a common wall between two adjacent cells, j and k. Because of the thin-wall assumption the variation of S over the wall thickness must be approximately linear. Hence, with reference to Eq. (2–42),

$$\sigma_{xs} = -\frac{\partial S}{\partial n_j} \simeq -\frac{S_j - S_k}{t(s_j)}. \tag{2–51}$$

Thus, σ_{xs} is uniformly distributed over the wall-thickness as illustrated in Fig. 2–9. The shear stress component σ_{xn} vanishes along Γ_j as well as Γ_k. It then follows from continuity that σ_{xn} is ignorable in the interior of the wall as well, *i.e.*

$$\sigma_{xn} \simeq 0. \tag{2–52}$$

Insertion of Eq. (2–51) into Eq. (2–41) provides:

$$\sum_k (S_j - S_k) \int_{\Gamma_{jk}} \frac{ds_j}{t(s_j)} = 2A_j G \frac{d\theta}{dx}, \qquad j = 1, 2, \ldots, N \tag{2–53}$$

where the summation on the left-hand side is extended over all cavities adjacent to cell j. Notice that $S_k = 0$ at the part of cell j adjacent to the outer periphery. Then, Eq. (2–53) represents N coupled linear equations for the determination of $S_j, j = 1, 2, \ldots, N$.

Subsequently the shear stress σ_{xs} in all interior and exterior walls is determined from Eq. (2–51). According to Eq. (2–29), the torsional moment is given as

$$M_x = 2 \sum_{j=1}^{N} A_j S_j, \tag{2–54}$$

where the contribution $\int_A S \, dA$ can be ignored due to the thin-wall approximation. Then, the torsional constant follows from Eq. (2–3):

$$K = \frac{M_x}{G d\theta/dx} = 2 \sum_{j=1}^{N} A_j \frac{S_j}{G d\theta/dx}. \tag{2–55}$$

Since S_j turns out to be proportional to $G d\theta/dx$, the right-hand side of Eq. (2–55) will be independent of this quantity.

Example 2.6 Homogeneous torsion of a rectangular thin-wall profile with two cells

Figure A shows a rectangular thin-walled cross-section with two cells exposed to homogeneous torsion from the torsional moment M_x. The wall-thickness is everywhere $t \ll a$.

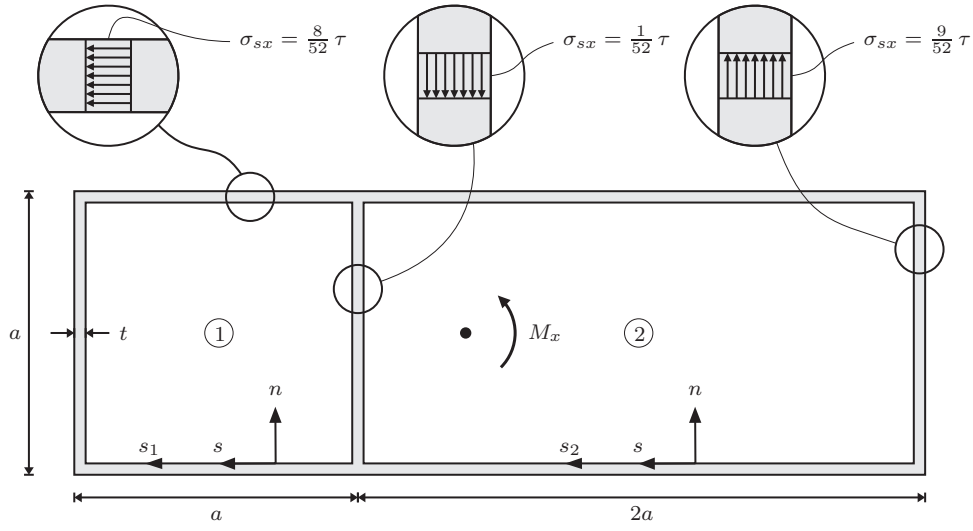

Figure A Homogeneous torsion of a rectangular thin-walled cross-section with two cells. Definition of local coordinate systems and distribution of shear stresses with $\tau = M_x/(a^2 t)$. *(continued)*

For the two cells, Eq. (2–53) takes the form:

$$(S_1 - 0)\frac{a}{t} + (S_1 - 0)\frac{a}{t} + (S_1 - 0)\frac{a}{t} + (S_1 - S_2)\frac{a}{t} = 2a^2 G\frac{d\theta}{dx}, \tag{a}$$

$$(S_2 - 0)\frac{2a}{t} + (S_2 - S_1)\frac{a}{t} + (S_2 - 0)\frac{a}{t} + (S_2 - 0)\frac{2a}{t} = 2 \cdot 2a^2 G\frac{d\theta}{dx}. \tag{b}$$

$$4S_1 - S_2 = 2atG\frac{d\theta}{dx}, \qquad -S_1 + 6S_2 = 4atG\frac{d\theta}{dx}. \tag{c}$$

The solution of Eq. (c) reads

$$S_1 = \frac{16}{23}atG\frac{d\theta}{dx}, \qquad S_2 = \frac{18}{23}atG\frac{d\theta}{dx}, \tag{d}$$

and by Eq. (2–54), the torsional moment is derived as

$$M_x = 2a^2 S_1 + 22a^2 S_2 = \frac{104}{23}a^3 tG\frac{d\theta}{dx} \qquad \Rightarrow \qquad G\frac{d\theta}{dx} = \frac{23}{104}\frac{M_x}{a^3 t}. \tag{e}$$

Then, S_1 and S_2 may be written as

$$S_1 = \frac{8}{52}\frac{M_x}{a^2}, \qquad S_2 = \frac{9}{52}\frac{M_x}{a^2}. \tag{f}$$

The shear stresses σ_{xs} follow from Eq. (2–51) and Eq. (f). The distribution has been shown in Fig. A with their direction of action. The quantity $\tau = M_x/(a^2 t)$ represents a normalisation quantity for the shear stresses.

The torsional constant follows from Eq. (2–55) and Eq. (d)

$$K = 2 \cdot a^2 \cdot \frac{16}{23}at + 2 \cdot 2a^2 \cdot \frac{18}{23}at = \frac{104}{23}a^3 t. \tag{g}$$

If the interior wall is skipped, the corresponding quantities become:

$$S_1 = \frac{1}{6}\frac{M_x}{a^2}, \qquad \sigma_{sx} = -\frac{1}{6}\frac{M_x}{a^2 t}, \qquad K = \frac{9}{2}a^3 t. \tag{h}$$

Hence, the interior wall *increases* the shear stress in the exterior cell walls of the right cell from $\frac{1}{6}\tau$ to $\frac{9}{52}\tau$ (1.3%). The torsional constant is increased merely from $K = \frac{9}{2}a^3 t$ to $K = \frac{104}{23}a^3 t$ (2.2%). □

As indicated by Example 2.6, only a small increase of the torsional stiffness is achieved by the inclusion of internal walls in a cross-section. Hence, from an engineering point of view, the benefits of applying structural members with a cellular cross-sections are insignificant in relation to torsion. Since the advantages regarding flexural deformations are also limited, and profiles with two or more cavities are not easily manufactured, it may be concluded that open cross-sections are generally preferred for beams loaded in unidirectional bending. Likewise, closed cross-sections with a single cavity (pipes or box girders) are preferable when the beam is primarily subjected to torsion and/or bending in two directions.

Finally it is noted that the solution method based on Prandtl's stress-function will only be used in relation to hand calculation for thin-walled cross-sections with at most two or three cells. Otherwise, for thick-walled sections or multi-cell problems, the homogeneous torsion problem will be solved numerically by a finite-element approach or another spatial discretization method based on the Neumann boundary problem specified in Box 2.1.

2.3 Shear stresses from bending

In the previous section, the shear stresses occurring due to homogeneous torsion of a beam have been analysed. A second contribution to the shear stresses stem from bending or flexural deformations of a beam and with a proper choice of coordinates, the two contributions decouple. Figure 2–10 shows a cross-section exposed to bending without torsion. Correspondingly, the loads per unit length q_y and q_z as well as the shear forces Q_y and Q_z have been referred to the shear centre S, the position of which is discussed in this section.

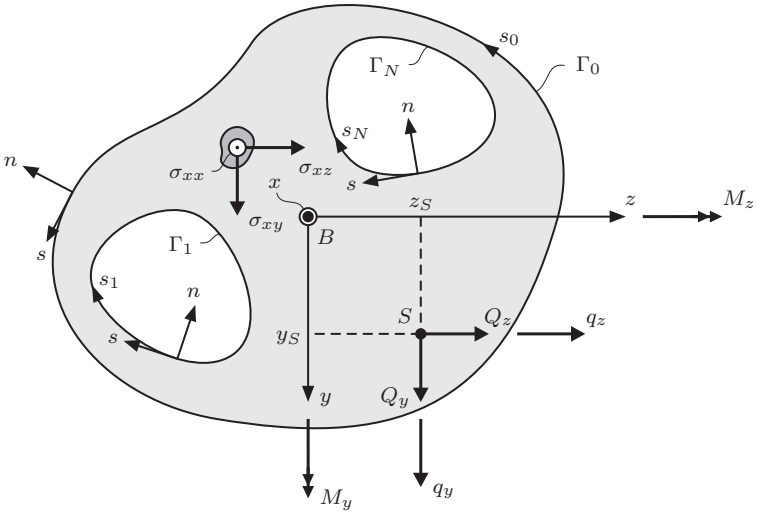

Figure 2–10 Cross-section exposed to bending.

The cross-section has the external boundary Γ_0 and may have a number of cavities, N, bounded by the interior boundary curves Γ_j, $j = 1, 2, \ldots, N$. Again, a local arc-length coordinate s_j is defined along each boundary, orientated clockwise for all interior boundaries, $j = 1, 2, \ldots, N$, whereas the arc-length coordinate s_0 along the outer boundary curve is orientated anti clockwise. At any point along the outer and inner boundary curves, local right-handed (x, n_j, s_j)-coordinate systems are defined as shown in Fig. 2–10. The (x, y, z)-coordinate system with origin at the bending centre B is assumed to be a principal-axes coordinate system.

On the cross-section, the normal stress σ_{xx} as well as the shear stresses σ_{xy} and σ_{xz} are acting. With reference to Eq. (2–7), these stresses fulfil the equilibrium equation

$$\frac{\partial \sigma_{xx}}{\partial x} + \frac{\partial \sigma_{xy}}{\partial y} + \frac{\partial \sigma_{xz}}{\partial z} = 0, \tag{2–57}$$

where σ_{xx} is determined from Navier's formula (1–75), *i.e.*

$$\sigma_{xx}(x, y, z) = \frac{N(x)}{A} + \frac{M_y(x)}{I_y} z - \frac{M_z(x)}{I_z} y. \tag{2–58}$$

It then follows that

$$\frac{\partial \sigma_{xx}}{\partial x} = \frac{dN}{dx}\frac{1}{A} + \frac{dM_y}{dx}\frac{z}{I_y} - \frac{dM_z}{dx}\frac{y}{I_z} = -\frac{q_x}{A} + (Q_y + m_z)\frac{y}{I_z} + (Q_z - m_y)\frac{z}{I_y}, \tag{2–59}$$

where the following equilibrium equations have been used in the statement:

$$\frac{dN}{dx} + q_x = 0, \qquad \frac{dM_y}{dx} - Q_z + m_y = 0, \qquad \frac{dM_z}{dx} + Q_y + m_z = 0. \tag{2–60}$$

A stress function $T = T(x, y, z)$ is introduced with the defining properties

$$\sigma_{xy} = \frac{\partial T}{\partial y}, \qquad \sigma_{xz} = \frac{\partial T}{\partial z}. \tag{2–61}$$

Hence, T is defined differently from the somewhat similar Prandtl's stress function, cf. Eq. (2–15). Insertion of Eqs. (2–59) and (2–61) into Eq. (2–57) provides the following Poisson partial differential equation for T:

$$\frac{\partial^2 T}{\partial y^2} + \frac{\partial^2 T}{\partial z^2} = \frac{q_x}{A} - (Q_y + m_z)\frac{y}{I_z} - (Q_z - m_y)\frac{z}{I_y}. \tag{2–62}$$

With reference to Eqs. (2–10) and (2–11), the boundary conditions read

$$\sigma_{xn} = \sigma_{xx}n_x + \sigma_{xy}n_y + \sigma_{xz}n_z = \sigma_{xy}n_y + \sigma_{xz}n_z = 0, \tag{2–63}$$

where $n_x = 0$ because the beam is cylindrical. Insertion of Eq. (2–61) into this equation provides the following homogeneous Neumann boundary conditions to be fulfilled on all exterior and interior boundary curves:

$$\frac{\partial T}{\partial n} = \frac{\partial T}{\partial y}n_y + \frac{\partial T}{\partial z}n_z = 0. \tag{2–64}$$

The boundary value problems defined by Eqs. (2–14) and (2–22) for the warping function and Prandtl's stress function, respectively, are independent of x, *i.e.* the solution applies for all cross-sections of the beam. In contrast, the corresponding boundary value problem defined by Eqs. (2–62) and (2–64) for $T = T(x, y, z)$ must be solved at each cross-section defined by x, where the shear stresses are determined. This is so, because q_x, m_y, m_z, Q_y and Q_z entering the right-hand side of Eq. (2–62) may vary along the beam. The solution to Eq. (2–62) with boundary conditions given by Eq. (2–64) is unique save an arbitrary function $T_0 = T_0(x)$ which has no influence on the shear stresses. The method can be applied to thick-walled or thin-walled cross-sections with or without interior cavities. Normally the boundary value problem can only be solved numerically based on a discretization of the Laplace operator entering Eq. (2–62). The boundary value problem for the stress function T has been summarised in Box 2.3.

Box 2.3 Boundary value problem for the stress function determining shear stresses in bending

For a given cross-section determined by the abscissa the stress-function $T = T(x, y, z)$ is obtained from the Poisson partial differential equation

$$\frac{\partial^2 T}{\partial y^2} + \frac{\partial^2 T}{\partial z^2} = \frac{q_x(x)}{A} - (Q_y(x) + m_z(x))\frac{y}{I_z} - (Q_z(x) - m_y(x))\frac{z}{I_y}, \qquad (y, z) \in A \tag{2–65a}$$

with the homogeneous Neumann boundary conditions

$$\frac{\partial T}{\partial n} = 0, \qquad (y, z) \in \Gamma_0 \cup \Gamma_1 \cup \cdots \cup \Gamma_N. \tag{2–65b}$$

The indicated method is not applicable for hand-calculations. For this purpose a method will be devised in the following sub-sections, which solves the problem for thin-walled open cross-sections and closed thin-walled sections with few cells.

2.3.1 Shear stresses in open thin-walled cross-sections

Figure 2–12 shows the same open thin-walled cross-section as shown in Fig. 2–7, when exposed to homogeneous torsion. Now the shear stresses σ_{xs} and σ_{xn} defined in local (x, n, s)-coordinates are requested, caused by the shear forces Q_y and Q_z acting through the shear centre S. We shall return to the definition and determination of the shear centre later in this chapter.

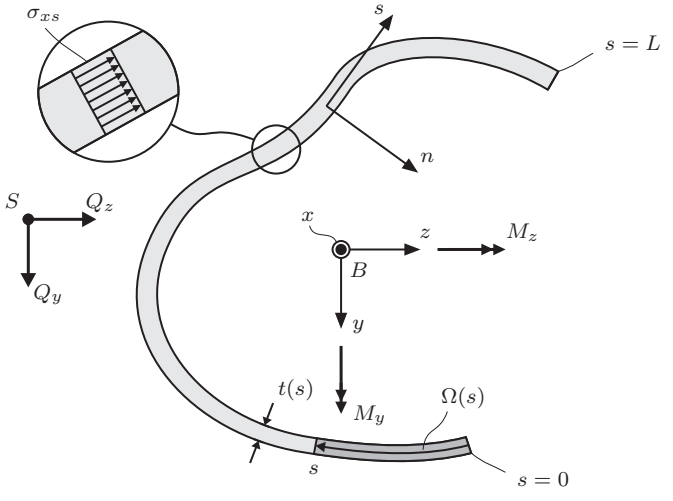

Figure 2–11 Cross-section exposed to bending.

The shear stress component σ_{xn} still vanishes at the surfaces $n = \pm\frac{1}{2}t(s)$, cf. Eq. (2–34). For continuity reasons, Eq. (2–43) remains valid in the interior of the wall, *i.e.*

$$\sigma_{xn}(x, n, s) \simeq 0. \tag{2–66}$$

Then, with reference to Eq. (2–57), the equilibrium equation of stress components in the (x, n, s)-coordinate system reduces to

$$\frac{\partial \sigma_{xx}}{\partial x} + \frac{\partial \sigma_{xs}}{\partial s} \simeq 0. \tag{2–67}$$

From Eq. (2–58) follows that σ_{xx} varies linearly over the cross-section. Thus it must be almost constant over the thin wall and can be replaced by its value at the midst of the wall. From Eq. (2–67) it then follows that σ_{xs} must also be approximately constant in the n-direction, *i.e.*

$$\sigma_{xs}(x, n, s) \simeq \sigma_{xs}(x, s). \tag{2–68}$$

The constancy of the shear stress component σ_{xs} in the thickness direction has been illustrated in Fig. 2–12. This variation should be compared to Eq. (2–34) for homogeneous torsion of an open cross-section, where a linear variation with n is obtained as illustrated in Fig. 2–7.

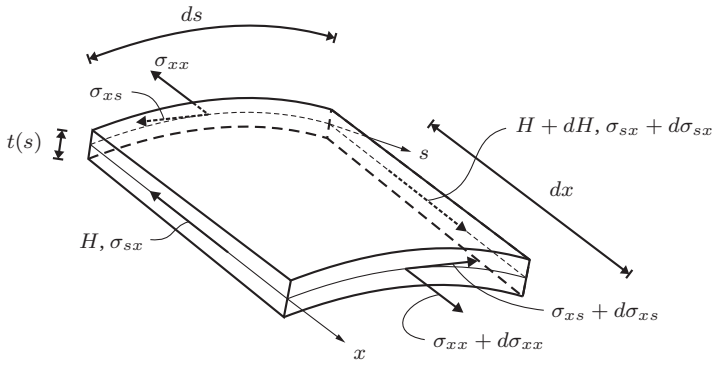

Figure 2–12 Differential element of a thin-walled cross-section.

A differential element with the side lengths dx and ds is cut free from the wall at the axial coordinate x and at the arc-length coordinate s, see Fig. 2–12. On the sections with the arc-length coordinates s and $s + ds$, the shear forces per unit length H and $H + dH$ are acting, where

$$H(x,s) = \int_{-t/2}^{t/2} \sigma_{sx}(x,n,s)dn \simeq \sigma_{xs}(x,s)t(s). \tag{2–69}$$

Here it has been exploited that $\sigma_{sx} = \sigma_{xs}$, and Eq. (2–68) has been utilised. On the sections with the axial coordinates x and $x + dx$, the normal stresses σ_{xx} and $\sigma_{xx} + d\sigma_{xx}$ are acting (see Fig. 2–12). Equilibrium in the x-direction then provides

$$(\sigma_{xx} + d\sigma_{xx})t(s)ds - \sigma_{xx}t(s)ds + (H + dH)dx - Hdx = 0 \quad \Rightarrow$$
$$\frac{\partial H}{\partial s} + t(s)\frac{\partial \sigma_{xx}}{\partial x} = 0, \tag{2–70}$$

where it has been utilised that σ_{xx} has an ignorable variation in the thickness direction. It has therefore been replaced with a constant value equal to the value present at the midst of the wall. Alternatively, Eq. (2–70) may be obtained simply by multiplication of Eq. (2–67) with $t(s)$ and use of Eq. (2–69).

With $H_0(x)$ representing an integration constant, integration of Eq. (2–70) provides the solution

$$H(x,s) = H_0(x) - \int_0^s \frac{\partial \sigma_{xx}}{\partial x} t(s)ds. \tag{2–71}$$

Especially, in the open thin-walled section the boundary condition $\sigma_{sx} = 0$ applies at the ends of the profile, corresponding to the arc-length coordinates $s = 0$ and $s = L$, *i.e.*

$$H(x,0) = H(x,L) = 0. \tag{2–72}$$

Thus, for an open thin-walled cross-section, the integration constant in Eq. (2–71) is $H_0(x) = 0$.

The partial derivative $\partial\sigma_{xx}/\partial x$ is given by Eq. (2–59). In what follows it is for ease assumed that $q_x = m_y = 0$. Equation (2–59) then reduces to

$$\frac{\partial \sigma_{xx}(x,s)}{\partial x} = \frac{Q_y(x)}{I_z} y(s) + \frac{Q_z(x)}{I_y} z(s), \tag{2–73}$$

where $(y(s), z(s))$ denotes the principal-axes coordinate of a position on the wall determined by the arc-length coordinate s.

Then, insertion in Eq. (2–71) and use of Eq. (2–69) provide the following solution for σ_{xs}:

$$\sigma_{xs}(x,s) = \frac{1}{t(s)} H(x,s) = -\frac{Q_y(x)}{t(s)I_z} S_{\Omega z}(s) - \frac{Q_z}{t(s)I_y} S_{\Omega y}(s), \tag{2–74a}$$

where it has been utilised that $H_0(x) = 0$ for the open section, and

$$S_{\Omega y}(s) = \int_0^s z(s)t(s)ds = \int_\Omega z dA, \qquad S_{\Omega z}(s) = \int_0^s y(s)t(s)ds = \int_\Omega y dA. \tag{2–74b}$$

The quantities $S_{\Omega y}(s)$ and $S_{\Omega z}(s)$ denote the statical moment around the y- and z-axes of the area segment $\Omega(s)$, shown with a dark grey signature in Fig. 2–12 and defined as

$$\Omega(s) = \int_0^s t(s)ds = \int_\Omega dA. \tag{2–75}$$

Equation (2–74) is known as *Grashof's formula*. The formula is valid for Timoshenko as well as Bernoulli-Euler beams with a thin-walled open cross-section. In this context it is noted that Bernoulli-Euler beam theory is based on the kinematic constraint that plane cross-sections orthogonal to the beam axis in the referential state remain plane and orthogonal to the deformed beam axis. In turn this implies that the angular strains γ_{xy} and γ_{xz} vanish, and hence that $\sigma_{xy} = \sigma_{xy} = 0$. Hence, the shear stresses in bending cannot be determined from the beam theory itself. Instead, these are determined from Eqs. (2–66) and (2–74) which are derived from static equations alone and, hence, are independent of any kinematic constraints.

The shear strain caused by the shear stress σ_{xs} is given as

$$\varepsilon_{xs} = \frac{1}{2G}\sigma_{xs} = \frac{1}{2Gt(s)} H(x,s). \tag{2–76}$$

The shear strain ε_{xs} implies a warping $u_{x0}(x,0)$ of the cross-section, additional to the displacement in the x-direction caused by the axial force and the bending moments. The latter is described by the kinematic conditions defined by Eqs. (1–11a) and (1–15) for Bernoulli-Euler beam theory. Hence, the displacements of the cross-section relative to the principal-axes coordinate system can be written as

$$u_x(x,s) = w_x(x) - \frac{dw_y(x)}{dx} y(s) - \frac{dw_z(x)}{dx} z(s) + u_0(x,s), \tag{2–77a}$$

$$u_y(x,s) = w_y(x), \tag{2–77b}$$

$$u_z(x,s) = w_z(x). \tag{2–77c}$$

The component $u_s(x,s)$ of the displacement vector $\mathbf{u}(x,s)$ in the tangential s-direction in the local (x,n,s)-coordinate system shown in Fig. 2–12 is given as

$$u_s(x,s) = \mathbf{s}^T \mathbf{u}(x,s) = \begin{bmatrix} \frac{dy(s)}{ds} \\ \frac{dz(s)}{ds} \end{bmatrix}^T \begin{bmatrix} u_x(x,s) \\ u_y(x,s) \end{bmatrix} = \frac{dy(s)}{ds} u_x(x,s) + \frac{dz(s)}{ds} u_y(x,s), \tag{2–78}$$

where $\mathbf{s}^T = \mathbf{s}^T(s) = [dy/ds, dz/ds]$ signifies the unit tangential vector. Then, the strain $\varepsilon_{xs}(x,S)$ follows from Eqs. (2–77) and (2–78):

$$\varepsilon_{xs} = \frac{1}{2}\left(\frac{\partial u_s}{\partial x} + \frac{\partial u_x}{\partial s}\right) = \frac{1}{2}\left(\frac{dy}{ds}\frac{dw_y}{dx} + \frac{dz(s)}{ds}\frac{dw_z}{dx} - \frac{dy}{ds}\frac{dw_y}{dx} - \frac{dz}{ds}\frac{dw_z}{dx} + \frac{\partial u_{x0}}{\partial s}\right) \quad \Rightarrow$$
$$\varepsilon_{xs} = \frac{1}{2}\frac{\partial u_{x0}}{\partial s}. \tag{2–79}$$

The warping $u_{x0}(x,s)$ is next determined by integration of Eq. (2–79):

$$u_{x0}(x,s) = 2\int_0^s \varepsilon_{xs}(x,s)ds + u_0(x). \tag{2–80}$$

The arbitrary function $u_0(x)$ is adjusted, so that $u_{x0} = 0$ at the bending centre B. When ε_{xs} is determined from Eq. (2–76), the warping of the cross-section additional to displacements in the x-direction predicted by Bernoulli-Euler beam theory can be determined by Eq. (2–80).

Example 2.7 Shear stresses and warping due to bending of a rectangular cross-section

Figure A shows a rectangular beam of height h and thickness t exposed to a shear force Q_y. The bending moment of inertia, the area segment $\Omega(s)$ and static moment $S_{\Omega z}(s)$ around the z-axis become

$$I_z = \frac{1}{12}h^3 t, \qquad \Omega(s) = st, \qquad S_{\Omega z}(s) = -st\left(\frac{h}{2} - \frac{s}{2}\right). \tag{a}$$

where the arc-length parameter is defined from the upper edge of the profile, *i.e.* $s = \frac{h}{2} + y$. Then, $\sigma_{xs} = \sigma_{xy}$ is determined from Eq. (2–74), that is

$$\sigma_{xy} = -\frac{Q_y}{tI_z}S_{\Omega z}(s) = 6\left(\frac{s}{h} - \frac{s^2}{h^2}\right)\frac{Q_y}{ht} = \frac{3}{2}\left(1 - 4\frac{y^2}{h^2}\right)\frac{Q_y}{ht}. \tag{b}$$

Equation (b) specifies a parabolic distribution over the cross-section, where $\sigma_{xy} = 0$ at the edges $y = \pm\frac{h}{2}$ in agreement with the boundary conditions, and the maximum value $\frac{3}{2}\frac{Q_y}{ht}$ is achieved at the bending centre B at $y = 0$.

Next, the warping is determined from Eqs. (2–76) and (2–80) together with Eq. (b):

$$u_{x0}(x,s) = u_0 + \frac{1}{G}\int_0^s \sigma_{xs}ds = u_0 + 6\frac{Q_y}{Ght}\int_0^s \left(\frac{s}{h} - \frac{s^2}{h^2}\right)ds = \frac{Q_y}{Gt}\left(3\frac{s^2}{h^2} - 2\frac{s^3}{h^3} - \frac{1}{2}\right), \tag{c}$$

where u_0 is adjusted, so $u_{x0} = 0$ at the bending centre, *i.e.* at $s = \frac{h}{2}$. With $s = \frac{h}{2} + y$, the warping displacements become

$$u_{x0}(y) = \frac{Q_y}{4Gt}\left(3\frac{2y}{h} - \left(\frac{2y}{h}\right)^3\right). \tag{d}$$

Equation (d) specifies a cubic polynomial variation, leading to an S-shape of the warping function. The distribution of $\sigma_{xy}(y)$ and $u_{x0}(y)$ has been shown in Fig. A. *(continued)*

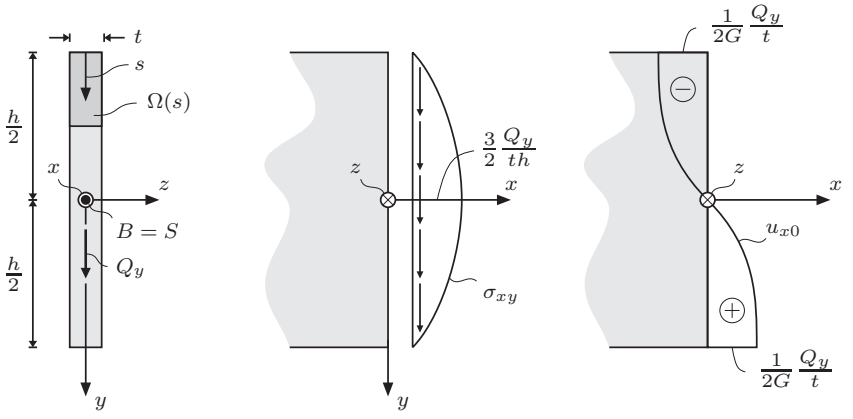

Figure A Rectangular cross-section subjected to bending: Area segment (left); shear stresses (centre); warping (right). □

Example 2.8 Shear stresses due to bending of a double-symmetric I-profile

Figure A (left) shows a double-symmetric cross-section exposed to the shear forces Q_y and Q_z. The wall thickness is everywhere $t \ll a$, *i.e.* the thin-wall assumption applies. The cross-sectional area and the principal bending moments of inertia become

$$A = 3at, \qquad I_y = 2 \cdot \frac{1}{12} a^3 t = \frac{1}{6} a^3 t, \qquad I_z = 2 \cdot \left(\frac{a}{2}\right)^2 at + \frac{1}{12} a^3 t = \frac{7}{12} a^3 t. \tag{a}$$

Due to the symmetry, the bending and shear centres are coinciding.

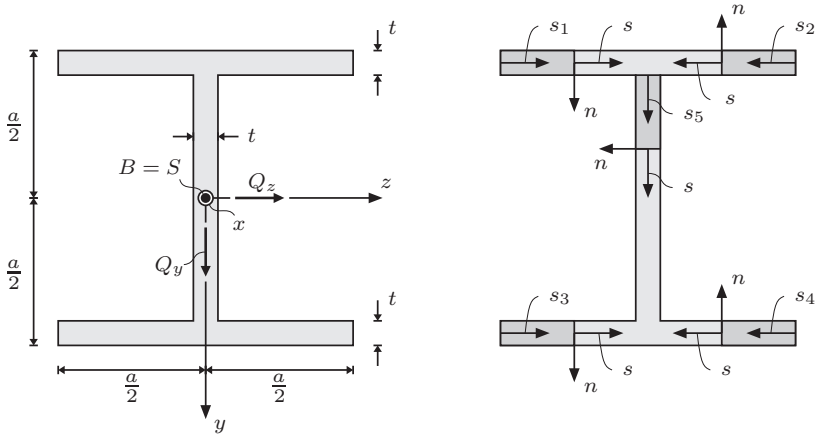

Figure A Double-symmetric I-profile: Geometry (left); definition of arc-length coordinates and local coordinate systems (right).

At first the shear stresses caused by Q_z are considered. For each of the four branches and the web of the profile, arc-length coordinates s_j and local right-handed (x, n_j, s_j)-coordinate systems are defined as shown in Fig. A (right). At the free edge, the shear stresses are $\sigma_{xs} = 0$. Hence, the shear force per unit length $H(x, s_j)$ vanishes at this point, and Eq. (2–71) becomes valid for each branch. *(continued)*

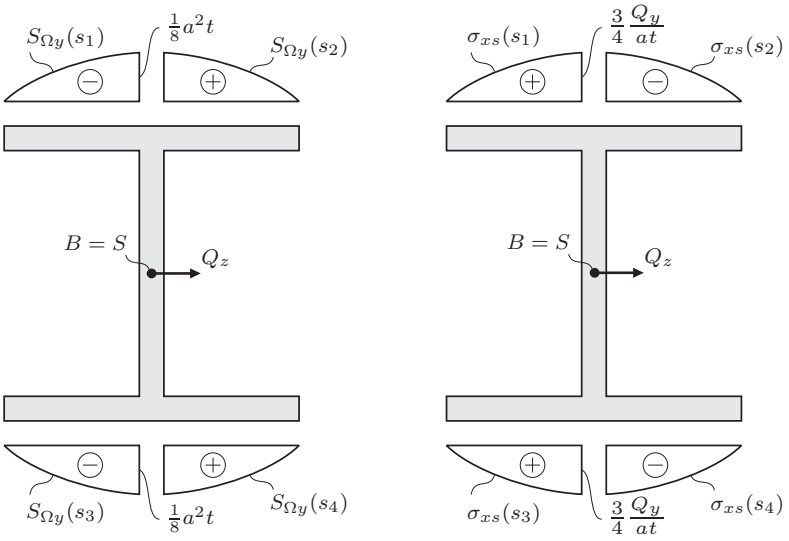

Figure B Double-symmetric I-profile: Distribution of statical moment of the area segment $\Omega(s_j)$ around the y-axis (left); distribution of the shear stresses $\sigma_{xs}(s_j)$ from Q_z (right).

On the five branches, the area segments become $\Omega(s_j) = s_j t$. These have been shown with a dark grey signature in Fig. A (right). For the flanges, the statical moments of $\Omega(s_j)$ around the y-axis become

$$S_{\Omega y}(s_1) = \frac{1}{2}ts_1(s_1 - a), \qquad S_{\Omega y}(s_2) = -\frac{1}{2}ts_2(s_2 - a), \tag{b}$$

$$S_{\Omega y}(s_3) = \frac{1}{2}ts_3(s_3 - a), \qquad S_{\Omega y}(s_4) = -\frac{1}{2}ts_4(s_4 - a). \tag{c}$$

Further, $S_{\Omega y} = 0$ along the web. The distribution has been shown in Fig. B (left).

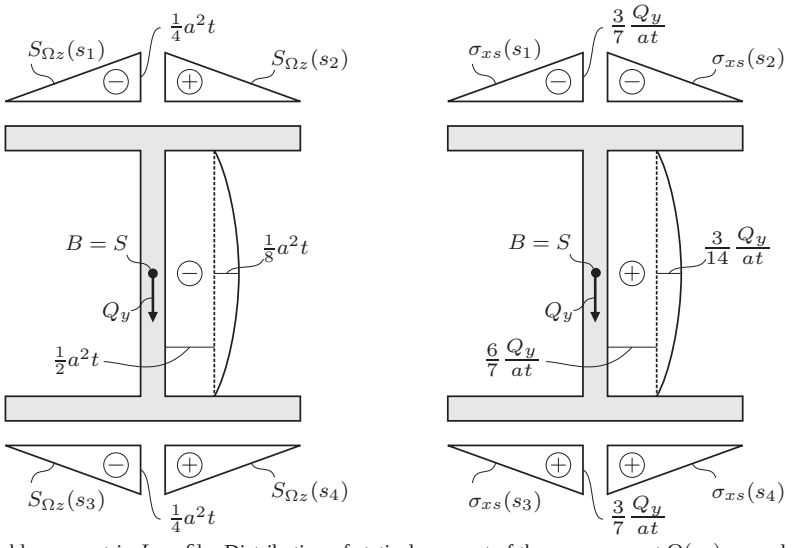

Figure C Double-symmetric I-profile: Distribution of statical moment of the area segment $\Omega(s_j)$ around the z-axis (left); distribution of the shear stresses $\sigma_{xs}(s_j)$ from Q_y (right). *(continued)*

The shear stresses $\sigma_{xs}(s_j)$ follow from Eq. (2–74):

$$\sigma_{xs}(s_1) = -\frac{Q_z}{tI_y} S_{\Omega y}(s_1) = 3\frac{Q_z}{a^3 t} s_1(a - s_1), \qquad \sigma_{xs}(s_2) = -3\frac{Q_z}{a^3 t} s_2(a - s_2), \tag{d}$$

$$\sigma_{xs}(s_3) = 3\frac{Q_z}{a^3 t} s_3(a - s_3), \qquad \sigma_{xs}(s_4) = -3\frac{Q_z}{a^3 t} s_4(a - s_4), \qquad \sigma_{xs}(s_5) = 0. \tag{e}$$

The distribution has been shown in Fig. B (right). The sign refers to the local x, n_j, s_j)-coordinate system. Hence, a negative sign implies that the shear stress is acting in the negative s_j-direction and, hence, is co-directional to Q_z. Then, the shear stresses in the flanges are distributed parabolically in the same way as stresses in the rectangular cross-section considered in Example 2.7. Each flange carries the shear force $Q_y/2$, and no shear force is carried by the web in the present case.

Next, the shear stresses caused by Q_y are analysed. The statical moment of the area segment $\Omega(s_j)$ around the z-axis becomes:

$$S_{\Omega z}(s_1) = -\frac{1}{2} a t s_1, \qquad S_{\Omega z}(s_2) = -\frac{1}{2} a t s_2, \tag{f}$$

$$S_{\Omega z}(s_3) = \frac{1}{2} a t s_3, \qquad S_{\Omega z}(s_4) = \frac{1}{2} a t s_4, \qquad S_{\Omega z}(s_5) = -\frac{a}{2} a t - \frac{1}{2} t s_5(a - s_5), \tag{g}$$

and by Eq. (2–74) the shear stresses $\sigma_{xs}(s_j)$ are determined as

$$\sigma_{xs}(s_1) = -\frac{Q_y}{tI_z} S_{\Omega z}(s_1) = \frac{6}{7}\frac{Q_y}{a^2 t} s_1, \qquad \sigma_{xs}(s_2) = \frac{6}{7}\frac{Q_y}{a^2 t} s_2, \tag{h}$$

$$\sigma_{xs}(s_3) = -\frac{6}{7}\frac{Q_y}{a^2 t} s_3, \qquad \sigma_{xs}(s_4) = -\frac{6}{7}\frac{Q_y}{a^2 t} s_4, \qquad \sigma_{xs}(s_5) = \frac{6}{7}(a^2 + s_5 a - s_5^2)\frac{Q_y}{at}. \tag{i}$$

The distribution of $\Omega(s_j)$ and $\sigma_{xs}(s_j)$ has been shown in Fig. C. □

2.3.2 Determination of the shear centre

So far in this section we have only considered double-symmetric cross-sections for which the shear centre S coincides with the bending centre B. However, in the general case, the shear centre will be different from the bending centre as suggested by Fig. 2–1. In any case, the shear forces Q_y and Q_z must be statically equivalent to the shear stresses integrated over the cross-section, *i.e.*

$$Q_y = \int_A \sigma_{xy} dA, \qquad Q_z = \int_A \sigma_{xz} dA. \tag{2–83}$$

In the present case, we are concerned with bending uncoupled from torsion. Hence, the torsional moment M_x stemming from the shear stresses on the cross-section should vanish. According to Eq. (2–25), this implies the identity

$$\int_A \left((y - y_s)\sigma_{xz} - (z - z_s)\sigma_{xy}\right) dA = 0. \tag{2–84}$$

Combining Eqs. (2–83) and (2–84) provides the relation for the coordinates of the shear centre:

$$-Q_y z_s + Q_z y_s = \int_A (-z\sigma_{xy} + y\sigma_{xz}) dA. \tag{2–85}$$

For a thin-walled cross-section, this identity may be recast in terms of the local (x, s, n)-coordinates, providing

$$-Q_y z_s + Q_z y_s = \int_L h(s)\sigma_{xs}(x,s)t(s)ds, \tag{2–86}$$

where $h(s)$ is the moment arm of the differential shear force $\sigma_{xs}(x,s)t(s)ds$,

$$h(s) = y(s)\frac{dz(s)}{ds} - z(s)\frac{dy(s)}{ds}. \tag{2–87}$$

It is noted that, with the given definition, $h(s)$ may have positive as well as negative values.

Insertion of Eq. (2–74) into Eq. (2–86) provides the identity

$$-Q_y z_s + Q_z y_s = -\frac{Q_z}{I_y}\int_L S_{\Omega y}(s)h(s)ds - \frac{Q_y}{I_z}\int_L S_{\Omega z}h(s)ds \tag{2–88}$$

which holds for arbitrary Q_y and Q_z. This implies the following solutions for the coordinates of the shear centre:

$$y_s = -\frac{1}{I_y}\int_L S_{\Omega y}(s)h(s)ds, \qquad z_s = \frac{1}{I_z}\int_L S_{\Omega z}(s)h(s)ds. \tag{2–89}$$

In particular, for a thin-walled section without branching, $S_{\Omega y}(s)$ and $S_{\Omega z}(s)$ become

$$S_{\Omega y}(s) = \int_0^s z(s)t(s)ds, \qquad S_{\Omega z}(s) = \int_0^s y(s)t(s)ds. \tag{2–90}$$

Hence, Eq. (2–89) involves a double integration with respect to the arc-length parameter over the length L. We shall arrange the calculation in a way such that only a single line integral needs to be evaluated.

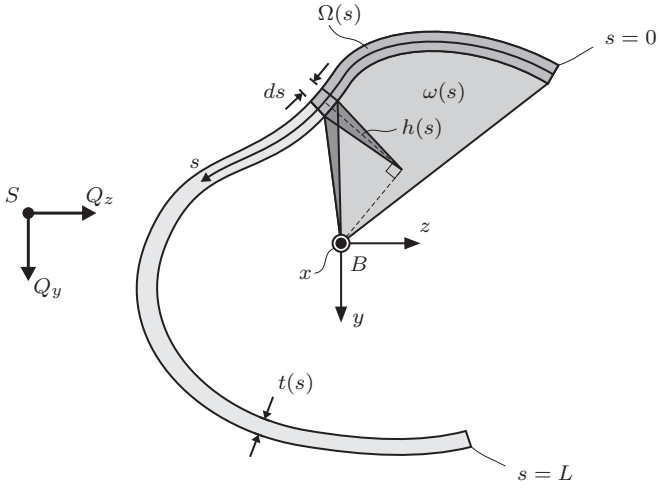

Figure 2–13 Cross-section exposed to bending.

At first the so-called sector coordinate $\omega(s)$ with pole B is introduced. The sector coordinate $\omega(s)$ is equal to the area shown in Fig. 2–13, delimited by the bending centre B and the area segment $\Omega(s)$. Thus, $\omega(s)$ is given as

$$\omega(s) = \int_0^s h(s)ds. \tag{2–91}$$

It follows that $\omega(s)$ may be considered as an integral of $h(s)$ with respect to s, *i.e.* $\frac{d}{ds}\omega(s) = h(s)$. Hence, from Eq. (2–90) follows that the derivation of $S_{\Omega y}(s)$ and $S_{\Omega z}(s)$ with respect to s become

$$\frac{d}{ds}S_{\Omega y}(s) = z(s)t(s), \qquad \frac{d}{ds}S_{\Omega z}(s) = y(s)t(s). \tag{2–92}$$

Then, integration by parts of Eq. (2–89) and use of Eq. (2–92) provides

$$y_s = -\frac{1}{I_y}\left(\Big[S_{\Omega y}(s)\omega(s)\Big]_0^L - \int_0^L z(s)\omega(s)t(s)ds\right) \tag{2–93}$$

Now, $S_{\Omega y}(L) = S_y = 0$, because the (x, y, z)-coordinate system has origin in the bending centre. Further, both $S_{\Omega y}(0) = 0$ and $\omega(0) = 0$, so the first term within the parentheses vanishes in both limits and, hence,

$$y_s = \frac{I_{\omega z}}{I_y}, \qquad I_{\omega z} = \int_0^L \omega(s)z(s)t(s)ds = \int_A \omega z dA. \tag{2–94a}$$

Similarly, it can be shown that

$$z_s = -\frac{I_{\omega y}}{I_z}, \qquad I_{\omega y} = \int_0^L \omega(s)y(s)t(s)ds = \int_A \omega y dA. \tag{2–94b}$$

The quantities $I_{\omega y}$ and $I_{\omega z}$ are denoted *sector centrifugal moments*. An arbitrary constant ω_0 can be added to $\omega(s)$ in Eq. (2–94) without changing the value of $I_{\omega z}$ and $I_{\omega y}$. This is so because $\int_A \omega_0 y dA = \omega_0 \int_A y dA = 0$ and $\int_A \omega_0 z dA = 0$. Hence, the sector coordinate is determined within an arbitrary constant.

As a third method, the coordinates of the shear centre may be determined from Eq. (2–86), if the shear stress $\sigma_{xs}(x, s)$ is calculated from Q_y and Q_z separately. Thus,

$$y_s = \frac{1}{Q_z}\int_L \sigma_{xs}(x, s)h(s)t(0)ds \qquad \text{for} \qquad Q_y = 0, \tag{2–95a}$$

$$z_s = \frac{1}{Q_y}\int_L \sigma_{xs}(x, s)h(s)t(s)ds \qquad \text{for} \qquad Q_z = 0. \tag{2–95b}$$

Obviously, if the profile has a line of symmetry, then the shear centre is placed on this line.

Finally, a note is made regarding the notation in this chapter. Previously, $\omega(x, y)$ has denoted the *normalised warping function* or, simply, the warping function. However, we shall later see that for open thin-walled sections the warping function is identical to the sector coordinate, which motivates the naming of the latter quantity.

Example 2.9 Determination of the shear centre for an I-profile with a single line of symmetry

The thicknesses of the flanges and the web of the profile shown in Fig. A (left) are all t. Due to the symmetry around the y-axis, the y-axis as well as the z-axis become principal axes. The bending centre is placed as shown in the figure and the principal moments of inertia become:

$$I_y = \frac{91}{12}a^3t, \qquad I_z = \frac{1044}{13}a^3t. \tag{a}$$

The profile is exposed to a horizontal shear force Q_z, and the position of the shear centre will be determined both by Eqs. (2–89), (2–94) and (2–95). Due to the symmetry, the shear centre is placed on the y-axis, *i.e.* $z_s = 0$.

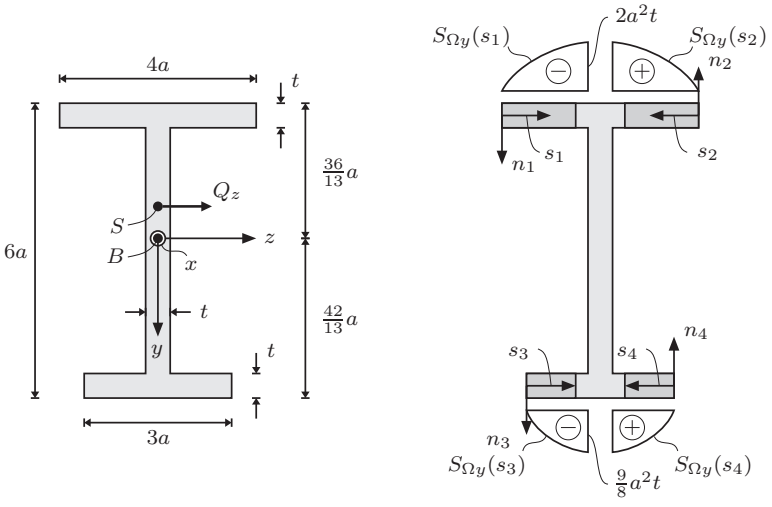

Figure A Single-symmetric I-profile: Geometry (left); definition of arc-length coordinates and distribution of static moments (right).

For each of the four branches indicated in Fig. A (right), an arc-length parameter s_j and a local (x, n_j, s_j) coordinate system are defined. The statical moments $S_{\Omega y}(s_j) = \int_\Omega z(s_j)t(s_j)ds_j$ become:

$$S_{\Omega y}(s_1) = -\int_0^{s_1}(2a - s)tds_1 = -\frac{1}{2}(4a - s_1)s_1t, \qquad S_{\Omega y}(s_2) = \frac{1}{2}(4a - s_2)s_2t, \tag{b}$$

$$S_{\Omega y}(s_3) = -\int_0^{s_3}\left(\frac{3}{2}a - s_3\right)tds_3 = -\frac{1}{2}(3a - s_3)s_3t, \qquad S_{\Omega y}(s_4) = \frac{1}{2}(3a - s_4)s_yt. \tag{c}$$

The shear stresses $\sigma_{xs}(x, s_j)$ are positive, when acting in the direction of the arc-length parameter s_j. These follow from Grashof's formula (2–74):

$$\sigma_{xs}(s_j) = -\frac{Q_z}{tI_y}S_{\Omega y}(s_j) = -\frac{12}{91}\frac{Q_z}{a^3t^2}S_{\Omega y}(s_j). \tag{d}$$

The distribution of shear stresses has been shown in Fig. B (left). *(continued)*

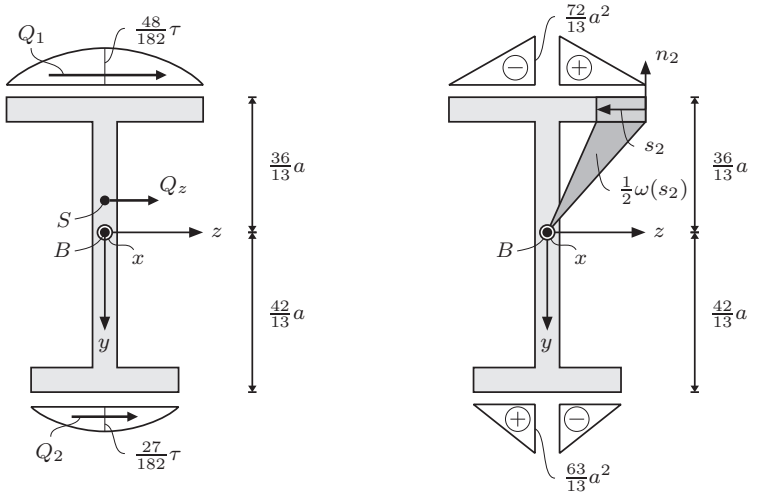

Figure B Single-symmetric I-profile: Shear stresses from the shear force Q_z with $\tau = Q_z/(at)$ (left); distribution of the sector coordinate $\omega(s)$ (right).

The shear stress resultants Q_1 and Q_2 in the top and bottom flanges become:

$$Q_1 = \frac{2}{3}\cdot\frac{48}{182}\cdot 4at\cdot\frac{Q_z}{at} = \frac{64}{91}Q_z, \qquad Q_2 = \frac{2}{3}\cdot\frac{27}{182}\cdot 3at\cdot\frac{Q_z}{at} = \frac{27}{91}Q_z. \tag{e}$$

The shear centre then follows from Eq. (2–95):

$$Q_z y_s = -Q_1\frac{36}{13}a + Q_z\frac{42}{13}a \qquad \Rightarrow \qquad y_s = -\frac{90}{91}a. \tag{f}$$

Next, employing another approach, the moment arm $h(s_j)$ defined by Eq. (2–87) is negative on the branches described by arc length parameters s_1 and s_2, and positive along the arc-length parameters s_2 and s_3. Then, from Eq. (b) it follows that

$$\begin{aligned}
&\int_L S_{\Omega y}(s)h(s)ds \\
&\quad= \int_0^{2a} -\frac{1}{2}(4a-s_1)s_1 t\left(-\frac{36}{13}a\right)ds_1 + \int_0^{2a}\frac{1}{2}(4a-s_2)s_2 t\left(+\frac{36}{13}a\right)ds_2 \\
&\quad+ \int_0^{3a/2} -\frac{1}{2}(3a-s_3)s_3 t\left(+\frac{42}{13}a\right)ds_3 + \int_0^{3a/2}\frac{1}{2}(3a-s_4)s_4 t\left(-\frac{42}{13}a\right)ds_4 \\
&\quad= \frac{96}{13}s^4 t + \frac{96}{13}a^4 t - \frac{189}{52}a^4 t - \frac{189}{52}a^4 t = \frac{15}{2}a^4 t.
\end{aligned} \tag{g}$$

Then, from Eqs. (2–89) and (a) it follows that

$$y_s = -\frac{1}{\frac{91}{12}a^3 t}\cdot\frac{15}{2}a^4 t = -\frac{90}{91}a. \tag{h}$$

This result is identical to the result achieved in Eq. (f). However, it is noted that the result in Eq. (h) has been achieved without the determination of the shear stresses. Hence, the second approach may appear to be simpler than the first approach, but it does not provide any information about the stress distribution.

(continued)

Finally, the same calculation is performed by means of Eq. (2–94). The distribution of the sector coordinate $\omega(s_j) = \int_0^{s_j} h(s)ds$ with the pole B for each of the four branches becomes:

$$\omega(s_1) = -\frac{36}{13}a\int_0^{s_1} ds_1 = -\frac{36}{13}as_1, \qquad \omega(s_2) = \frac{36}{13}as_2, \tag{i}$$

$$\omega(s_4) = -\frac{42}{13}a\int_0^{s_4} ds_4 = -\frac{42}{13}as_4, \qquad \omega(s_3) = \frac{42}{13}as_4. \tag{j}$$

The sector centrifugal moment $I_{\omega z} = \int_A \omega z dA = \int_L \omega(s)z(s)t(s)ds$ becomes:

$$I_{\omega z} = 2\int_0^{2a}(2a - s_1)\cdot\frac{36}{13}as_1\cdot 2tds_1 + 2\int_0^{2a}\left(-\frac{3}{2}a + s_4\right)\cdot\frac{42}{13}as_4\cdot 2tds_4 = -\frac{15}{2}a^4t, \tag{k}$$

where the symmetry of the integrand $\omega(s)z(s)$ has been exploited. Then, from Eqs. (2–94) and (a) the shear centre is determined as

$$y_s = -\frac{1}{\frac{91}{12}a^3t}\frac{15}{2}a^4t = -\frac{90}{91}a. \tag{l}$$

Hence, the three different approaches lead to the same result. □

Example 2.10 Determination of the shear centre for a symmetric U-profile

The bending centre of the U-profile has the position shown in Fig. A. Since the profile is symmetric, the indicated (x, y, z)-coordinate system is a principal axis system. The moments of inertia with respect to the principal axes become:

$$I_y = \frac{64}{15}a^3t, \qquad I_z = \frac{26}{3}a^3t. \tag{a}$$

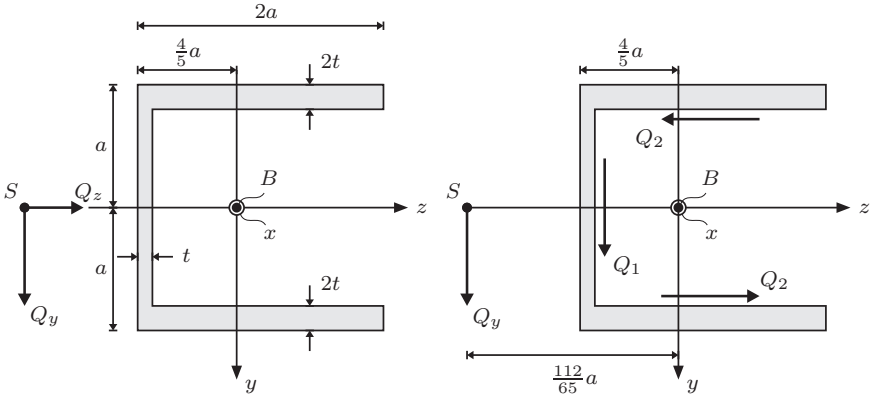

Figure A Symmetric U-profile: Geometry (left); position of the shear centre (right).

Local arc length coordinates s_1, s_2 and s_3 are introduced as indicated in Fig. B. The distributions of the static moments $S_{\Omega y}(s_j)$ and $S_{\Omega z}(s_j)$ are shown in the figure. The analytic expressions are given as

(continued)

$$S_{\Omega y}(s_1) = \int_0^{s_1} \left(\frac{6}{5}a - s_1\right) 2t ds_1 = \left(\frac{12}{5}as_1 - s_1^2\right) t, \tag{b}$$

$$S_{\Omega y}(s_2) = \frac{4}{5}a^2t + \int_0^{s_2} \left(-\frac{4}{5}a\right) t ds_2 = \frac{4}{5}at(a - s_2), \tag{c}$$

$$S_{\Omega y}(s_3) = -\frac{4}{5}a^2t + \int_0^{s_3} \left(-\frac{4}{5}a + s_3\right) 2t ds_3 = -\frac{4}{5}a^2t - \frac{8}{5}as_3t + s_3^2t, \tag{d}$$

$$S_{\Omega z}(s_1) = \int_0^{s_1} (-a) 2t ds_1 = -2as_1t, \tag{e}$$

$$S_{\Omega z}(s_2) = -4a^2t + \int_0^{s_2} (-a + s_2) t ds_2 = -4a^2t - as_2t + \frac{1}{2}s_2^2t, \tag{f}$$

$$S_{\Omega z}(s_3) = -4a^2t + \int_0^{s_3} a \cdot 2t ds_3 = -4a^2t + 2as_3t. \tag{g}$$

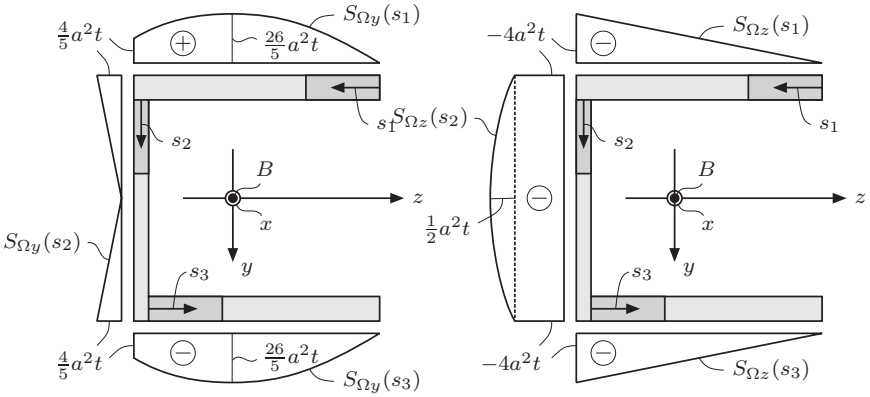

Figure B Symmetric U-profile: Distribution of the static moments $S_{\Omega y}(s_j)$ (left) and $S_{\Omega z}(s_j)$ (right).

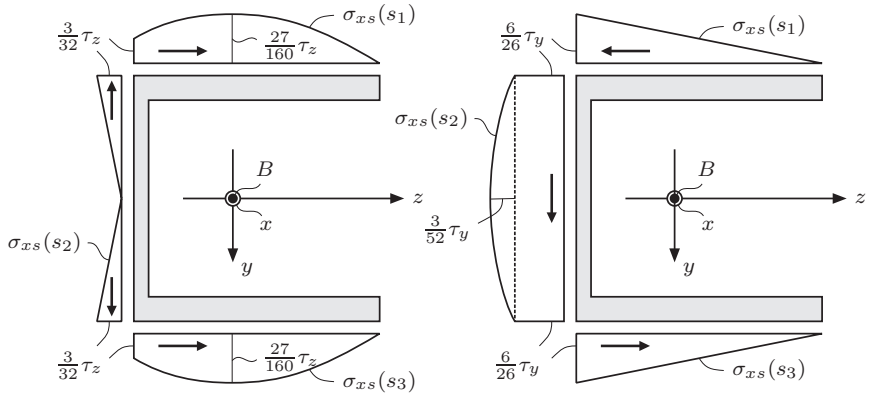

Figure C Symmetric U-profile: Distribution of the shear stresses from the shear forces Q_z with $\tau_z = Q_z/(at)$ (left) and Q_y with $\tau_y = Q_y/(at)$ (right). *(continued)*

The shear stresses follow from Grashof's formula (2–74). Figure B (left) shows the distribution of shear stresses from Q_z, and Fig. B (right) shows the distribution from Q_y. The position of the shear centre is given by Eq. (2–95). Since the shear stresses σ_{xs} from Q_z are distributed symmetrically around the z-axis it follows that $y_s = 0$, reflecting the fact that the z-axis is a line of symmetry.

The resulting shear forces Q_1 and Q_2 in Fig. A then become

$$Q_1 = 2t \cdot \frac{1}{2} \cdot 2a \cdot \frac{6}{26}\tau_y = \frac{6}{13}Q_y, \qquad Q_2 = t \cdot \left(\frac{2}{3} \cdot \frac{3}{52} + \frac{6}{13}\right) 2a\tau_y = Q_y. \tag{h}$$

Finally, from Eq. (2–95) follows that

$$z_s = -\frac{1}{Q_y}\left(Q_1 \cdot a + \frac{4}{5}a \cdot Q_2 + Q_1 a\right) = -\frac{112}{65}a. \tag{i}$$

Hence, for a U-profile the shear centre lies at a considerable distance outside the profile. □

2.3.3 Shear stresses in closed thin-walled sections

Figure 2–14 shows a closed single-cell section of a thin-walled beam. The shear force $H(x, s)$ acting within the wall per unit length of the beam (see Fig. 2–12) in a corresponding open section is uniquely determined by Eq. (2–71) due to the condition $H(x, 0) = H_0(x) = 0$ at the boundary $s = 0$. However, in a closed section $H(x, s)$ is not a priori known in one or more points of the periphery Γ_1, for which reason the shear stresses cannot be determined from static equations alone. Hence, a geometrical condition must be introduced, from which the initial value $H_0(x)$ at $s = 0$ can be determined. The derivation of this geometric condition will be considered at first.

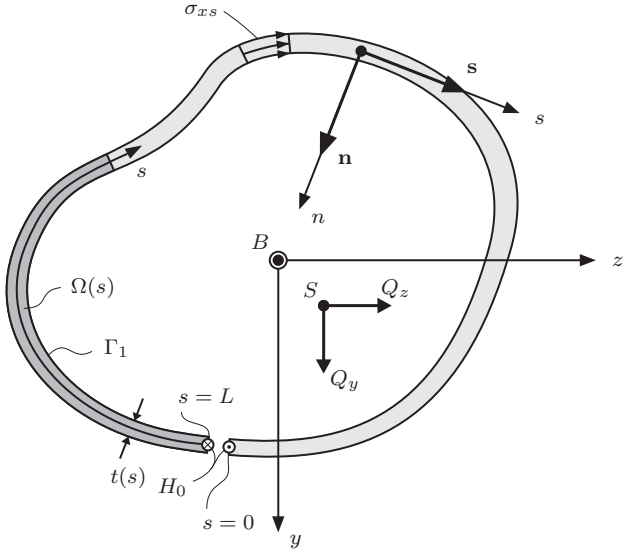

Figure 2–14 Closed single-cell section exposed to bending.

The arc-length coordinate s is orientated clock-wise with an arbitrarily selected origin O. Then, the local (x, n, s)-coordinate system is orientated with the n-axis orientated toward the interior of the cell. The shear stress $\sigma_{xs}(x, s)$ follows from Eqs. (2–71) and (2–73):

$$\sigma_{xs}(x,s) = \frac{1}{t(s)}H(x,s) = \frac{H_0(x)}{t(s)} - \frac{Q_y(x)}{t(s)I_z}S_{\Omega z}(x,s) - \frac{Q_z(x)}{t(s)I_y}S_{\Omega y}(x,s). \tag{2–98a}$$

where the static moments of the area segment $\Omega(s)$ are again given as

$$S_{\Omega y}(s) = \int_0^s z(s)t(s)ds = \int_\Omega z dA, \qquad S_{\Omega z}(s) = \int_0^s y(s)t(s)ds = \int_\Omega y dA. \tag{2–98b}$$

Equation (2–98a) is the equivalence of Grashof's formula (2–74) for a closed thin-walled section. Unlike the case of the open section, $H_0(x)$ is generally different from zero and the determination of $H_0(x)$ is part of the problem.

The shear strain ε_{xs} in the local (x, n, s)-coordinate system is given by Eq. (2–76) which is valid for open as well as closed thin-walled sections. This implies the warping $u_0(x, s)$ defined by Eq. (2–80), where it is recalled that $u_0(x, s) = 0$ in the bending centre B. This is so, because $w_x(x)$ has been defined as the total displacement in the x-direction of B. Now, for the closed section, the displacement $u_x(x, s)$ must be continuous as a function of s along the periphery Γ_1. The axial and bending contributions, *i.e.* the first three contributions on the right-hand side of Eq. (2–77), are always continuous. A possible discontinuity then stems from the warping. If the profile is open, as illustrated in Fig. 2–12, the ends at $s = 0$ and $s = L$ can move freely relatively to each other. Hence, a warping discontinuity develops between these two endpoints. However, in a closed section, the warping of these points must be identical. Hence, the geometrical condition can be formulated as

$$u_{x0}(x,0) = u(x,L) = u_0(x). \tag{2–99}$$

Insertion of Eqs. (2–76) and (2–99) into Eq. (2–80) provides

$$u_0(x) = u_0(x) + 2\int_0^L \varepsilon_{xs}(x,s)ds = u_0(x) + \frac{1}{G}\int_0^L \frac{H(x,s)}{t(s)}ds \qquad \Rightarrow$$
$$\int_0^L \frac{H(s)}{t(s)}ds = \oint_{\Gamma_1} \frac{H(s)}{t(s)}ds = 0. \tag{2–100}$$

Insertion of Eq. (2–98a) gives the following formulation of the geometrical condition from which the initial condition H_0 can be determined:

$$H_0(x)\oint_{\Gamma_1}\frac{ds}{t(s)} - \frac{Q_z}{I_y}\oint_{\Gamma_1}\frac{S_{\Omega y}}{t(s)}ds - \frac{Q_y}{I_z}\oint_{\Gamma_1}\frac{S_{\Omega z}}{t(s)}ds = 0. \tag{2–101}$$

With $H_0(x)$ determined, $H(x, s)$ and the shear stress $\sigma_{xs}(x, s)$ can next be determined from Eq. (2–98a).

Example 2.11 Shear stresses in a symmetric thin-walled single-cell section

Figure A shows a double-symmetric thin-walled single-cell profile. The thickness is everywhere t. We want to determine the shear stresses from a shear force Q_y acting at the shear centre. *(continued)*

The cross-sectional area and moment of inertia around the z-axis become

$$A = 8at, \qquad I_z = \frac{5}{3}a^3 t. \tag{a}$$

The origin of the arc length coordinate is chosen at the lower left corner. The corresponding distribution of the static moment $S_{\Omega z}(s) = \int_0^s z(s)t(s)ds$ has been shown in Fig. B.

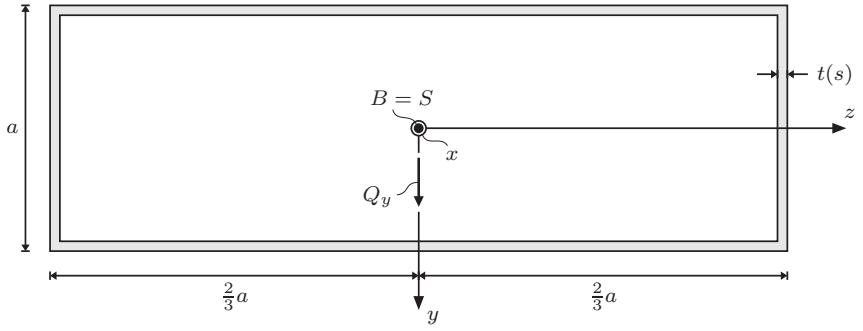

Figure A Geometry of the symmetric rectangular thin-walled single-cell section.

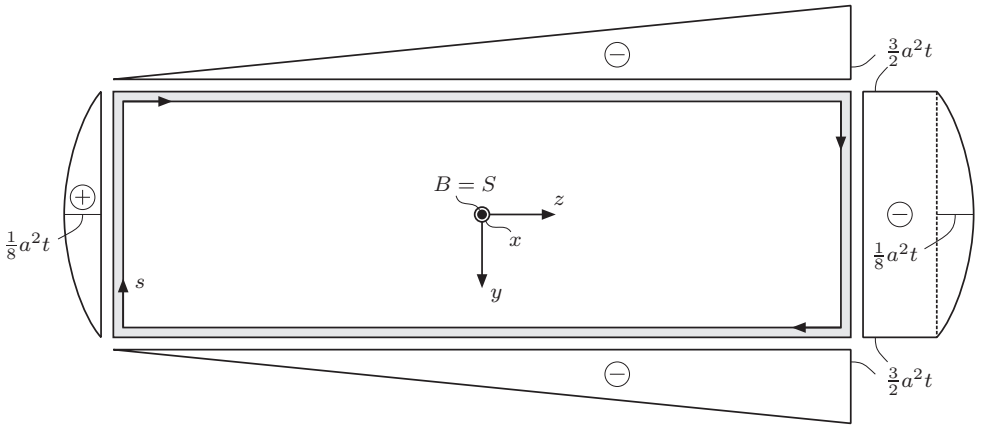

Figure B Distribution of the static moment $S_{\Omega z}(s)$ in the symmetric rectangular thin-walled single-cell section.

Next, the following line integrals are calculated:

$$\oint_{\Gamma_2} \frac{ds}{t} = \frac{1}{t}(a + 3a + a + 3a) = \frac{8a}{t}, \tag{b}$$

$$\oint_{\Gamma_1} \frac{S_{\Omega z}(s)}{t} ds$$
$$= \frac{1}{t}\left(\frac{2}{3}\cdot\frac{1}{8}a^2t\cdot a - \frac{1}{2}\cdot 3a\cdot\frac{3}{2}a^2t - \frac{3}{2}a^2t\cdot a - \frac{2}{3}\cdot\frac{1}{8}a^2t\cdot a - \frac{1}{2}\cdot 3a\cdot\frac{3}{2}a^2t\right) = -6a^3. \tag{c}$$

(continued)

From Eq. (2–101) then follows that

$$H_0 \cdot \frac{8a}{t} - \frac{Q_y}{\frac{5}{3}a^3 t}(-6a^3) = 0 \qquad \Rightarrow \qquad H_0 = -\frac{9}{20}\frac{Q_y}{at}. \tag{d}$$

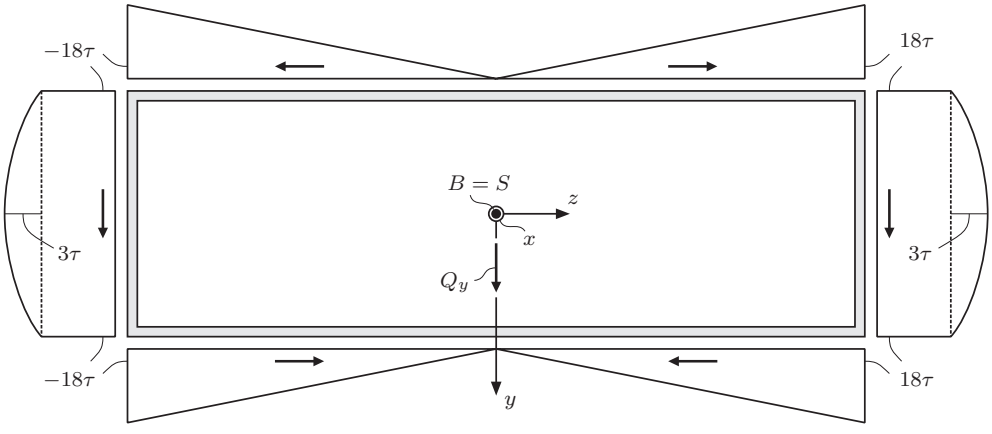

Figure C Shear stresses in the symmetric rectangular thin-walled single-cell section with $\tau = Q_y/(40at)$.

The distribution of shear stresses $\sigma_{xs}(x, s)$ follows from Eq. (2–98a) and has been indicated in Fig. C. The arrows indicate the positive direction of the shear stresses. These will be referred to as the *shear flow* in what follows, due to the analogous behaviour of water flowing down through a system of pipes. □

As shown in Example 2.11, a symmetric thin-walled single-celled profile exposed to a shear force acting along the line of symmetry will have a symmetric distribution of shear stresses. Especially, the shear stress at the line of symmetry vanishes. Hence, if the origin of arc-length coordinate is placed at the line of symmetry we must have $H_0(x) = 0$, entailing that a single-celled symmetric profile can be analysed from the static equations alone.

For a thin-walled profile with N cells, arc-length parameters s_j are introduced for all cells, orientated clock-wise as shown in Fig. 2–15. The origins $O_1, O_2, \ldots, O_N$ for the arc-length coordinates are chosen arbitrarily. The shear forces per unit length $H_{0j}(x)$ at the origins are unknown and must be determined from geometrical conditions in addition to the static shear flow equations. Similarly to Eq. (2–99) these are determined by the conditions that the warping must be continuous along all the peripheries Γ_j of the cells.

At first, the static moments $S_{\Omega y}$ and $S_{\Omega z}$ for the open profile in Fig. 2–15 are determined. Especially, the variation of $S_{\Omega y}(x, s_j)$ and $S_{\Omega z}(x, s_j)$ along Γ_j as a function of s_j are registered. Next, the calculation of the shear force per unit length $H_j(x, s_j)$ within each cell can be arranged as illustrated in Fig. 2–16. Firstly, the shear force per unit length $H_{sj}(s_j)$ of the open, branched profile is calculated, orientated in the direction of the arc-length coordinate s_j. This is given by Grashof's formula (2–74), *i.e.*

$$H_{sj}(s_j) = -\frac{Q_z}{I_y} S_{\Omega y}(s_j) - \frac{Q_y}{I_z} S_{\Omega z}(s_j). \tag{2–103}$$

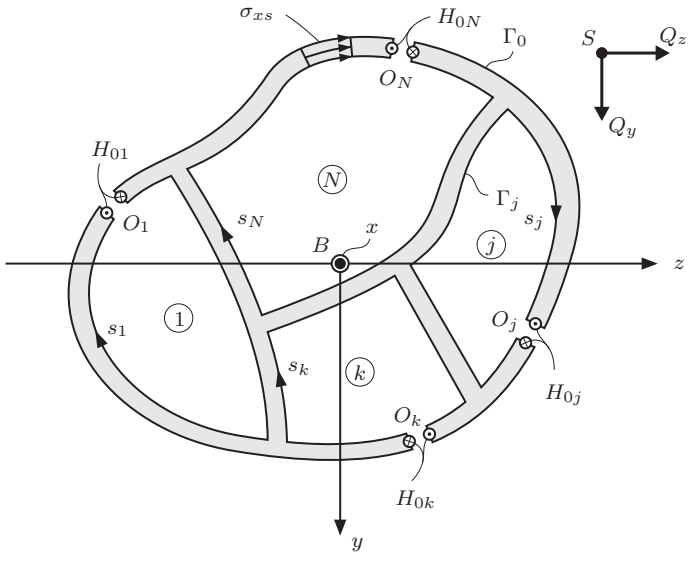

Figure 2–15 Closed multi-cell section exposed to bending.

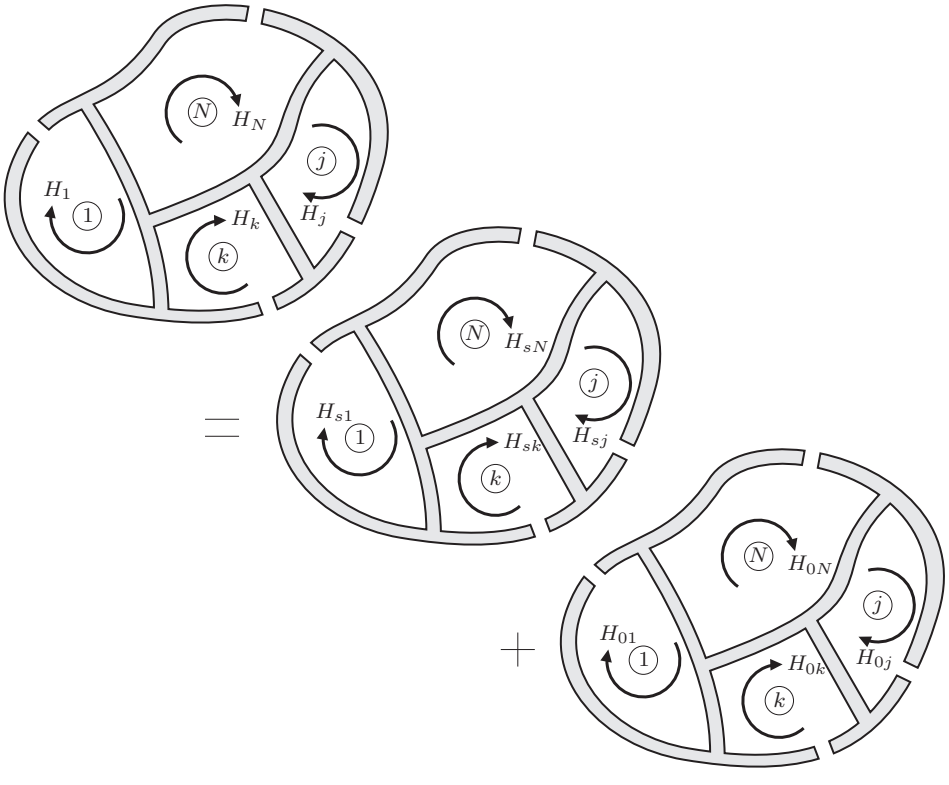

Figure 2–16 Arrangement of calculations of shear forces per unit length within cells.

In each cell, the initial conditions induce a constant shear force per unit length H_{0j}. Due to the chosen sign convention, the net shear force on the periphery segment Γ_{jk} between cell j and cell k becomes $H_{sj} - H_{0k}$. Hence, on this segment the total shear force per unit length becomes

$$H_j(s_j) = H_{sj}(s_j) + H_{0j} - H_{0k}. \tag{2–104}$$

Continuity requires that Eq. (2–101) is fulfilled for all N cells, *i.e.*

$$\oint_{\Gamma_j} \frac{H_j(s_j)}{t(s_j)} ds_j = 0, \qquad j = 1, 2, \ldots, N. \tag{2–105}$$

Insertion of Eq. (2–104) leads to the following N linear equations for the determination of $H_{01}, H_{02}, \ldots, H_{0N}$:

$$\sum_{k=1}^{N} (H_{0j} - H_{0k}) \int_{\Gamma_{jk}} \frac{ds_j}{t(s_j)} = -\oint_{\Gamma_j} \frac{H_{sj}(s_j)}{t(s_j)} ds_j, \qquad j = 1, 2, \ldots, N. \tag{2–106}$$

The coefficient matrix in Eq. (2–106) is identical to this for the determination of Prandtl's stress function S_j in the cells in the corresponding St. Venant torsion problem. With H_{0j} determined from Eq. (2–106), $H_j(s_j)$ can be calculated from Eq. (2–104). Finally, the shear stresses $\sigma_{xs}(s_j)$ follow from Eq. (2–98a) with positive sign when acting in the direction of s_j.

Example 2.12 Shear stresses in a single-symmetric double-cell section

The profile shown in Fig. A is identical to that considered in Example 2.11. However, a partition with the wall thickness t has been included as shown in the figure. The bending centre B is placed as indicated. Because the section is symmetric around the z-axis the indicated coordinate system with origin in B is a principal axis coordinate system. The section is still exposed to a shear force Q_y acting through the shear centre S. Due to the symmetry the shear centre is placed on the z-axis ($y_S = 0$). The z_s will be determined as a part of the solution. The cross-sectional area and inertial around the z-axis become

$$A = 9at, \qquad I_z = \frac{7}{4} a^3 t. \tag{a}$$

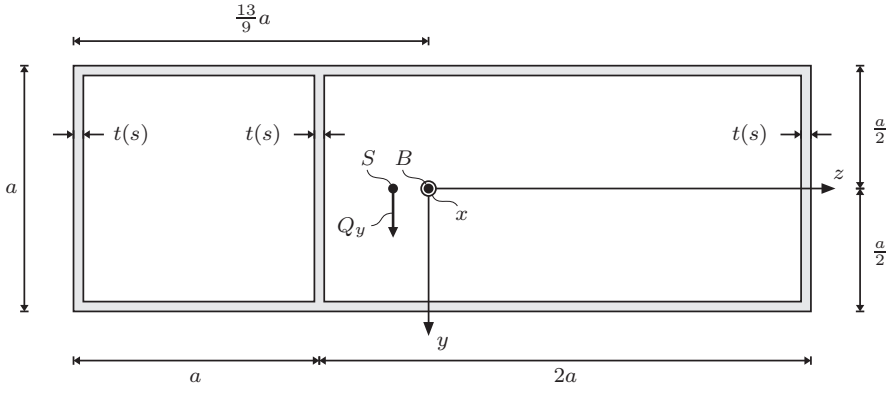

Figure A Geometry of the rectangular thin-walled double-cell section.

(continued)

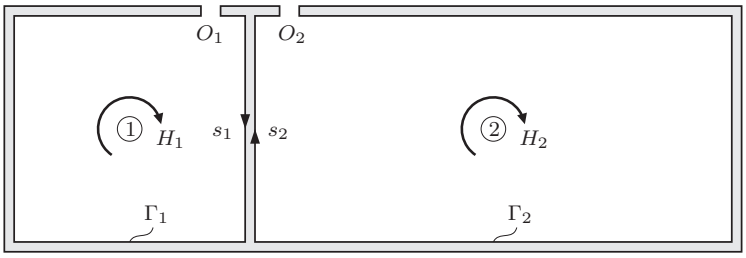

Figure B Definition of the origins of the arc-length coordinates in the rectangular thin-walled double-cell section.

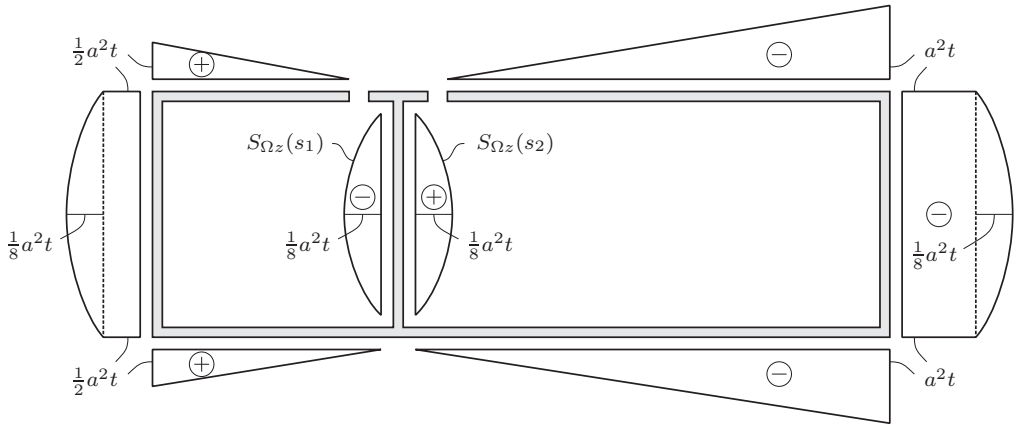

Figure C Distribution of the static moments $S_{\Omega z}(s1)$ and $S_{\Omega z}(s2)$ in the rectangular thin-walled double-cell section.

The origin of the arc-length coordinates are chosen as shown in Fig. B. The static moments $S_{\Omega z}(s_1)$ and $S_{\Omega z}(s_2)$ are next calculated with the sign and magnitude as indicated in Fig. C. Especially, it is seen that $S_{\Omega z}(s_1) = -S_{\Omega z}(s_2)$. The shear force per unit length in the open profile is given by Eq. (2–103):

$$H_{sj}(s_j) = -\frac{Q_y}{I_z} S_{\Omega z}(s_j), \qquad j = 1, 2. \tag{b}$$

Next, Eq. (2–106) provides

$$(H_{10} - H_{20})\frac{a}{t} + (H_{10} - 0)\frac{a}{t} + (H_{10} - 0)\frac{a}{t} + (H_{10} - 0)\frac{a}{t} = -\oint_{\Gamma_1} \frac{H_{sj}(s_1)}{t(s_1)} ds_1, \tag{c}$$

$$(H_{20} - 0)\frac{2a}{t} + (H_{20} - 0)\frac{a}{t} + (H_{20} - 0)\frac{2a}{t} + (H_{20} - H_{10})\frac{a}{t} = -\oint_{\Gamma_2} \frac{H_{sj}(s_2)}{t(s_2)} ds_2. \tag{d}$$

The right-hand sides are calculated by insertion of Eq. (b) with the distribution of $S_{\Omega z}(s_j)$ shown in Fig. C. The results become

$$\oint_{\Gamma_1} \frac{H_{sj}(S_1)}{t(s_1)} ds_1 = \frac{4}{7}\frac{Q_y}{a^3t^2}\left(\frac{2}{3}a \cdot \frac{a^2t}{8} - \frac{a}{2} \cdot \frac{a^2t}{2} - a\frac{a^2t}{2} - \frac{2}{3}a\frac{a^2t}{8} - \frac{s}{2}\frac{a^2t}{2}\right) = -\frac{4}{7}\frac{Q_y}{t}, \tag{e}$$

$$\oint_{\Gamma_2} \frac{H_{sj}(s_2)}{t(s_2)} ds_2 = -\frac{4}{7}\frac{Q_y}{a^3t^2}\left(\frac{2a}{2} \cdot a^2t + a \cdot a^2t + \frac{2}{3}a \cdot a^2t + \frac{2a}{2}a^2t - \frac{2}{3}a\frac{a^2t}{8}\right) = \frac{12}{7}\frac{Q_y}{t}. \tag{f}$$

(continued)

Then, the following solutions are obtained for the initial values of the shear forces per unit length:

$$4H - 10 - H_{20} = -\frac{4}{7}\frac{Q_y}{a}, \qquad -H_{10} + 6H_{20} = -\frac{12}{7}\frac{Q_y}{a}, \tag{g}$$

which implies that

$$H_{10} = \frac{24}{322}\frac{Q_y}{a}, \qquad H_{20} = -\frac{88}{322}\frac{Q_y}{a}. \tag{h}$$

Next, $H_j(s_j)$ is calculated from Eqs. (2–103) and (2–104) along both peripheries Γ_1 and Γ_2. Finally, the shear stresses $\sigma_{xs}(s_j)$ are computed from Eq. (2–98a). Due to the constant wall thickness this reduces to

$$\sigma_{xs}(s_j) = \frac{1}{t}H_j(s_j), \qquad j = 1, 2. \tag{i}$$

The flow of the shear stresses σ_{xs} has been shown in Fig. E.

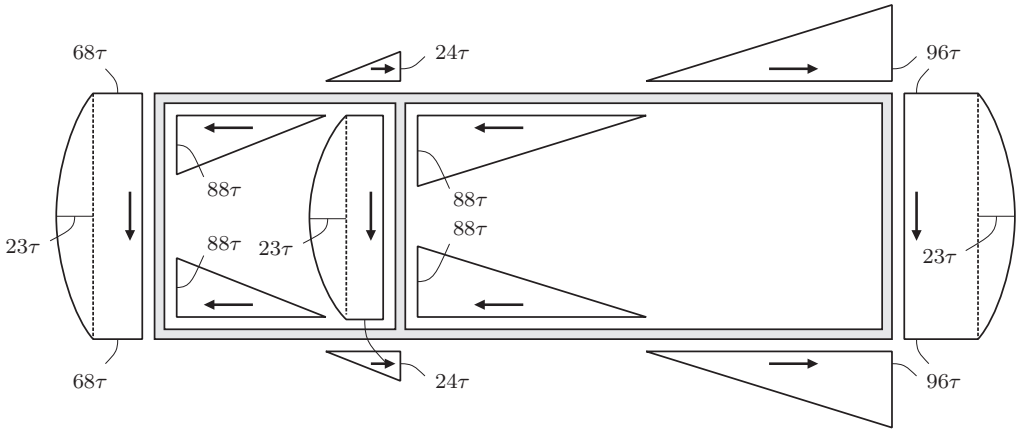

Figure D Distribution of the shear stresses in the rectangular thin-walled double-cell section with $\tau = Q_y/(322at)$.

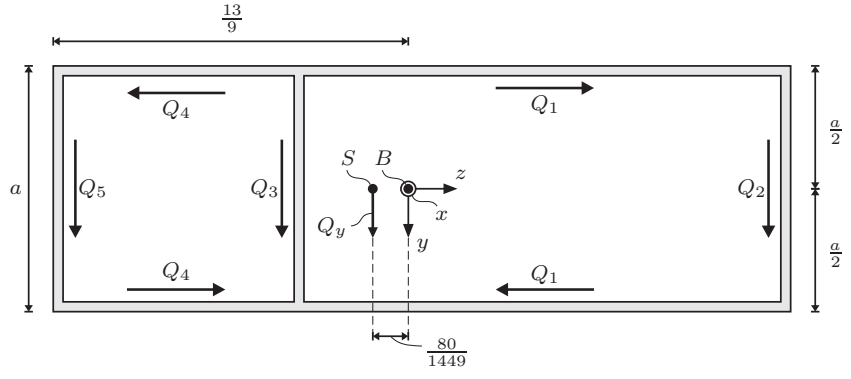

Figure E Shear forces in the wall segments of the rectangular thin-walled double-cell section. *(continued)*

Next, the shear forces Q_1, Q_2, Q_3, Q_4 and Q_5 in the wall segments shown in Fig. E are calculated. These become:

$$Q_1 = \frac{1}{2}(96-88)\cdot 2a\cdot t\cdot \frac{1}{322}\frac{Q_y}{at} = \frac{12}{483}Q_y, \tag{j}$$

$$Q_2 = (96+\frac{2}{3}\cdot 23)\cdot a\cdot t\cdot \frac{1}{322}\frac{Q_y}{at} = \frac{167}{483}Q_y, \tag{k}$$

$$Q_3 = (112+\frac{2}{3}\cdot 23)\cdot a\cdot t\cdot \frac{1}{322}\frac{Q_y}{at} = \frac{191}{483}Q_y, \tag{l}$$

$$Q_4 = \frac{1}{2}(68-24)\cdot a\cdot t\cdot \frac{1}{322}\frac{Q_y}{at} = \frac{33}{483}Q_y, \tag{m}$$

$$Q_5 = (68+\frac{2}{3}\cdot 23)\cdot a\cdot t\cdot \frac{1}{1288}\frac{Q_y}{at} = \frac{125}{483}Q_y. \tag{n}$$

It is seen that $Q_2+Q_3+Q_5 = Q_y$. The static equivalence (2–83) of the shear stresses is then fulfilled. The position z_s of the shear centre follows from Eq. (2–95):

$$z_s = -\frac{1}{Q_y}\left((Q_4-Q_1)a - Q_2\cdot\frac{14}{9}a + Q_3\cdot\frac{4}{9}a + Q_5\frac{13}{9}a\right) \quad \Rightarrow \quad z_s = -\frac{80}{1449}a. \tag{o}$$

The position of the shear centre has been illustrated in Fig. E. □

Example 2.13 Distribution of shear stresses in open and closed sections due to bending and St. Venant torsion

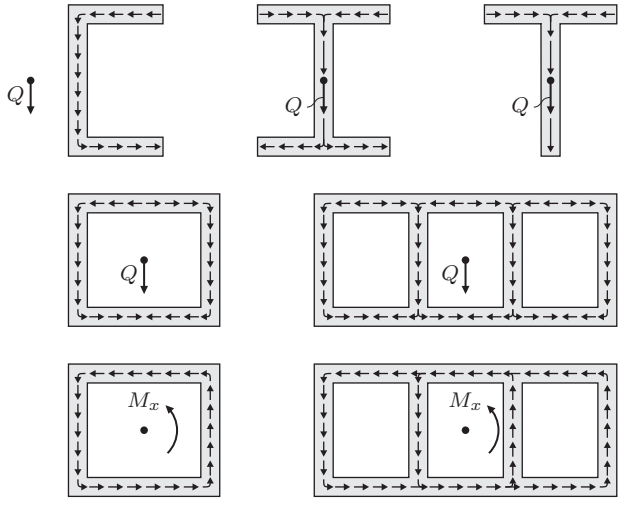

Figure A Shear flow in open and closed sections due to transverse shear forces and torsional moments.

Fig. A shows the shear flow in open and closed thin-walled sections exposed to a transverse shear force Q or a torsional moment M. For closed sections the shear stresses $\sigma_{xs}(x,s)$ are uniformly distributed over the wall thickness for both loadings. For open section this is only the case in the case for the shear force loading, whereas the shear stresses for St. Venant torsion is linearly varying in the thickness direction around the mid-line of the wall. □

2.4 Summary

The computation of shear stresses in beams has been the focus of this chapter with detailed explanation of the theory for thin-walled sections subjected to torsion and/or bending. A brief summary of the main findings is given in the following.

Uncoupling of bending and torsion requires that the shear force acts through the so-called shear centre. The shear centre always lies on a line of symmetry within a symmetric cross-section. Hence, the position of the shear centre coincides with that of the bending centre for double-symmetric sections.

St. Venant torsion is characterised by the fact that the beam is allows to warp freely, leading to a homogeneous twist of the cross-section along the beam axis. The homogenous torsion problem can be defined in terms of the warping function or, alternatively, in terms of Prandtl's stress function.

Shear stresses due to homogeneous torsion vary linearly over the thickness of the wall in open thin-walled profiles. However, in a closed thin-walled section with one or more cells, the shear stresses due homogeneous torsion is homogeneous over the thickness.

Homogeneous torsion induces warping in a beam. The warping increases linearly with the torsional moment. However, in a circular profile (a cylinder as well as a tube) there is no warping.

The torsional stiffnesses of open and closed cross-sections are different . Thus, a closed cross-section has a much higher torsional stiffness than an open cross-section with a similar cross-sectional area. Likewise, the ultimate strength of a closed section is higher than that of a similar open section.

Shear stresses from bending can generally be analysed by means of the so-called stress function. However, this requires the use of a numerical scheme, *e.g.* the finite-element method.

Grashof's formula defines the shear stresses from bending in open thin-walled sections. For closed thin-walled sections, Grashof's formula must be adjusted be an additional term that

Warping takes place due to bending since the shear stresses are accompanied by shear strains. For a rectangular cross-section, the beam warps into an S-shape.

Shear flow is a graphical interpretation of the direction in which the shear stresses are acting on the cross-section of a beam. In the case of bending, this forms an analogy to water streaming down a system of pipes.

Internal walls in a section will not increase the torsional stiffness and strength significantly. However, the inclusion of an internal wall oriented in the direction of the shear force will provide an increase of the shear strength and stiffness.

The theory presented in this chapter can be used for the determination of the shear stresses and warping deformations in beams subjected to any combination of bending and homogeneous torsion. However, if torsion is prevented, *e.g.* at one end of the beam, another theory must be applied as described in the next chapter.

References

Krenk, S. (2001). *Mechanics and analysis of beams, columns and cables* (2nd ed.). Springer Verlag.

SaintVenant, B. (1855). Memoire sur la torsion des prismes. *Mem. Acad. Sci. Savants Etrangers* **14**, 233–560.

Timoshenko, SP (1921). On the correction for shear of the differential equation for transverse vibrations of static bars. *Philosophical Magazine, Series 6* **41**, 744–746.

Vlasov, V.Z. (1961). Thin-walled elastic beams. *Israel Program for Scientific Translations*.

ISSN 1901-7278
DCE Lecture Notes No. 23